TÉCNICO LISBOA

Comparative study of the contact pressures in hip joint models with femoroacetabular impingment with different cephalic deformities

Iryna Havenko

Thesis to obtain the Master of Science Degree in

Biomedical Engineering

Supervisors: Prof. Fernando Manuel Fernandes Simões

Dr. Paulo Renato Amaral Rego

Examination Committee

Chairperson: Prof. Paulo Rui Alves Fernandes

Supervisors: Prof. Fernando Manuel Fernandes Simões

Members of the Committee: Prof. Carlos Miguel Fernandes Quental

October 2017

Abstract

In this study, finite element analyses of hip joint models with femoroacetabular impingment of the cam-type are performed. For comparative purposes, patient-specific three-dimensional geometries of the hip joint structures are obtained by manual segmentation from arthro-MRI sequences of images in two pathologic cases presenting different cephalic deformities characterized by alpha-angles equal to 60º and 81º, respectively.

In the numerical simulations, the pathologic hip joints are submitted to a physiological compression force and to several physiological hip motions. In all the analyses the bony structures are considered rigid and the soft tissues are considered as linear elastic and isotropic materials. The contact pressures and the von Mises stresses are registered and compared in these pathologic hip models in order to better understand the mechanism of aggression of the intra-articular tissues and to justify and validate the current medical treatment. Moreover, this study aims at understanding the role of the labrum in the pathologic hip joints. Thus, numerical simulations of the hip models without the presence of the labral tissue are also performed.

The magnitudes of the contact pressures obtained in the two pathological cases are in coherence with published data and are higher than the ones obtained in normal hip joints. As a consequence of the increased severity of the cam impingement, increased contact pressure magnitudes are observed in the pathologic hip with larger alpha angle. When the labrum is absent from the model, the magnitudes of the contact pressures are moderately smaller than the ones obtained in the complete models. However, the regions that are now subjected to pressure are wider, suggesting that the labrum has a supportive and protective action that preserves some regions of the cartilage structures from high pressures.

Resumo

Neste estudo, foram analisados pelo método dos elementos finitos modelos de articulações da anca que apresentam conflito femoroacetabular do tipo cam. Para efeitos de comparação, geometrias tridimensionais baseadas na anatomia específica dos pacientes são obtidas através da segmentação manual a partir de imagens de artro-ressonância magnética radial correspondentes a dois casos patológicos que apresentam diferente deformidade cefálica caracterizada por ângulos alfa de 60º e 81º, respetivamente.

Nas simulações numéricas, as articulações patológicas da anca são submetidas a uma força de compressão fisiológica e a vários movimentos fisiológicos característicos da anca. Em todas as análises, as estruturas ósseas são consideradas rígidas e os tecidos moles são considerados como materiais elásticos lineares e isotrópicos. As pressões de contacto e as tensões de von Mises são registadas e comparadas nestes modelos patológicos da articulação da anca, de forma a interpretar melhor o mecanismo de agressão dos tecidos intra-articulares e justificar e validar o tratamento cirúrgico corrente. Este estudo tem também como objetivo compreender o papel do labrum nas articulações patológicas da anca. Assim, simulações numéricas dos modelos da anca sem a presença do tecido labral são também realizadas.

As magnitudes das pressões de contacto obtidas nos dois casos patológicos são coerentes com os resultados publicados e são maiores do que as obtidas nas articulações normais da anca. Como consequência do aumento da severidade do conflito cam, as maiores magnitudes de pressão de contacto são observadas na anca patológica com maior ângulo alfa. Quando o labrum está ausente do modelo, as magnitudes das pressões de contacrfto são moderadamente menores do que as obtidas nos modelos completos. No entanto, as regiões agora sujeitas a pressão são mais amplas, sugerindo que o labrum tem uma ação de suporte e proteção que preserva algumas regiões das estruturas da cartilagem das altas pressões.

Acknowledgments

I would like to thank professor Fernando Simões for all the incessant support, availability and advices given throughout all the phases of this thesis. Also, Dr. Paulo Rêgo for providing the arthro-MRI images of the patients and for clarifying relevant characteristics of the present hip pathology. I would like also to thank my friends in Instituto Superior Técnico, in Lisbon and in Aveiro for all the remarkable experiences shared during all these 5 years and also for the support during the elaboration of the present project. To my family, I am thankful for the everyday support and for this unique academic opportunity.

Table of Contents

List of figures

List of Tables

List of Acronyms

FAI	Femoroacetabular Impingement
OA	Osteoarthritis
THA	Total hip arthroplasty
FE	Finite element
MRI	Magnetic Resonance Imaging
FEA	Finite element analysis
FEM	Finite element method
MRA	Arthro-MRI imaging

1. Introduction

The hip joint is one of the most important human joints in the body. The complexity of its anatomical and functional specifications provides equilibrium and balance, resulting in notorious firmness and permitting different motions with a broad range in distinct anatomical planes. It plays a major role in the gait cycle, and in the normal daily living activities. The structure of this type of joint promotes the accommodation of the human body weight and allows the spreading of the loads on the body.

The femoroacetabular impingement (FAI) in the hip joint is an abutment mechanism, due to the abnormal hip morphology, between the femoral head/neck and the acetabular rim, resulting in cartilage and labrum aggression. Mostly prevalent in active adults, the individuals usually reveal hip pain and decreased hip mobility [1][2]. As a result of the abnormal (non-physiological) stresses and contact pressures experienced within the intra-articular structures, this pathological mechanism may lead to hip dysfunction. The pathological mechanism of FAI has been commonly associated as a potential cause of cartilage degeneration and posterior development of early osteoarthritis (OA) of the hip. Early diagnosis and accurate treatment should be performed in order to avoid extreme cartilage damage and to improve the patient's mobility and life quality [3].

There are two types of impingement distinguished so far: the cam-type impingement and the pincer-type impingement. The former is characterized by an abnormal (non-spherical) shape of the femoral head with decreased femoral head/neck offset. The latter, is characterized by an abnormal local or global overcoverage of the acetabulum [4]. Mixed impingement can also be observed. Cam-type lesions mostly affect the articular cartilage and may lead to labrum tear. Pincer-type lesions affect predominantly the labral tissue.

FAI of the cam-type impingement, the focus in this study, is characterized by an abnormal value of the alpha angle, a geometrical parameter. The alpha angle is a measurable anatomical characteristic of the hip morphology and quantifies the morphological deformity of the femoral head. Normal hip morphology is characterized by alpha angles in the range of 40-50º [5]. The deformity in the femoral head is located usually at the anterosuperior rim and the repetitive impacts between the abnormal femoral head and the acetabulum lead to excessive stresses and contact pressures in the intra-articular structures [6].

Mostly prevalent in young athletic male adults, the femoroacetabular (FAI) of the cam-type is observed when the hip is submitted to flexion and internal rotations movements, required in intense sports activities and also in normal routine activities. For advanced cam-type impingement, individuals usually present pain and limited hip motions when submitted to experimental clinical tests. Currently, imaging techniques such as magnetic resonance imaging arthrograms (arthro-MRI) are performed to identify the cam-type abnormality in the hip and to assess the severity of the aggression of the soft tissues. More extensive diagnosis may be useful to identify, in some cases, cartilage inflammation and

chondromalacia [6]. The treatment of FAI of the cam-type is mainly surgical. It consists on restoring the sphericity of the femoral head, by trimming the aspherical shape observed on the femoral head/neck junction and can be done by open surgery or by arthroscopy [7].

Several studies have already been performed with the aim of evaluating and measuring the contact pressures and stresses in hips with abnormal morphology, while simulating the loadings and motions of normal daily living activities. The key aspect throughout these studies was to obtain a correlation between the morphological deformity of the hip joint and the measured intra-articular contact pressures. Chegini et al. [5] analyzed the contact pressures and stress distributions of virtual pathological hip joint models, including FAI of the cam and pincer types and dysplastic joints, using finite element analysis (FEA). Hip joints with normal morphology were also considered. Jorge et al. [8] developed three-dimensional finite element models of a normal hip and of a hip with femoroacetabular impingement of the cam-type obtaining the corresponding contact pressures and stress distributions. The FE meshes of the hip joints were based on the reconstruction of patient-specific real anatomies. More recently, Lourenço et al. [9], using the same reconstruction method of the hip models as in Jorge et al. [8] based on real patient-specific anatomy, compared and evaluated the intra-articular stresses and contact pressures in a hip joint with femoroacetabular impingement of the cam-type before and after hip surgical intervention. It was observed that the computed contact pressures in the cam-type model before treatment were larger than the ones obtained after surgical intervention.

The goal of this study is to compare the intra-articular von Mises stresses and contact pressures in hips with femoroacetabular impingement of the cam-type with various degrees of morphological deformity, with and without the presence of the labral tissue aiming at improving and validating the current treatment techniques. Individuals with FAI of the cam-type with distinct values of alpha angles are considered in order to assess its influence on the values of the stresses and contact pressures and the consequent intensity of the aggression of the soft tissues (articular cartilages and labrum). The patient-specific real geometries of the hip joint are obtained from arthro-MRI sequences of images. Based on the same reconstruction method as used in Lourenço et al. [9], three-dimensional (3D) finite element (FE) meshes of the femoral cartilage, acetabular cartilage and labrum are obtained, and the corresponding models are analysed under the action of physiological hip forces and physiological rotational motions.

The finite element (FE) contact analyses in real patient-specific geometry models, comparatively to those performed in idealized/artificial models [5], provides a personalized diagnosis and treatment procedure for each individual. Thus, this study, in our opinion, will help to justify and validate the current medical treatment interventions that delay the aggression of the soft tissues and its progression eventually resulting in OA. Also, this study aims at understanding the role of the labrum in the pathologic hip joints.

The present thesis is divided in six distinct chapters. The present chapter is the introductory chapter, providing an overall view of the performed work. Chapter two provides a review of the femoroacetabular impingement as well as the theoretical background of the hip anatomy, the hip biomechanics, and the current diagnosis and treatment techniques of the pathology. Chapter three contains the literature review

presenting the already performed works and analyses and chapter four describes the used reconstruction methodology to obtain the final 3D models of the pathologic hip joints. In chapter five the results and the subsequent discussion of the results of the finite element analyses are presented. In the last chapter, chapter six, conclusions and future perspectives are discussed.

2. Cam-type femoroacetabular impingement

2.1. Hip anatomy review

The knowledge of the structural components of the hip and its anatomical orientations are the basis for understanding the principles of the hip joint biomechanics and the associated pathologic conditions. Anatomically, the hip joint is defined by its osseous architecture, articular cartilage surfaces, acetabular labrum, ligaments, and fibrous capsule elements. Nevertheless, the muscles surrounding the hip joint are necessary in providing hip firmness and permit a variety of hip movements. The hip joint anatomical structures and surrounding tissues are represented in Figure 1.

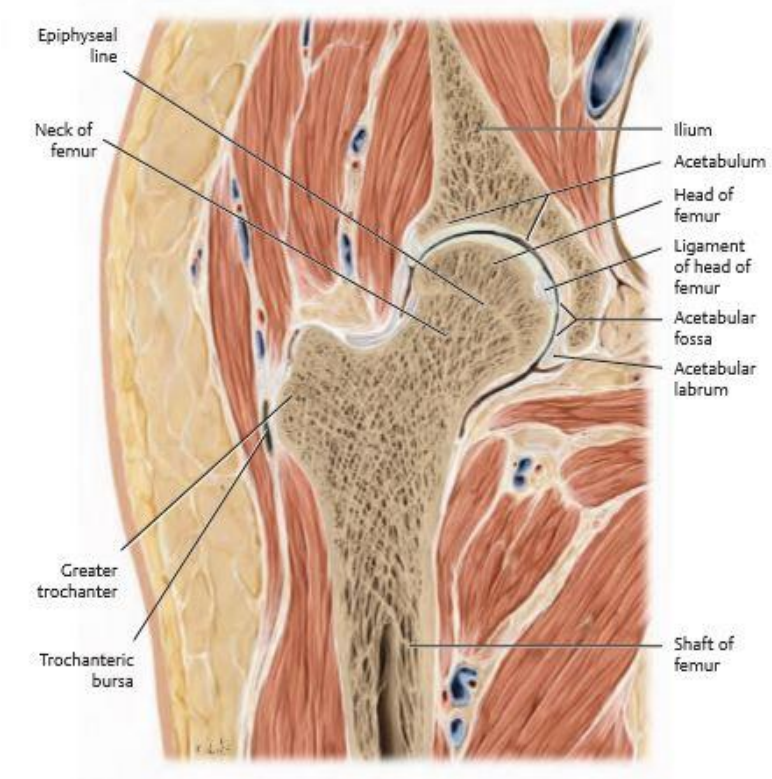

Figure 1: Right hip joint: anterior view in coronal section [10].

Characterized by the rotational movements that allows between the femoral head and the acetabular cavity of the pelvis, the hip joint constitutes a multi-axial ball-and-socket type of synovial joint [10].

2.1.1. Articular Surfaces

The articular surfaces of the hip joint are the head of the femur and the acetabular cavity. The head of the femur is characterized by its spherical shape which is layered with cartilage. Extended to the extremities of the acetabular labrum, the articular cartilage thickness is most commonly thinner at the outer border of the femoral head and tends to increase its thickness to the medial area of the femoral head [11]. In addition, it achieves its highest thickness in the anterolateral zone of the femoral head, a zone where the fundamental loadings of the hip joint are most noticeable. Medially, on the surface of the femoral head there is a *locus*, named fovea capitits, which receives the ligament of the head of the femur, the ligamentum teres responsible for the blood supply and that can be observed in Figure 2.

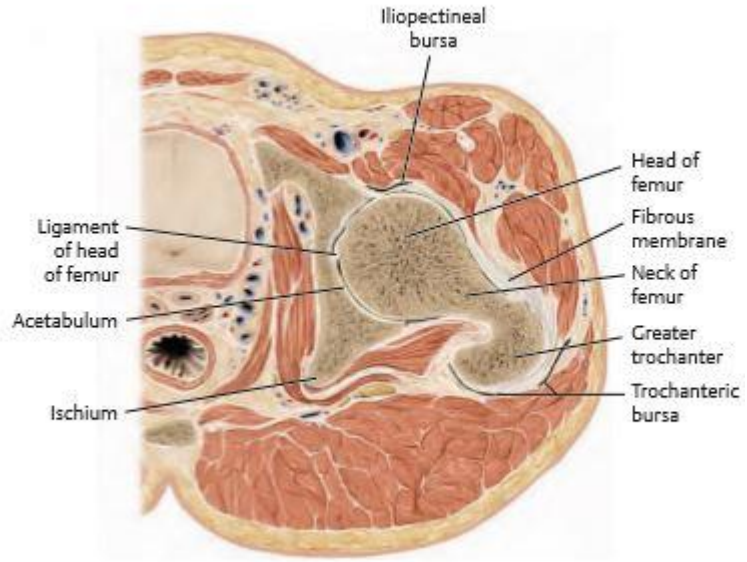

Figure 2: Head of the femur of the right hip joint: superior view [10].

The acetabulum is a concave (cup) shaped structure composed by the involvement of segments of bones from the pelvis, the ilium, ischium, and pubis. Initially in an early developmental stage, in newborns, these three bones are separated by specific cartilage, the triradiate cartilage. The fully developed and united skeletal structure of these bones is achieved by the age of 22-24 years [12]. The diverse structures that can be identified within the acetabulum are the lunate surface, acetabular fossa, acetabular notch (roof), and the acetabular rim. The acetabular components are represented in Figure 3.

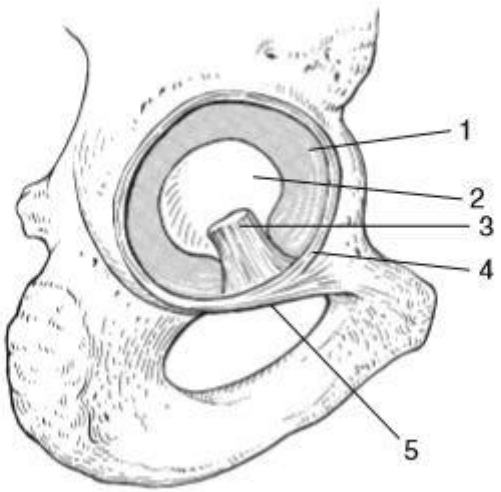

Figure 3: Lateral view of the acetabulum of the left hip joint: 1- lunate surface; 2- acetabular fossa; 3- ligamentum teres; 4- acetabular labrum; 5- transverse acetabular ligament [55].

The lunate surface of the acetabulum is described as an unclosed ring that is coated with articular cartilage. It forms the articular surface zone of the acetabulum, connects directly to the head of the femur. It is expanded anterosuperiorly, absorbing the pressure of the body weight which falls in the straight posture [11]. The acetabular cartilage has the highest thickness in the anterosuperior area, where the surface is broader, which is fundamental to carry and support the loads that act on the hip joint [13]. Absent in articular cartilage, the acetabular fossa is coated by the synovial membrane medially on the lunate surface.

The acetabular labrum is a complex ring-shaped structure composed of fibrocartilaginous tissue that frames the acetabular socket. It is attached to the acetabular rim and links by the transverse acetabular ligament, at the lower portion along the acetabular notch [11]. From a cross-sectional view, it is triangular shaped, outlines the acetabular cavity and holds the head of the femur. The continuity of the acetabular labrum within the transverse acetabular ligament creates an ideal joint environment, increasing the adaptation between the articulating surfaces, the femoral head and the acetabulum [13].

The acetabular labrum enters the acetabulum by 20-25% and enhances the acetabulum surface area by 25-30% [13]. Due to its joint deepening, provides additional stability to the hip joint, by confining the extreme movements of the head of the femur. It plays a major role in the allocation and accommodation of forces experienced within the joint, aiming to decrease the intra-articular pressures [14]. It has been suggested that the acetabular labrum aids to preserve the synovial fluid and its internal pressures within the intra-articular structures, controlling the merging of the articular cartilages and thus, leading to decreased stresses. The pressures in the synovial fluid within the intra-articular structures create an increased hydrostatic fluid pressurized environment, which avoids the direct interaction of the cartilages from the femoral head and the acetabular cavity [12]. The labrum (triangular shaped structure)

and its surroundings are represented Figure 4. Some, studies were also performed in order to assess and clarify the role and the mechanical characteristics of the labral tissue [15].

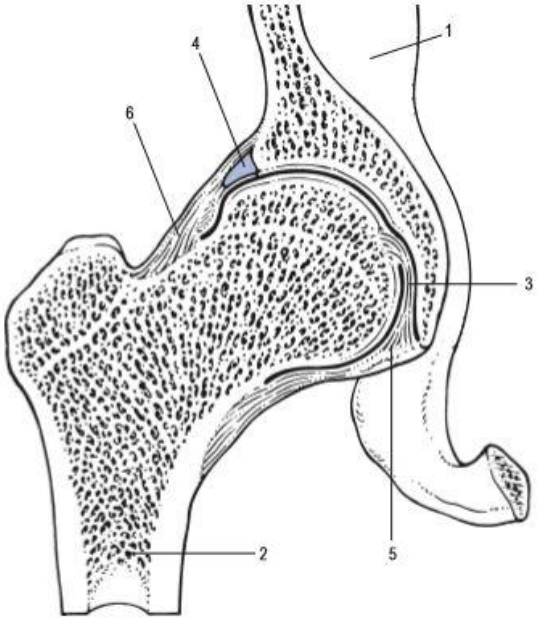

Figure 4: Right hip joint: sectional view. 1-ilium; 2-femur; 3-ligamentum teres; 4-acetabular labrum; 5-transverse acetabular ligament; 6-joint capsule [55].

2.1.2. Ligaments and Synovial membrane

The ligaments that constitute the hip joint are the iliofemoral, pubofemoral, ischiofemoral and the transverse acetabular ligaments, which major role is to control the movements of the hip. The surrounding ligaments provide an overall increased and intensifying stability to the joint during normal daily motions. Additionally, as a characteristic of this type of joint, it presents a tissue between the capsule and its cavity, the synovial membrane. It synthesizes the synovial fluid observed in the intra-articular joint environment, contributing to a lubricated and nourished joint. The main function of the synovial fluid is to reduce friction between the articular cartilages of the joint surfaces and to absorb shocks. The anatomical structure and morphology of the synovial membrane is represented in Figure 5. The synovial fluid also nourishes the cells of the articular cartilages which are avascular tissues.

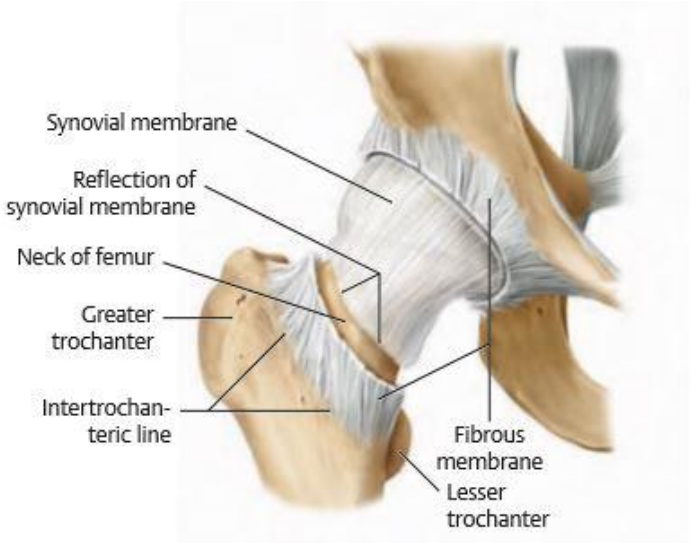

Figure 5: Right hip joint: anterior view. Joint capsule is represented with the exposed synovial membrane [11].

2.2. Biomechanics of the hip joint

The biomechanics of the hip joint provides an understanding of the development, evolution, and treatment of many disorders associated to this joint. The hip joint plays a fundamental role in hip movements and weight-bearing during routine and sports activities. Since the hip joint offers resistance to the experienced loads and forces, and also supports and accommodates the extreme impacts, distinct importance must be delivered in the understanding of the injury mechanism of the hip and its subsequent consequences. Failures of the articular cartilages in the hip joint, most commonly lead to deformed biomechanics of the hip, damaging the surrounding tissues. Anatomical and morphological deformities are usually the instigators of the biomechanical hip disorders. Loss of structural integrity compromises hip's normal physiological function, promoting inflammatory responses and originating pathologic conditions, such as human osteoarthritis (OA).

The hip joint is a diarthrodial type of joint, allowing the movement between its articular structures and enables the spreading of the experienced loadings within the intra-articular structures. The hip joint is characterized by a unique osseous stability, in which alterations of the morphology significantly influence its physiological biomechanical properties. The major characteristic of this joint is the fact that it is always subjected to a specific compressive force. The magnitude of the compressive force is due to the weight-bearing [13]. Muscular surrounding tissue of the hip joint is the main contributor to this compressive force.

The mechanical loadings experienced within the hip articulation vary according to the performed activity. For normal routine activities, and due to the hip joint motions, the hip cartilage experiences a wide range of mechanical loadings. Athletic activities may lead to an extremely increased loading across the hip joint. Maximal forces registered across the human hip joint can reach 2.5 to 4.5 times the body weight during walking activity [16]. Nevertheless, the impact of the high physical stresses on the hip joint during athletic activities may lead to pathologic hip joint processes.

Pathologic conditions such as anatomical abnormalities or conditions such as obesity, and FAI, contribute to the loss of mechanical integrity of the hip joint and lead to increased pressures and stresses. The understanding of the biomechanical function of the hip is a fundamental step that may aid the physician in the diagnosis of such pathological conditions and delay severe damage with appropriate treatment procedures [17].

2.2.1. Articular cartilage responses to mechanical loading

The articular cartilage is a specialized connective tissue that covers the articular structures of the hip joint. An understanding of the arrangement of this type of tissue and its mechanical responses to the experienced loadings are key aspects in identifying the features of the pathological and structural damage of hip osteoarthritis.

The bone ends of the articular structures of the hip joint, such as the femoral head and the cavity of the acetabulum are covered with articular cartilage, providing a bearing contact between these articular structures. Comparing to bone articular cartilage stiffness is much decreased, which results in admissible stresses within the joint [17]. The most important characteristic of the articular cartilage is in providing a hydrated surface for the motions and in facilitating the spreading of loads with a low friction coefficient.

The mechanical behavior of the articular cartilage results from the integrity offered by its components and the ability to sustain and transmit the experienced normal physiological loadings. The articular cartilage has associated some characteristic properties that define its behavior. The assessment and definition of its mechanical properties, such as Poisson’s coefficient and Young’s modulus, enables the identification of how differently it behaves to a specific environment.

The mechanical behavior of articular cartilage is described by a biphasic model characteristic. It consists on its solid and fluid components. In healthy articular cartilage tissue, it has been noticed that major loadings are supported by the fluid components, with a relatively small contribution of the solid components. On the other hand, in the case of pathologic cartilage tissue, such as osteoarthritic cartilages, the major contribution for the support of the experienced cartilage loadings is performed by the components of the solid phase, which lead to cartilage fatigue and loss of integrity between the

components that constitute the solid matrix. This mechanical alteration of the articular cartilage components results in higher cartilage deformation due to the reduced stiffness [17].

2.2.2. Instigative processes of osteoarthritis (OA)

As already mentioned, the normal physiological functioning of the articular cartilage is the result of the interaction between its mechanical structural properties and mechanical responses enabling the performance of free daily normal movements essential in the individuals lives. Several alterations of the biochemical or mechanical properties of the cartilage are potential initiators of cartilage degeneration which lead to the subsequent development of osteoarthritis [18].

Osteoarthritis is the most common chronic joint disease that results from cartilage degenerative processes. Individuals presenting signs of joint degeneration and early development of OA may reveal hip pain, disability and restricted hip motions. Extremely developed OA may lead to cartilage failure. The loss of integrity between the articular cartilage components responsible for retaining the mechanical stiffness leads to a sequence of degenerative processes. Such cartilage disorders are characterized by the loss of proteoglycans and thus, leading to high levels of pressure, result in increased cartilage deformation. Also, cartilage displacement is emphasized in response to low stiffness. Gradual loss of articular cartilage is observed as a result of metabolic abnormalities. In response to the metabolic and biochemical abnormalities of the articular cartilage, inflammatory processes of the synovial membrane initiate, leading to an intensified mechanism of cartilage damage.

The development of human hip osteoarthritis may be the result of numerous factors that lead to a nonfunctional joint. The cause for OA has been proposed to be primary or secondary [3]. It is considered primary, when the origin is not known but it is proposed to be subsequent to some cartilage or osseous abnormalities. Secondary osteoarthritis may be the result of any congenital and developmental abnormalities or joint injury. Nevertheless, and according to the cause, the increasing age has influence in the prevalence of hip osteoarthritis. The changes on the functioning and metabolic physiological maintenance of the chondrocytes (the cartilage cells) may have age-related basis. Deficient functioning of the chondrocytes leads to articular cartilage changes and thus, in these cases, the individual is more susceptible to develop osteoarthritis, and also to give rise to its progression. Considering the age-related issues of the instigative processes of the OA, the most affected individuals are older than 60, but apart from the increasing age prevalence, children and middle aged adults are also affected.

2.3. Femoroacetabular impingement: overview

Femoroacetabular impingement (FAI) is currently associated as a major cause of hip osteoarthritis (OA) [3]. It is a pathomechanical process of the hip characterized by an abnormal morphological anatomy of the osseous structures of the hip joint (incronguity between the femoral head and the acetabulum). The osseous alterations or deficient spatial orientation of the femoral head/neck junction may increase the stresses on the hip joint and, overtime, the pathologic condition of FAI may develop. It is described by an abutment mechanism between the proximal femur and the acetabular rim, in which the repetitive impacts of the hip may result in severe damage of the surrounding soft tissues of the hip joint [19]. The determinant motions that influence the pathological condition of the hip joint are the flexural and internal rotations of the hip and the predominant location of FAI is the anterosuperior rim region. Mostly affecting young male active adults, individuals presenting FAI usually reveal groin pain and limited hip motions. Increased levels of activity may aggravate the hip joint status and lead to highly symptomatic conditions.

The etiology of FAI is not clear and it is still under investigation. Some pediatric diseases and hip deformities have been proposed as possible predisposes of FAI. Diseases such as Legg-Calvé-Perthes, slipped capital femoral epiphysis (SCFE), and hip dysplasia may lead to the development of FAI. Also, high-impact athletic activities and genetic factors represent a potential cause for FAI. Today evidences suggest that FAI may also develop without any previous history of hip diseases.

FAI was first distinguished by Ganz et al. [4] as an underlying cause for idiopathic hip OA. By assessing, through open surgical dislocation, the hip structures and their aggression patterns, enabled the identification of different FAI morphologies. Also, Wagner et al. [2] provided conclusions that were consistent with the fact that osseous deformities of the femoral head/neck are the predominant factor for early joint degeneration, based on biochemical findings. Samples of patients with femoroacetabular impingement of the cam-type presenting an aspherical femoral head were selected and the biochemical signs and patterns of the articular cartilage modification were compared with osteoarthritic joints. The authors concluded that the biochemical signs of cartilage degeneration in patients with FAI presenting abnormal osseous morphology were identical with those existing in osteoarthritic human hip joints.

There are two types of impingement that have been identified, explaining the articular cartilage aggression and the patterns of failure mechanisms of the hip: the cam-type impingement and the pincer-type impingement. Although the two types of femoroacetabular impingement may occur separately, it is common to observe a version of both types of impingement in the same hip joint. Cam lesions are described by the cam effect resulting from the abnormal aspherical portion of the femoral head or lack of the offset in the femoral head-neck junction, mostly affecting the femoral cartilage and the labrum. Pincer lesions are explained by the rotation of the femoral head in the acetabular region that is overcovered, predominantly affecting the labrum [7]. Both lesions and mixed version can be observed in Figure 6.

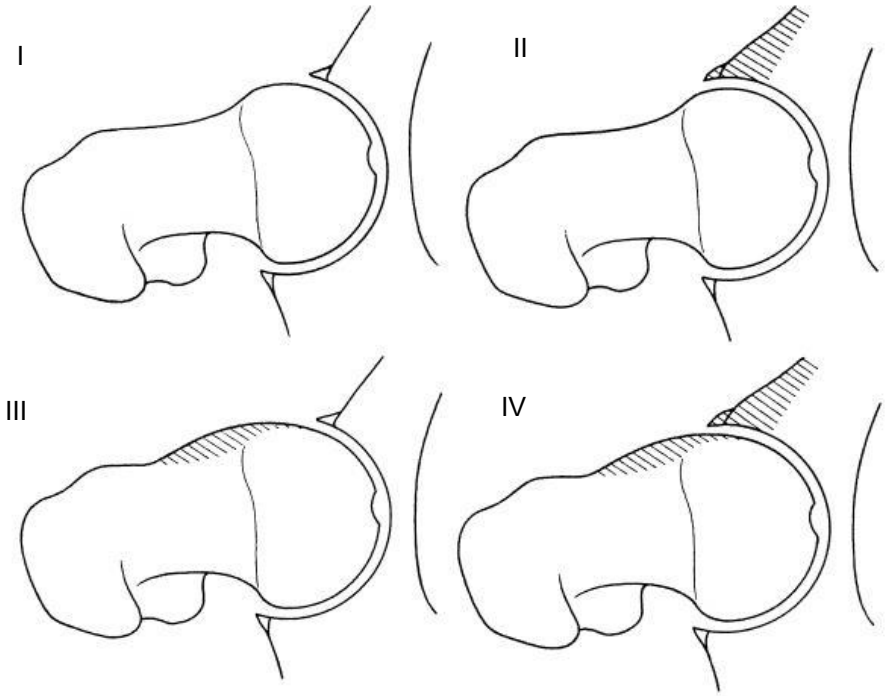

Figure 6: Representation of normal and pathologic joints. I-normal; II-pincer-type impingement; III-cam-type impingement; IV- mixed impingement (cam and pincer lesions). Adapted from [23].

FAI of the cam-type, characterized by an aberrant asphericity of the femoral head is predominantly located in the anterosuperior region of the transition to the anatomical neck, as one can observe in figure 6 - III. Several motions of the hip may lead to the damage of the cartilage and of the surrounding tissues. Pure flexural rotation and pure internal rotation movements are most symptomatic. Due to this movements and its repetitive impacts between the abnormal femoral head and the acetabular cavity, the articular cartilage structures and the labrum are submitted to excessive stresses and non-physiological intra-articular contact pressures. Contrarily to cam lesions, the pincer-type aggression mechanism is slightly attenuated and the joint degeneration is reduced [2].

Most individuals presenting FAI are under the age of 45 and the overall prevalence of FAI pathology is from 11% to 16%. The cam-type mostly affects male adults with ages between 17-35 years and is more prevalent in individuals with high levels of athletic demands. The pincer-type affects predominantly women with ages between 35-50 years and is significantly less destructive than the cam-type impingement [3]. A recent study proposed by Pun et al. [20] reported data for the epidemiology of FAI of the US population. Based on a study of 400 human hips, individuals with mean age of 25-35 years and where 55% were women without a history of any previous hip disease, the prevalence of the cam-type impingement was 15% in which almost 80% were men. In an elder group population, based on 3620 individuals with mean age of 55-65 years and where 60% were women, also without any previous disease, the reported values for the cam-type impingement prevalence in men and in women, were respectively 19.5% and 5%. The prevalence for the pincer-type lesions was significantly decreased, for men, when compared to cam-type. In conclusion, and in contrast to pincer-type impingement, cam-type impingement is more common and affects mostly men. Also, in a study conducted by Ito et al. [21] it has

been concluded that age and gender have influence in the prevalence of femoroacetabular impingement of the cam-type. The results demonstrate that symptomatic male young adults and symptomatic older female individuals present the same characteristics of this type of impingement.

Diagnosis and treatment techniques of FAI are fundamental in providing an effective management and follow-up of the progression of the pathological mechanism due to FAI. Individuals with FAI are usually submitted to clinical tests which are performed to validate the presence of FAI, providing a confirmative impingement test. More comprehensive and deep understanding of soft tissues status and damage are achieved through open surgical technique. Treatment interventions of FAI are fundamental in order to relief pain, avoid irreversible chondral and labral damages and is determinant in the long-term success of FAI treatment procedures. Successful surgical treatment of FAI requires appropriate and rectification of the osseous hip anatomy and morphology that led to the abnormal contact mechanics of the hip and its subsequent symptomatic conditions. In addition, early correction of the FAI pathology may delay the development of OA [22].

2.3.1. Cam-type impingement

Cam-type impingement is described by its jamming mechanism of the aspherical femoral head into the acetabulum [4]. The asphericity of the femoral head is characterized by an abnormal contour usually of the anterosuperior region of the head of the femur and decreased femoral head/neck offset, resulting in an abutment mechanism of the head of the femur with increasing radius of curvature into the acetabular cavity. Osseous bumps, responsible for the abnormal contour of the head of the femur, are most seen on radiographs of pathologic hips as characteristic of FAI of the cam-type, and are usually located at the anterosuperior region of the head of the femur (see Figure 7).

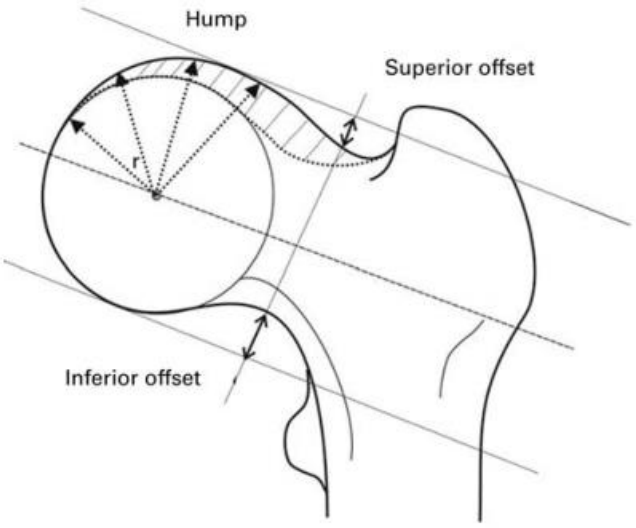

Figure 7: Representation of a cam-type pathological femur and its morphological characteristics - the formation of the osseous bump in the anterosuperior area of the femoral head with notable decreased femoral head/neck superior offset and the increase in the radius (r) of the curvature of the femoral head [28].

Hip motions seem to be a determinant factor for the damage patterns of the intra-articular structures of the hip joint. Repetitive hip impacts between the abnormal femoral head and the acetabular cavity result in non-physiologic stresses, which in long-term causes damage of the articular cartilages and labrum, leading to the separation between the cartilage and labrum and also to detachment of the cartilage from the subchondral bone [23]. The damages of the acetabular cartilage are commonly associated to inflammatory responses which lead to the pathologic condition, known as chondromalacia. This pathologic condition, assessed through arthroscopic intervention of the hip joint is represented in Figure 8.

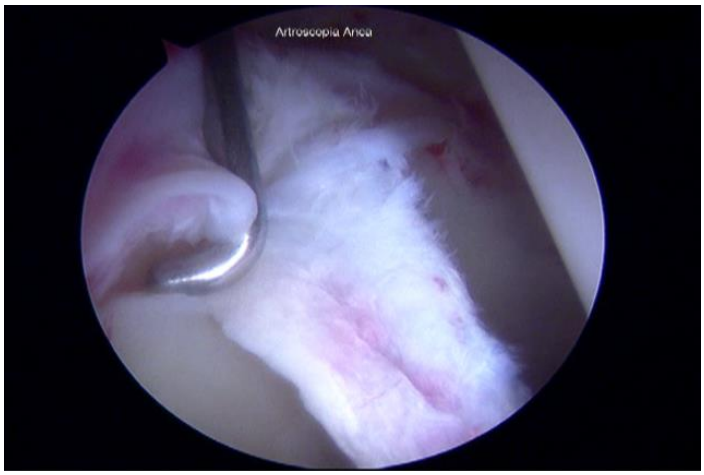

Figure 8: Arthroscopic intervention of a cam-type hip joint with visible signs of chondromalacia (red-ish inflammatory signs).

Due to the impact of the abnormal femoral head into the acetabulum, high stresses and severe damage are more notable during repetitive hip flexion and internal rotations movements. In the early stages of FAI of the cam-type, and depending on the severity of the pathology, the labrum may not reveal signs and patterns of aggression, but overtime labral tear may occur. The representation of the damage mechanism due to cam-type impingement is represented in Figure 9.

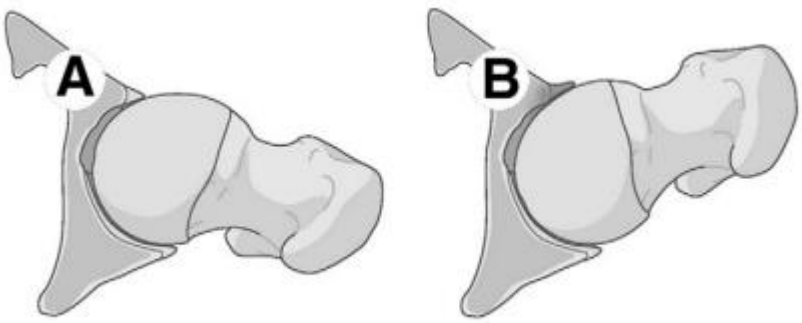

Figure 9: Damage mechanism of the cam-type impingement. A – Decreased femoral head/neck offset due to the asphericity of the femoral head. B – representation of a hip joint motion, in flexion and internal rotation the aspherical femoral head produces high stresses on the surrounding soft tissues, cartilage and labrum, due to the abutment [22].

The pathogenesis of cam-type impingement is unclear but, in the last decade some diseases such as slipped capital femoral epiphysis (SCFE), Perthes, and also genetic features have been proposed as risk aspects for the instigative processes of FAI of the cam-type [20]. Also, and more commonly, cam-type lesions have been associated to young male adults that are engaged in high-impact physical activities that require extreme hip motions, such as hockey and soccer. The athletic demands during adolescence play a major role in the development of cam-type impingement, since it is during adolescence that the maturation of the human skeleton occurs. Alterations in the osseous structure, such as new bone formation at the anterosuperior region of the femoral head or alterations in the contour of the growth plate, may occur as result of the shear stresses experienced at the unmatured hips during high athletic demands [1]. A deeper understanding of the instigative processes of FAI of the cam-type, regarding femoral malformations, is a center factor in order to provide effective and accurate preventive procedures.

2.3.2. Alpha-angle and center-edge angle

Abnormalities observed at the femoral head/neck junction, such as osseous excess or bumps defining the abnormal contour of the femoral head, provide quantifiable information that can be used to assess the degree of severity of the cam-type deformity. The quantifiable measure, known as the alpha-angle, was first described by Notzli et al. [24] with the aim of measuring the relationship between the femoral head and the neck junction. Also, a study conducted by Clohisy et al. [25] provided measurement techniques which quantified the femoral head deformity. The alpha angle is the angle between two lines: the first line from the center of the circle defining the femoral head and a point on the anterosuperior region at the periphery of the head of the femur where the asphericity starts to appear exactly beyond the circle that defines the femoral head, and the second line formed by a point in the center axis of the neck of the femur and the center of the circle defining the femoral head. In Figure 10 the representation of the hip joint with cam-type impingement is performed using radiographs on an anteroposterior view, in which the depiction of the alpha angle and its defining lines are specified.

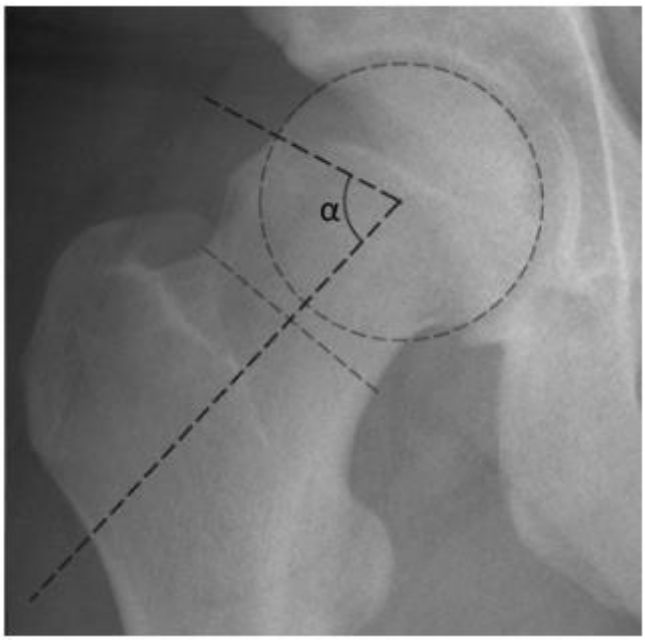

Figure 10: Radiograph presenting a hip joint on an anteroposterior view with the depiction of the lines defining the alpha angle [31]

Also, the morphology of the structure of pathologic hip joints can be assessed in Figure 11, in which one can identify an increasing pattern of the osseous bump on the anterosuperior region of the femoral head for increasing alpha-angles.

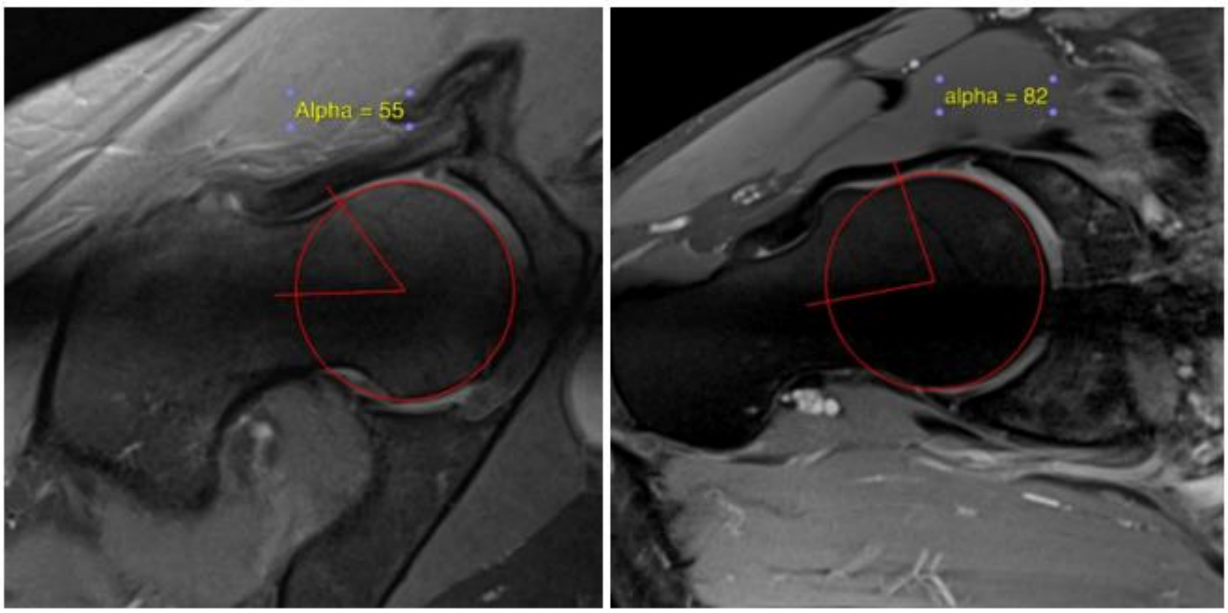

Figure 11: Representation of two measures of the alpha-angle in pathologic hip joints in arthro-MRI images. Left – depiction of a cam-type pathologic joint with an alpha angle of 55º. Right – depiction of a hip joint with a cam-type impingement with an alpha angle of 82º. The two lines quantifying the alpha angle: the first line from the center of the femoral neck to the center of the circle that defines the femoral head, and the second line from the center of the circle defining the femoral head to the anterior point on the femoral head in which the bump starts to appear beyond the femoral head circle.

The alpha angle can be quantified using radiographs, computed tomography or performing arthro-MRI technique on human hips. Also, it has been already validated in Barton et al. [26] the existence of an alternative method to measure the alpha angle, which reflects much more specificity and sensitivity, when compared to plain radiographs and the MRI technique. The lateral projections of the hip, more specifically the Dunn views technique for measurement of the alpha angle, have been used to assess the degree of the cam severity. Initially, the alpha angle was employed as a tool to assess the features of the coronal section of the hip joint in magnetic resonance imaging but in the last decade it has been used as a measurable instrument that quantifies the degree of femoral deformity and thus, its correlation with the severity of the cam-lesion in pathologic hips. Specific alpha-angles are assigned to pathologic and non-pathologic hips. Studies developed by Notzli et al. [24], Kassarjian et al. [27], Gosvig et al. [28] and Nou et al. [29] measured the alpha angle in human pathologic hip joints of patients presenting a femoroacetabular impingement of the cam-type with a positive impingement test, suggesting that abnormal alpha angles are greater than 55º, whereas for non-pathologic hip joints the physiological values for the alpha angles are in the range of 42 – 54º. The measured values for the alpha-angle in distinct hip joints are independent of the orientation of the neck of the femur and are only dependent of the observed osseous bump in the femoral head, located laterally to the physeal closure. As already mentioned, the cam-type geometries are characterized by decreased femoral head/neck superior offset (as seen in figure 8) which is in direct correlation with the abnormal contour of the femoral head. Significantly decreased offset occurs as the result of a highly aspherical femoral head.

Also, it has been noticed that individuals presenting FAI of the cam-type reveal different characteristics regarding the gender specification [30]. The gender has been considered in several analysis and experiments in the measurement of the alpha angle. A significant characteristic of the alpha angle is its variance regarding male and female individuals. Different values for the normal limiting degrees of the alpha angles are assigned to male and female individuals. More recently, a study conducted by Laborie et al. [31] specified the normal values regarding the gender specification in a group of healthy and young individuals. For anteroposterior views, the normal alpha angle assigned to male individuals is higher than the value assigned to female individuals, suggesting the gender specific values. For the former, the normal measured alpha angle is in the range of 61º – 63º and for the latter the normal measured alpha angles are in the range of 51º - 53º.

Quantification of the osseous bumps, as characteristic of the cam-type FAI, using the alpha angle, enabled the assessment of the severity of both, the deformity of the anterosuperior region of the femoral head and the acetabular labrum and cartilage damage observed in individuals with FAI of the cam type. Increased alpha angles are most commonly associated to higher femoral and acetabular cartilage damages, and to labral tear. Also, individuals with higher alpha angles, usually are more symptomatic than the individuals with lower alpha angles. Recently, Wright et al. [32] suggest that higher values of the alpha angle are associated with severe progression of the pathologic mechanism of the hip joint (FAI). Also, high values observed for the alpha angle are the determinant factor in the development of early osteoarthritis, resulting in most of the cases in tear of the acetabular labrum.

The alpha angle is thus, an important tool for the assessment of the severity of the cam type pathology of the hip joint, contributing for the comprehension of the aggression mechanisms regarding the degree of severity of the joint impingement. Individuals presenting cam type impingement reveal different levels of severity of the pathology, which are clinically significant, lead to different aggression patterns and mechanisms of the surrounding tissues of the hip joint and that may be quantified by the knowledge of the alpha angle. Providing quantitative information about the degree of severity of the aspherical femoral head, the alpha-angle also explains the decrease of the femoral head/neck offset observed in patients with femoroacetabular impingement of the cam-type and thus, aims at improving the knowledge of the pathology of the joint and the related clinical and mechanical consequences. Regarding the work and procedures throughout this thesis, the focus relies on an extensive comprehension of the mechanism of the impingement in individuals presenting FAI of the cam-type with different degrees of femoral head deformity characterized by the respective values of the alpha angle.

The quantification of the acetabular deformities commonly seen in individuals presenting pincer-type lesions is performed using the center-edge (CE) angle, also known as the Wiberg's angle. The center-edge angle is the angle between two lines: a vertical line that passes through the center of the femoral head and the line that connects the center of the femoral head and the edge of the acetabulum. It has been used as a quantifiable tool for the distinction of the several acetabular deformities, such as acetabular overcoverage and hip dysplasia. The physiological values for normal hips are in the range of 24º-26º. High values of the CE angle (higher than 35º) are associated to pincer-type pathologic hips (acetabular overcoverage). The CE angle associated to pathologic hips with dysplasia is lower than 14º-16º.

2.3.3. Tear of the labral tissue

FAI of the cam-type has been observed as a cause of labral tear [33]. Individuals presenting cam impingement in most severe and advanced cases usually reveal, as result of the pathologic mechanism of the hip joint, detachment of the acetabular labrum from the joint structure. The identification of labral tear is performed through the MRI imaging technique, but the surgical intervention (open surgery) also provides an evident diagnosis. In the early stages of the pathologic diagnosis, the acetabular labrum lesion is not significant, whereas for advanced cases and late diagnosis of the cam impingement, individuals present extreme hip pain and the labral separation is more common.

Due to its anatomical and morphological features, the acetabular labrum is important in the maintenance and support of the articular structures and thus allows the absorption of high stresses experienced in the hip joint during diverse hip movements. As already mentioned, the repetitive hip joint impacts in hips with cam impingement lead to extreme articular cartilage and labral damages. As proposed by McCarthy et al. [34] the articular cartilage damage is more severe in individuals that present labral aggression and/or labral detachment.

Histological studies have been performed in order to evaluate the status of the labral tissue in pathologic hips [35], in which the labral tissue components revealed lack of organization and are the basis for the labral dysfunction. Labral damage and posterior dysfunction are critical features in the pathologic mechanism of the cam impingement and have been associated to development and progression of hip osteoarthritis (OA) [36]. It is thus, of extreme importance to deliver an early diagnosis of the labral tissue aggression in order to delay the total separation of the labrum from the chondral structures and also, to prevent the progression of OA. The treatment of the labral tear is a crucial process in which the main focus is to restore the morphological characteristic of the labrum, by reattaching it to the joint structures, and it can be performed by open surgery or by arthroscopy. The representation of the labrum reattachment through arthroscopic surgery is shown in Figure 12.

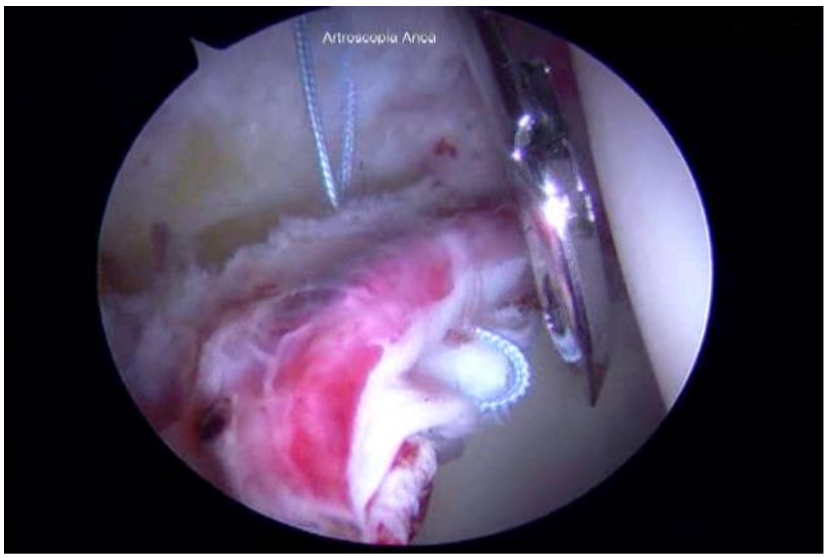

Figure 12: Arthroscopic hip joint surgery: labrum reattachment intervention.

2.4. Diagnosis and Treatment

The early diagnosis of the FAI hip pathology mechanism is a relevant procedure to delay severe joint damage providing the accurate preventive procedures. Several techniques are today available to facilitate the identification of this pathology of the hip. Patients presenting symptoms and signs, such as pain and limited flexural and internal rotation hip motions, are submitted to several clinical tests and the final diagnosis is confirmed through arthro-magnetic resonance imaging (arthro-MRI) [37]. Specific symptoms can be associated to the pathologic mechanism of the hip joint due to FAI. When submitted to the impingement tests, consisting in forced flexion and internal rotation of the hip joint, individuals with cam impingement usually reveal hip pain and reduced hip motion, which confirms the cam impingement, leading to a positive impingement test and positive clinical impingement diagnosis [1]. The impingement tests provide low sensibility and do not identify the features and specifications of the pathology, such as damage of the surrounding tissues of the articular joint.

For more extensive knowledge of the joint pathology, imaging techniques such as radiographs, MRI and also arthro-MRI (MRA) are performed. Radiographs provide useful information regarding the bony specifications, which not only identify the acetabular deformities but also allow the quantification of the asphericity of the femoral head through the measurement of the alpha angle. On the other hand, the MRI imaging technique allows the identification of the anatomical orientation of the cam impingement, providing information on the extension of the femoral osseous bump observed usually on the anterosuperior region of the femoral head in cam hip joints [38]. The assessment of tissue damage observed in the articular cartilages of the femoral head and acetabulum and also in the labrum, is performed by enhancing the contrast of the arthro-MRI (MRA) images, by injecting a gadolinium solution [39]. The injection of gadolinium improves the contrast of the arthro-MRI images and increases the resolution of the images, allowing the identification and distinction of the presence of labral damage and labral tear in cam joints. Nevertheless, and in order to provide a more detailed and precise diagnosis, improvements regarding the imaging techniques are on-the-go and aim at facilitating the identification of the articular cartilage and labral damage [1].

Currently the treatment of FAI of the cam-type, depending on the severity of the pathology, relies on either non-operative procedures, highlighting the need of avoiding extreme hip motions and reducing the level of physical activities, or surgical procedures. The operative intervention can be performed by an open surgery or an arthroscopic surgery or even by a combination of both techniques. It consist on the reshaping of the abnormal asphericity of the femoral head to reestablish the physiological sphericity of the femoral head which reduces pain and increases hip mobility [7]. Nevertheless, the success of the surgical interventions besides restoring the anatomical shape of the osseous structure should also enable the attenuation of the hip joint damage and the progression of hip OA, thus avoiding total hip arthroplasty (THA) [6].

Open surgery is an invasive technique and allows the confirmation and posterior correction of the osseous bumps observed usually in the anterosuperior region of the femoral head in cam joints. Consisting on the trimming of the femoral head, it restores the normal spherical shape of the femoral head, and thus, ceases the impinging process. Regarding the arthroscopic surgical intervention, it is a less invasive technique when comparing to open surgery [40]. As in the open surgical treatment, the arthroscopic procedure allows the correction of the femoral abnormalities, by reshaping the asphericity of the head of the femur. Also, the rectification of the damage observed on the articular cartilages of the

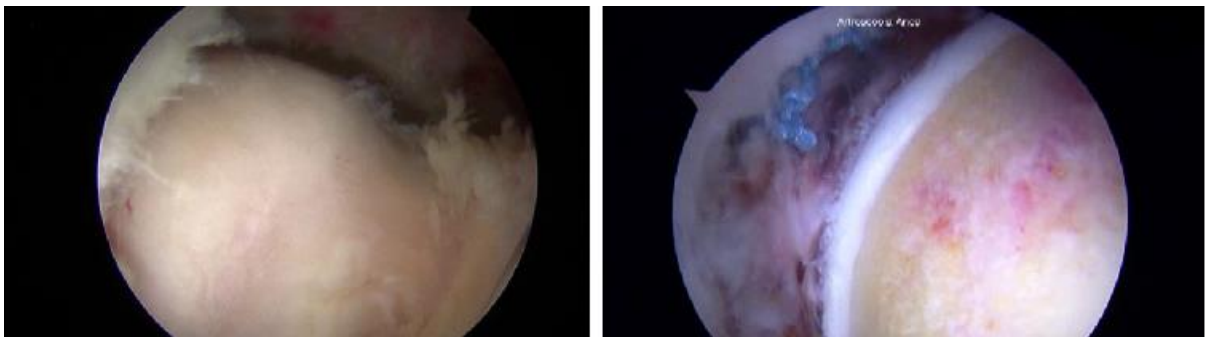

Figure 13: Arthroscopic intervention of a pathologic cam-type hip joint. Left: Representation of the cam lesion on the femoral head before femoral osteoplasty. Right: Representation of the femoral head after femoral osteoplasty (recovery of the sphericity of the femoral head).

femoral head and acetabulum and the reattachment of the labral tissue to its normal joint structure, may be performed through arthroscopic surgery. Regarding the morphologic features of cam lesions, the reshaping of the femoral head leads to a significant decrease in the alpha angle and increases the femoral head/neck offset, which relieves the joint from the impingement mechanism [37]. The arthroscopic intervention before and after femoral osteoplasty, representing the reshaping (restoring the sphericity) of the head of the femur is presented in Figure 13.

As result of the cam-type lesions, the delivery of an early diagnosis and correct clinical intervention procedures are key aspects in order to relief pain and recover the normal functioning of the hip joints that present FAI of the cam-type. Also, the understanding of the FAI mechanism influences the development of innovative surgical interventions, which not only may decrease the progression of cam-type FAI but also, prevent severe articular cartilage damage and delay hip joint OA.

3. Literature review

Several studies were performed in order to better interpret the damage mechanism of the hip joint in individuals presenting cam-type femoroacetabular impingement. This pathologic condition of the hip has been of major clinical interest, since some findings suggest that FAI of the cam-type is the underlying cause for human hip osteoarthritis (OA). Excessive contact pressures and stresses experienced in hip joints with abnormal anatomical relation of the femoral head-neck junction have been identified as an instigative mechanism of cartilage degeneration due to labral tear and osteochondral lesions.

Experimental and computational studies based on the measurement of contact pressures and stresses in normal hip joints were performed to evaluate the spreading of the experienced forces across the hip joint during normal daily activities. Experimental methods performed in several studies, such as studies conducted by Hodge et al. [41], Macirowski et al. [42], Eisenhart et al. [43] and also Anderson et al. [44] are based on the measurement of the stresses and contact pressures in the normal hip joint *in vivo* and *in vitro*, using pressure sensitive films. The values of the contact pressures measured in non-pathologic hips are cross-compared with the magnitudes of the contact pressures obtained in pathologic hips. In the last decade, computational studies based on virtual and on real subject-specific anatomy of hips with FAI of the cam-type were employed. Computational studies such as the ones by Macirowski et al. [42], Genda et al. [45], Yoshida et al. [46] Chegini et al. [5], Jorge et al. [8], Lourenço et al. [9] are today the prevalent and most used technique for measurements of intra-articular contact pressures. Computational methods, being vastly used to calculate stresses and contact pressures, provide a quantifiable relationship between hip morphological alterations of the osseous structure and the stresses experienced by the surrounding soft tissues [44]. The computational analyses of intra-articular stresses and contact pressures are performed using the Finite Element Method (FEM). Finite element (FE) analyses have been vastly employed as a tool for the prediction of the behavior of pathological hips.

Studies based on experimental measurements reported values for contact pressures in non-pathologic hips. Hodge et al [41] measured *in vivo* using a force plate, the contact pressures in the acetabulum during normal walking activity, simulating natural loading conditions. For single-leg stance during walking, the peak measured pressure was 6.72 MPa, with a load representing 103% of body weight and for the sitting to standing movement, the peak registered pressure was 7.14 MPa, with a load representing 45% of body weight. The magnitudes of the peak pressures for the single-leg stance and for sitting to standing movement were registered at different regions of the acetabulum. Afoke et al [47] measured the pressure distribution within the intra-articular structures using pressure sensitive films during stance phase of normal walking activity. The loadings applied simulated the heel-strike at 3.1 to 3.5 times of the body weight and the moment before toe-off at 3.6 to 4.1 times of the body weight. For a 27º flexion movement, the pressures were in a range of 4.9 to 10.2 MPa for applied loads varying from 1980 to 2555 N (3.1 to 3.5 times of the body weight). For a 18º extension movement, the pressures measured were in a range of 6.0 to 10.4 MPa for applied loads varying from 2160 to 2993 N (3.6 to 4.1 times of the body weight). Additionally, the cartilage surface where the highest pressures were measured

was located in the anterosuperior region with values superior to 10 MPa. Michaeli et al [48] used Fuji sensitive pressure films to measure contact pressures in normal hip joints. The values for the peak contact pressures were in a range of 4.5 to 8.5 MPa for compression loads varying from 800 to 1200 N. A study conducted by von Eisenhart et al [43] revealed quantitative information of the contact pressures in normal hips of individuals with ages from 18 to 75 years old, in which the thickness of the femoral and acetabular cartilages was considered. Load distributions were also assessed. The measurements were performed during a simulated loading of walking cycle for heel-strike with applied loading of 94% of the body weight, midstance with applied load of 345% of the total body weight, heel-off with loading of 223% of total body weight and toe-off with loading of 80% of the body weight. The reported values for the contact pressure in the acetabulum were 6.4 ± 1.75 MPa at heel-strike, 7.7 ± 1.95 MPa at midstance, 6.4 ± 1.33 MPa at the heel-off stance and 5.4 ± 1.7 MPa at toe-off stance. In addition, the load-bearing areas of the acetabulum for heel-strike and toe-off stance were identified at the acetabular margin, whereas for midstance and heel-off stance were reported at the central area of the lunate surface of the acetabulum. On the other hand, for the four phases of the walking cycle, the peak pressures were recorded at the ventro-superior region of the lunate surface of the acetabulum, which was coincident with the region of maximum acetabular cartilage thickness. Also, the registered values for the cartilage thickness suggest an inhomogeneous distribution of the cartilage thickness in the acetabulum and in the femoral head. Yoshida et al [46] developed three dimensional (3D) generic hip models, based on discrete element analysis (DEA), to measure the contact pressure distribution in the normal hip during routine daily activities. The loadings applied simulated normal walking, standing up and sitting down activities. The contact pressures obtained for normal walking revealed a peak pressure of 3.26 MPa on the lateral margin of the acetabulum, for standing up motion the registered value was of 8.97 MPa located at the posterior edge of the acetabulum and for the sitting down activity the contact pressure was the maximum in the overall measurements with a value of 9.36 MPa located in the same region as for the standing up motion. Anderson et al [44] performed experimental measurements to predict the contact pressures on normal hips for simulated loadings of stairs climbing, descending and normal walking. Additionally, computational analysis based on FEM were developed and validated. Using pressure sensitive films, the experimental measurements reported pressures in a range of 1.7 to 10 MPa, with an average pressure of 4.5 – 5.0 MPa. Computationally, the finite element models reported peak pressures of 10.78 MPa for walking, 12.73 MPa for descending stairs and 11.61 MPa for stair-climbing. In addition, the load-bearing regions of the FE models were located on the lateral margin of the acetabulum.

More recently, computational analyses of pathologic hips were developed. Chegini et al [5] developed 3D finite element models of virtual idealized hips with distinct pathologic conditions in order to study the relationship between abnormal hip morphologies and the experienced stresses on the hip joint cartilage during normal daily activities. Dysplastic hips and pincer hips were considered with CE angle varying from 0º (dysplastic hip) and 40º (pincer hip) and hips with femoroacetabular impingement of the cam-type were considered with alpha angles varying from 40º (normal hip) to 80º (cam-type hip joint). The loadings applied were mimicking the walking and standing to sitting daily movements. The maximum value for the contact pressure at the acetabular cartilage and labrum during standing to sitting movement

(loading with 156% of total body weight) was 12.84 MPa and it was observed in the cam-type hip joint with alpha angle of 80º and CE angle of 30º (considered normal), whereas for an alpha angle lower than 50º and CE angle between 20º and 30º the minimum contact pressures were identified with a value of 3.34 MPa. The peak pressure registered for the standing to sitting condition in the cam-type joint suggests major cartilage damage due to increased experienced pressures and is coincident with the maximal flexion and rotation movements. For the walking condition, the alpha angle did not influence the peak contact pressures with notable differences on the magnitudes of the contact pressures regarding the variation of the CE angles. The maximum contact pressure was registered for a dysplastic hip joint with a value of 9.92 MPa with CE angle of 0º, whereas the minimum value of 1.81 MPa corresponded to a pincer joint with CE of 40º. The authors concluded that the stresses and contact pressures within the joint where highly depend on the bony anatomy of the femoral head and acetabulum. Additionally, they observed that for alpha angles below 50º and for CE angles between 20º and 30º the stresses and contact pressures were minimized.

Computational analysis of the contact pressures distributions of real impinging hips were also developed. Jorge et at [8] developed a three dimensional finite element model of a real hip with femoroacetabular impingement of the cam-type based on patient-specific anatomy in order to evaluate stresses and contact pressures in the intra-articular soft structures while simulating physiological loadings. A model of a normal hip was also developed in order to cross compare the obtained magnitudes for the contact pressures and stresses. The reconstruction methodology was based on manual segmentation of the anatomical structures of interest based on arthrographic magnetic resonance images. Based on a set of 16 radial MRA images, the 3D finite element model of a hip presenting a cam-type deformity with an alpha angle of 98º (highly pathologic) and a CE angle of 30º (considered normal) was developed. The osseous structures of the hip, the femoral head and the acetabulum, were considered rigid. The soft tissues such as the femoral cartilage, the acetabular cartilage and the labrum were considered linear elastic and isotropic. Based on Shepherd et al [49], the mechanical properties used for the cartilages were a Young Modulus E = 12 MPa and a Poisson's ratio v =0.4. According to [5], the values E = 20 MPa and v =0.4, were assigned to the labrum. The applied loads simulated normal daily walking activity subjecting the hip joint to a compressive force with a horizontal component of 480 N and a vertical component of 2000 N. Also, the hip joint was subjected to flexural (90º) and internal (24º) rotations, simulating physiological routine motions. For the rotational movements several nodes were selected on the femoral cartilage in order to study the contact pressures variations according to the angular movement of the femoral head. The maximum contact pressures for the pure flexural movement of 90º were in the range of 12 to 13 MPa on the cartilages and 16 MPa on the labrum. Regarding the pure internal rotational movement of 24º, the maximum contact pressure observed was in the order of 13 to 14 MPa and of 15 MPa in the labrum. Regarding the contact pressures observed in the selected nodes during flexural and internal rotational movements, the magnitudes of the contact pressures tend to increase with node distance to the center of the femoral head. The high pressures experienced in the labrum justify the severe labral aggression observed in patients with femoroacetabular impingement of the cam-type. Recently, Lourenco et al [9] developed 3D finite element models of real individual-specific hips presenting femoroacetabular impingement of the cam-

type, before and after surgical intervention. The individual at the time was 21 years old, with a weight of 750 N and height of 1.82 m. The patient presented a cam-type deformity with an alpha angle of 90º (normal value up to 40-50º) before surgery and a CE angle of 30º (considered normal). After surgical intervention, the alpha angle decreased substantially to 41º, and the femoral head recovered its spherical shape. The stresses and contact pressures were obtained in the articular cartilages and labrum of the cam-type hip before and after surgery. The same reconstruction methodology already validated in Jorge et al [8] was performed; the mechanical properties of the soft tissues were assigned with identical values and the bones were also considered rigid. The hip joints before and after surgery were submitted to identical compressive forces and to the same rotational movements (flexural rotation of 90º and pure internal rotation of 40º), simulating physiological normal daily motions. The compression force was applied in the frontal plane with a horizontal component of 450 N and a vertical component of 1875 N. Bergmann et al. [50] observed the mentioned magnitudes for the compression force during the walking activity for an individual of 750 N. For the pure internal rotation movement of 40º, it was noticed an increase of the contact pressures reaching maximum values at the anterosuperior region of the hip joint; the same was observed for the flexural rotation of 90º. Regarding the magnitudes of the contact pressures for the internal rotation of 40º, the peak pressures on the femoral cartilage, acetabular cartilage and labrum were respectively, 12.45 MPa, 15.99 MPa and 15.82 MPa. The von Mises stresses presented an extremely high value for the labrum, reaching the value of 26.45 MPa. For flexural rotation of 90º, the peak pressures observed in the femoral cartilage, acetabular cartilage and labrum were respectively 7.11 MPa, 10.23 MPa and 7.08 MPa. Regarding the von Mises stresses, the maximum value was observed on the labrum with a value of 23.48 MPa. After surgical intervention, for the internal rotation of 40º, the peak pressures on the femoral cartilage, acetabular cartilage and labrum were respectively, 9.48 MPa, 9.62 MPa and 11.97 MPa. For flexural rotation of 90º, the peak pressures observed in the femoral cartilage, acetabular cartilage and labrum were respectively 6.82 MPa, 7.80 MPa and 9.98 MPa. Regarding the von Mises stresses, the maximum value was observed on the labrum with a value of 15.28 MPa. The values for the contact pressures and von Mises stresses obtained in the pathologic hip before surgical intervention were much higher than the ones obtained in the same hip after surgery, which suggest that the surgical intervention may prevent severe soft tissues damage and joint degeneration. Also, the extremely high stresses experienced by the labrum as consequence of the cam-type impingement support the lesions observed in the labrum, such as labral tear and tissue damage due to high impact. It was also concluded that the physiological rotational motions were the major factor for the extremely increased contact pressures and stresses for the pathologic hip, being the pure internal rotation of 40º the most aggressive motion.

More recently, a study conducted by Liu et al [51] predicted the contact pressures in a normal hip and in hips presenting femoroacetabular impingement of the cam-type with distinct alpha angles. As in the previous works, 3D finite element models were developed. The reconstruction methodology of the cam-type hips were based on the reconstructed model of the normal hip. A normal hip (alpha angle of 47º) from a healthy female individual was semi-automatically and manually segmented from CT imaging data. The cam-type models with varying alpha angles were obtained based on the normal hip reconstructed model, by modifying the femoral head/neck junction by creating bony bumps at the

anterosuperior region. Models with alpha angles varying from 60º to 90º were obtained. In contrast to the work developed by Lourenco et al [9] in which the soft tissues (articular femoral and acetabular cartilages and labrum) were meshed using tetrahedral linear elements, Liu et al meshed the cartilages using hexahedral elements, and the labrum was not included in the analyses. Also, the cortical bone of the femur was considered as a linear elastic material, to which tetrahedral mesh elements were assigned. The mechanical properties of the soft tissues were the same as in Lourenco et al [9] and Jorge et al [8]. The cortical bone was assumed as a homogeneous and isotropic material with a Young modulus E = 17 MPa and Poisson's ratio v=0.29, according to Dalstra et al [52]. The loadings and motions applied in the hip joints simulated the physiological motions of normal daily activities. Prior to the application of the loadings, the anatomical position of the femur was established and thus, oriented relatively to the pelvis. The obtained values for the peak contact pressures during normal walking activity in the acetabular cartilage revealed a reduced magnitude difference regarding the normal and cam-type hips. For higher hip motions, such as for standing to sitting movements, the peak pressures varied significantly within the distinct cam-type hips with varying alpha angles. The maximum contact pressures were observed for the most severe case of the pathological hip. For the sitting down motion, when the hip is in 59º flexion, the peak pressure observed in the normal hip had a magnitude of 4.097 MPa, whereas for the impinging cam-type hips the peak pressures were 5.353 MPa for the cam hip with alpha angle of 60º, 6.312 MPa for the cam hip with alpha angle of 70º, 8.167 MPa for the cam hip with alpha angle of 80º and the highest peak pressure was observed for the cam hip with 90º with a magnitude of 10.520 MPa. For the standing up motion, the measured peak pressures presented identical pattern when comparing to sitting down motion. The peak pressure for the normal hip was 4.571 MPa, whereas for the cam hips with alpha angles of 60º, 70º, 80º and 90º was respectively 6.295 MPa, 7.291 MPa, 10.620 MPa and 12.460 MPa. Additionally, it was observed a higher pressure distribution in the anterosuperior region of the acetabulum in cam hips, which is coincident with the location of the cam-type deformity. The authors concluded that there is a notable relation between the severity of the cam-type impingement, characterized by the alpha angle, and the abnormal experienced contact pressures within the intra-articular structures of the hip. Also, the obtained values for the cam-type hips enabled the identification of several hip motions which influence and are the determinant features for the abnormal contact mechanics in these hips. Regarding the severity of the cam-type hips, characterized by the alpha angle, cam hips that present alpha angles of 80º or higher lead to extremely large contact pressures within the intra-articular structures and are influenced by certain hip motions. It was first hypothesized but lately validated that 1) cam hips with varying alpha angles reveal abnormal contact pressures when compared to normal hips and 2) the various types of hip motions control the effects of cam-type abnormality on the modification of the contact mechanics in the cam hips.

4. Reconstruction Methodology

In the present work, models of the hip of two patients presenting cam impingement with distinct alpha angles of 60º and 81º were analyzed, in order to obtain the contact pressures and the stresses in the articular cartilages and labrum of the pathologic joints. Several methodological procedures and different computational softwares were employed in order to obtain the final three-dimensional (3D) models based on the real patient-specific anatomy of the hip joints with cam impingement and the respective numerical results of the mechanical simulations. For the purpose, two sets of arhtro-MRI sequence images with 16 radial images of the pathologic hip joints, were provided by an orthopaedical surgeon. The 3D reconstruction of the hip joints models and the FE analysis were performed using the following methodology already validated in [8] [9] [53]: manual image segmentation, surfaces and posterior solid creation, and finite element mesh generation and analysis.

A detailed description of the methodology is presented for one of the cam-type hip joints. The set of medical images for each case was provided in the DICOM (Digital Imaging and Communications in Medicine) format, which was primarily converted to a readable format and organized in order to obtain a correct sequence of images. The conversion of the images and also the assessment of the image properties (FOV, dimensions of the image) and collection of useful medical information (age and weight of the patient) was performed using the Philips DICOM viewer software.

4.1. Case 1 – Patient with cam-type: alpha angle 60º

The first case analysed corresponds to a male patient presenting a cam-type femoroacetabular impingement with an alpha angle of 60º. The set of medical images consists of 16 images obtained through magnetic resonance arthrography imaging (arthro-MRI) with gadolinium injection, in which the contrast is enhanced, enabling the identification of the structures of interest. At the date of acquisition (24/01/16) the patient was 28 years old, with a weight of 80kg. Regarding the image properties, the images present a field of view (FOV) of 165mm, pixel spacing of 0.52 and dimension of $384x384\ pixels^2$. The image acquisition was performed radially, with radial angle increment of 11.25º, varying from 0º to 180º and the rotational axis was coincident with the axis that defines the femoral neck and extends to the femoral head. The set of 16 images of the pathologic hip joint obtained through arthro-MRI is represented in Figure 14.

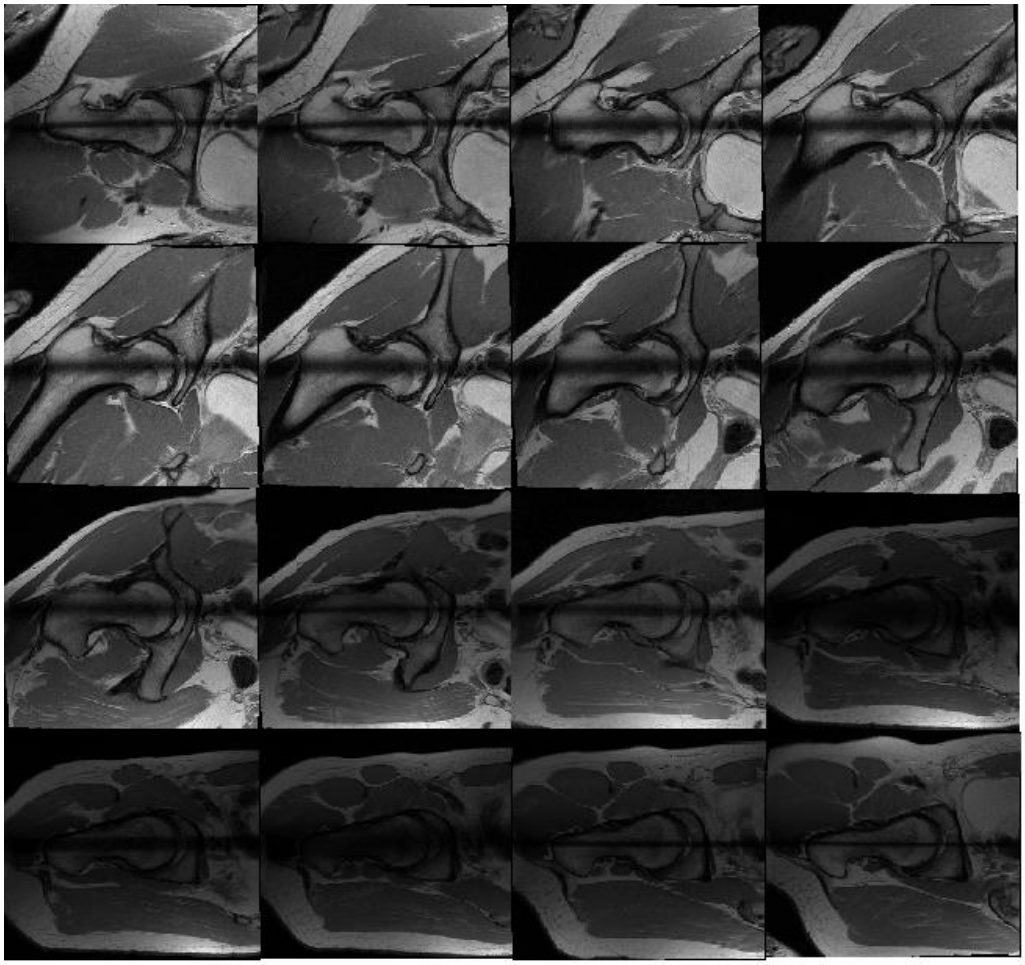

Figure 14: Case 1 - Set of 16 images obtained through arhtro-MRI from a patient presenting FAI of the cam-type with an alpha angle of 60º.

From the sequence of provided images, it is possible to identify specific images in which the cam protuberance is more visible. The aspherical contour of the head of the femur identified in the anterosuperior region of the femoral head is more visible in images 11 and 12 from the set of 16 images and is indicated by the grey circles in Figure 15.

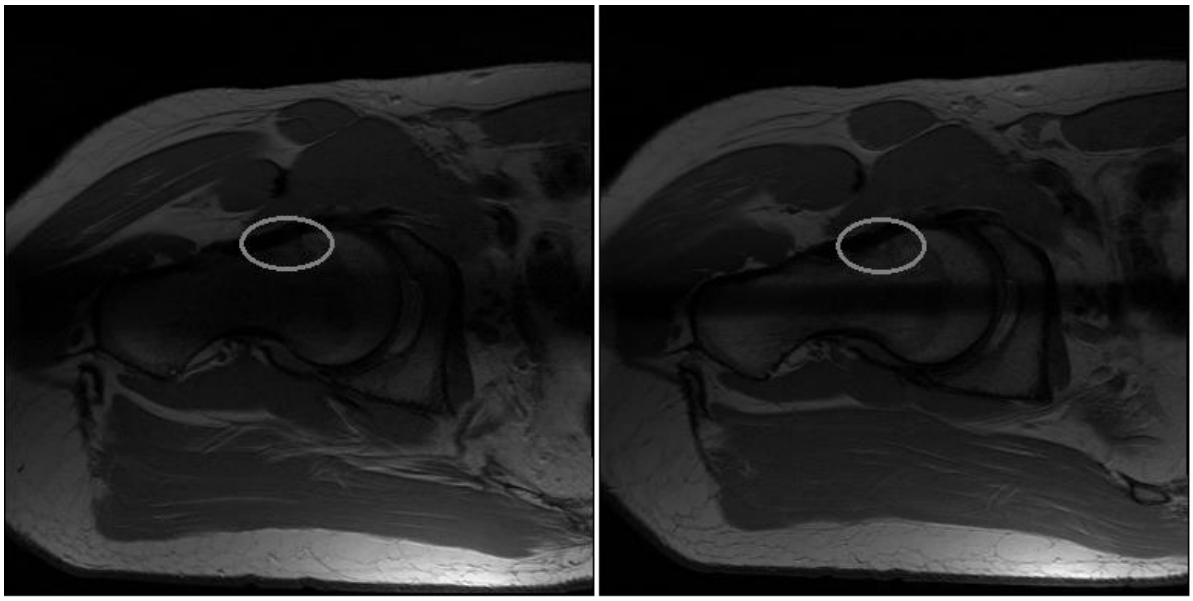

Figure 15: Case 1 - Sequence of two arhtro-MRI images from the set of 16 images (left: image 11; right: image 12) in which the cam deformity is more visible and is identified by the grey circles.

4.1.1. Manual Segmentation and 3D Reconstruction

The manual segmentation steps and the 3D reconstruction of the hip joint models were performed using the same, already validated procedures, as in [8][9][53]. For the segmentation purposes, Rhinocerus software was used in order to obtain the contours of the anatomical structures of interest and the posterior extraction of geometrical data relative to the structures that define the pathologic hip joint. The manual segmentation was performed in a base set of 16 squares, one square assigned to each of the 16 images from the arthro-MRI sequence in which the manual contours of the boundaries of the anatomical structures were made. The contours for each image were defined using spline curves and each one of the structures of interest was assigned with a different color. The manual segmentation of one of the images in one of the squares is represented in Figure 16, in which different structures can be observed. The main components are: the femur (green), the acetabulum and pelvic bone (red), the femoral cartilage (blue, green and red), the acetabular cartilage (red, cyan, blue and magenta) and the labrum (magenta, red and blue).

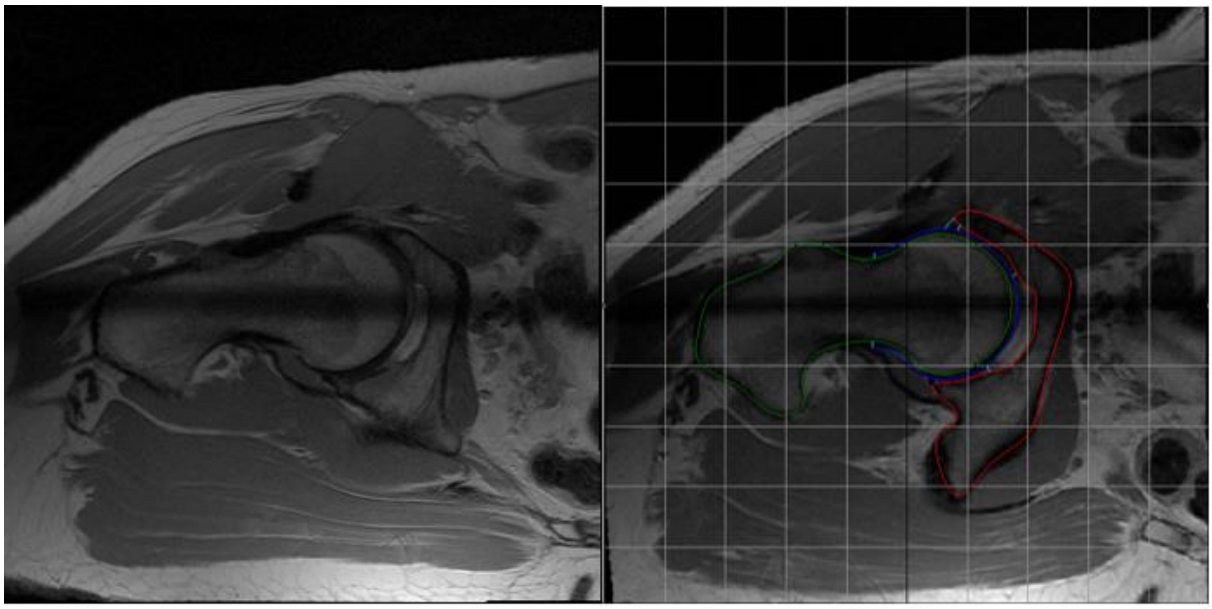

Figure 16: Case 1 - Left: image before segmentation. Right: manual segmentation of one of the images in the square limits (image 10 of the presented set of 16 images) and the depiction of the contours of the main structures of the hip joint: femur, acetabulum and pelvic bone, femoral and acetabular cartilage and labrum.

In order to obtain the 3D reconstruction of the structures of interest, subcurves from the existing curves delimiting the anatomical components were created. The anatomical structures of interest are the femoral cartilage, the acetabular cartilage and the labrum. The bony structures of the hip joint, the femur and the acetabulum, were considered rigid body structures and thus, only the soft tissues were reconstructed and considered. The reconstructed structures from the subcurves are posteriorly divided in a set of segments, which allows the drawing of circumferential isocurves through the generated points. The isocurves delimit the surfaces of these structures and are constructed through the connection point by point of the curves. The reconstructed soft tissues and the respective isocurves are represented in Figure 17 and Figure 18, respectively.

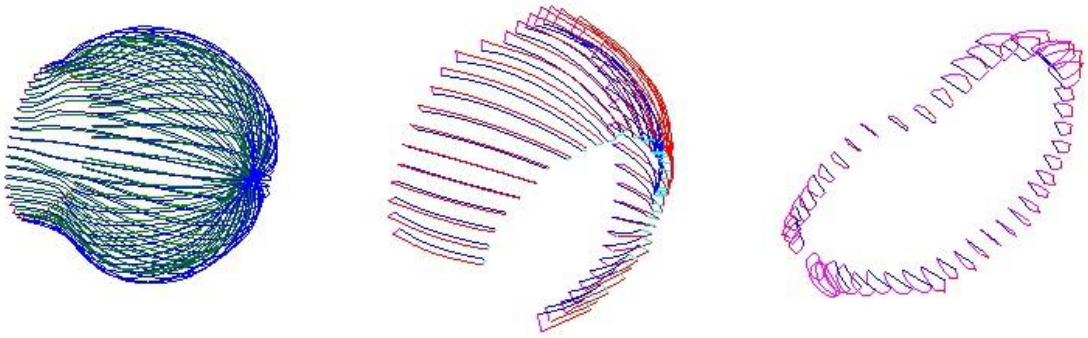

Figure 17: Case 1 - 3D representantion of the curves obtained from manual segmentation depicting the structures of interest. From left to right: femoral cartilage, acetabular cartilage and labrum.

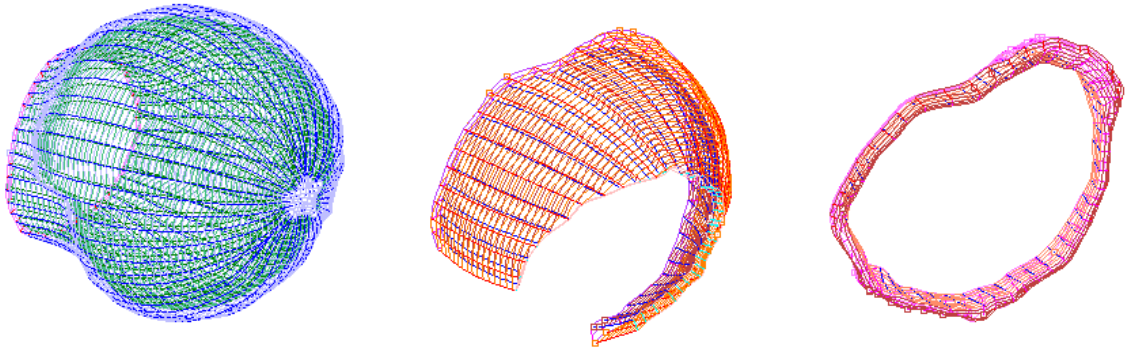

Figure 18: Case 1 - 3D representation of the anatomical structures formed by the circumferential isocurves. From left to right: femoral cartilage, acetabular cartilage and labrum.

The final 3D model of the hip joint with the anatomical structures is assembled in order to obtain the real model of the soft tissues of the hip joint. The assembly of the three structures from the hip joint is represented in Figure 19 and is the final structure obtained using Rhinocerus software.

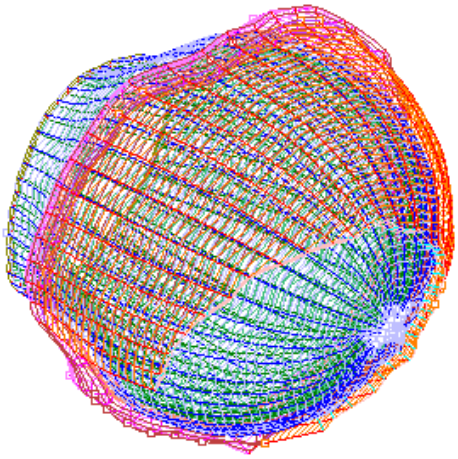

Figure 19: Case 1 - Final 3D model, obtained in Rhinocerus, representing the fully constructed model of the soft tissues of the hip joint.

Regarding the surfaces creation and the development of the solid model for each of the components of the soft structures, geometrical information was extracted from the final assembly represented in Figure 19. In order to define each surface of interest, the geometrical information, which consisted of clouds of points obtained from the isocurves of each component of the hip joint, was exported from Rhinocerus. The surface creation was performed using the same method as in Jorge et al. [8], Lourenço et al. [9] and Lourenço [53], which has also been confirmed in previous works as a successful method for medical information reconstruction [8][54]. The cloud point interpolation was performed using FastRBF (Fast Radial Basis Functions) toolbox especially designed for MATLAB, enabling the reconstruction and representation of the surfaces of interest.

4.1.2. Geometry treatment in Solidworks and mesh generation using Abaqus

The surfaces obtained from fastRBF toolbox were generated as .obj files. In order to create the three-dimensional solid models of each anatomical component, the .obj files were assessed using the Solidworks software, where the treatment procedures and creation of the assembled 3D model were performed. The 3D solid models of each structure, before surface treatment, obtained in SW from the surfaces generated by fastRBF are represented in Figure 20.

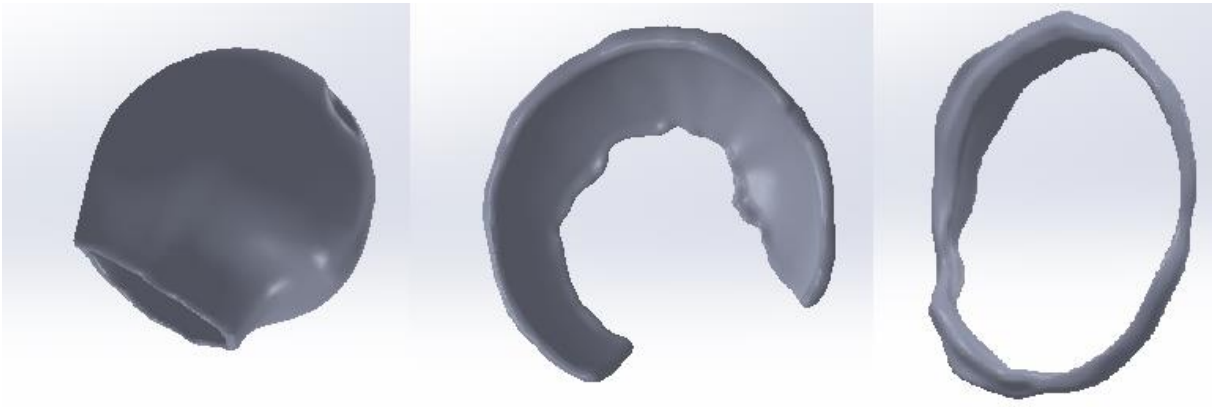

Figure 20: Case 1 - Representation of the 3D models of each anatomical component using SW, obtained from the surfaces generated by the fastRBF toolbox before treatment. (from left to right: femoral cartilage, acetabular cartilage and labrum)

Regarding geometry repair procedures, smoothing and surface localized treatment were performed for each anatomical component, in order to attenuate the edgy and striking structures which are notable on the solid models represented in Figure 20. Posteriorly to this treatment, the origin of the coordinate system is assigned to the centroid of the head of the femur and all the components are scaled with a factor of 16.5 due to the FOV (field of view) of the arthro-MRI images.

The anatomical soft structures of the hip joint are combined in order to obtain a logical coincident surface geometry between the three anatomical components. The combining procedure prevents possible structural warnings, such as interpenetrations between the components, which are critical during the numerical analysis.

The complete FE mesh of the model of the hip joint that was used in the numerical simulations was obtained using Abaqus software and is represented in Figure 21 and has a total of 288641 elements. Different mesh colors were assigned to each anatomical component of the hip joint in order to be straightforwardly distinguishable.

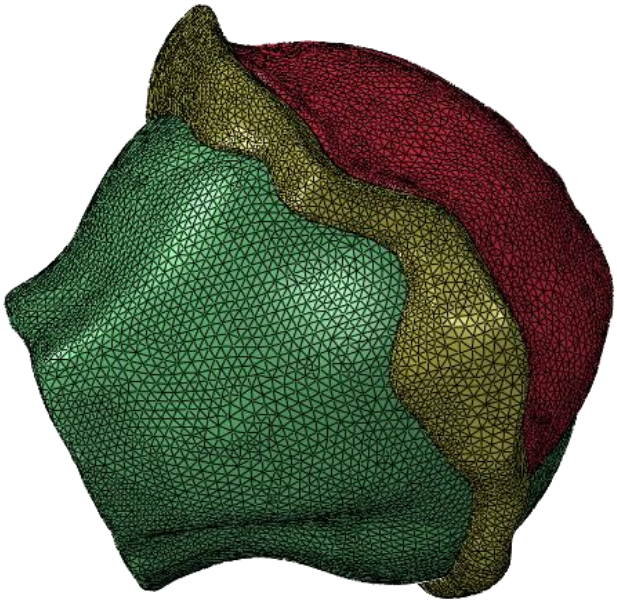

Figure 21: Case 1 - Complete FE mesh of the three structures of the hip joint. Green – femoral cartilage; Red – acetabular cartilage; Yellow – labrum.

In [8] a FE mesh with a total number of 109167 tetrahedral linear elements was used while in [9] and [53] meshes with 188635 and 270108 tetrahedral linear elements were used. Moreover, in [8] a study of the convergence of the mesh provided similar values for the maximum contact pressures when a mesh composed by the same number of tetrahedral quadratic elements was used. In [9], a study of the convergence of the mesh also provided similar values for the maximum contact pressures when a more refined mesh (with 737646 tetrahedral linear elements) was used. Therefore, the meshes used in the present analyses are believed to be able to provide accurate results.

4.2. Case 2 – Patient with cam-type: alpha angle 81º

The analysis of the second case regards a male patient with FAI of the cam-type with an alpha angle of 81º. The set of arthro-MRI images of the hip joint consist of 16 images, which enabled the identification of the anatomical structures of interest. The images present a FOV of 210mm, pixel spacing of 0.55 and dimension of $384x384\ pixels^2$. The image acquisition was performed with a radial angle increment of 11.25º, varying from 0º to 180º and the axis of radial rotation was equally coincident with the axis that defines the femoral neck and extends to the femoral head, as in the first case. The set of 16 images obtained from arthro-MRI is similar to the one illustrated for the first patient.

Identically as for the first case, in the present case it was also possible to identify sequences of images where the cam deformity is more visible. From the set of 16 medical images, the two images with the evident femoral asphericity are represented in Figure 22 and the region of the asphericity is denoted by the grey circles.

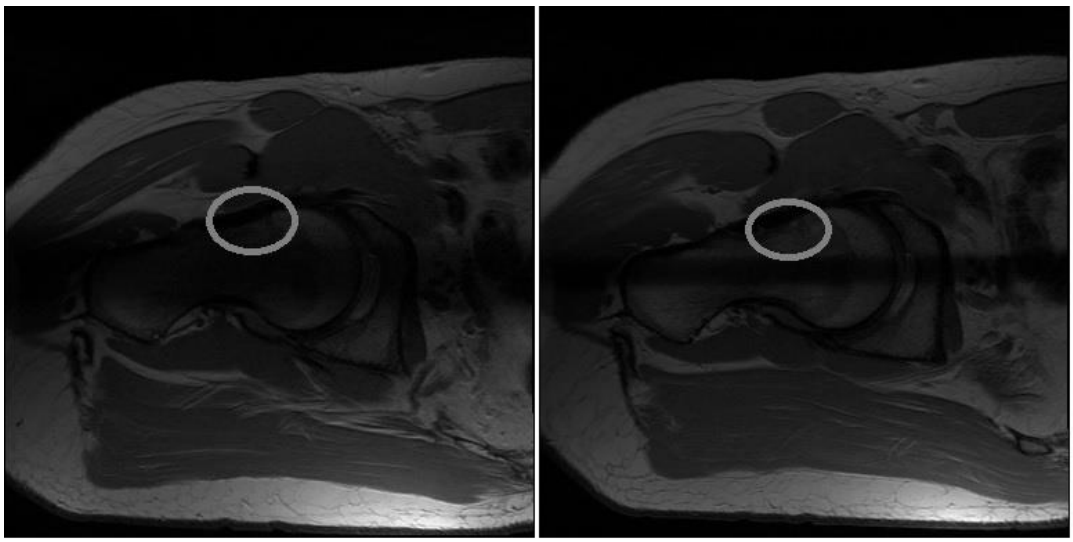

Figure 22: Case 2 - Sequence of two arhtro-MRI images from the set of 16 images (left: image 11; right: image 12, in which the cam deformity is more visible and is identified by the grey circles.

Since the manual segmentation and the 3D reconstruction procedures are the same as the ones used in the previous case, only the final models obtained from Rhinocerus and from Abaqus will be presented. The final structure obtained using Rhinocerus software can be observed in Figure 23 and represents the final assembled 3D model of the hip joint with the anatomical soft structures.

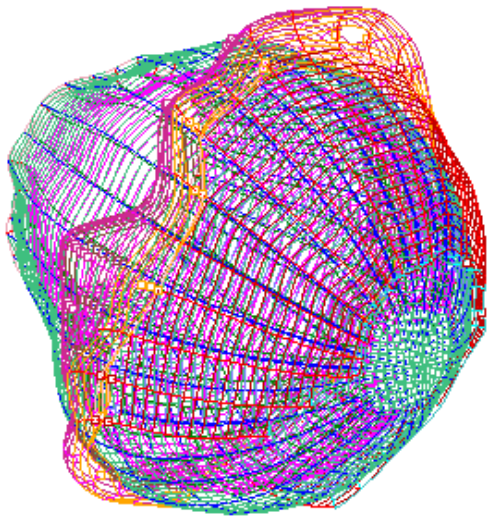

Figure 23: Case 2 - Final 3D model, obtained in Rhinocerus, representing the fully constructed model of the soft tissues of the hip joint.

As in the previous case, the following stage comprised the development of the surfaces of each structure using fastRBF tollbox for MATLAB. The surfaces obtained from fastRBF toolbox were generated as .obj files. In order to create the three-dimensional solid models of each anatomical component, the .obj files were assessed using the Solidworks software, that was next used for treatment and repair of the geometry. Moreover, for the combining processes, the scaling factor of each structure was 21.0 due to the FOV of the images and the origin was assigned to the centroid of the femoral head. The final assembly representation of the combined 3D solid model of the pathologic hip joint obtained after the treatment and the posterior FE mesh generation in Abaqus is represented in Figure 24. The complete FE mesh of the model of the hip joint that was used in the numerical simulations has a total of 363739 elements. In Figure 24, different mesh colors were assigned to each anatomical component of the hip joint in order to be plainly distinguishable.

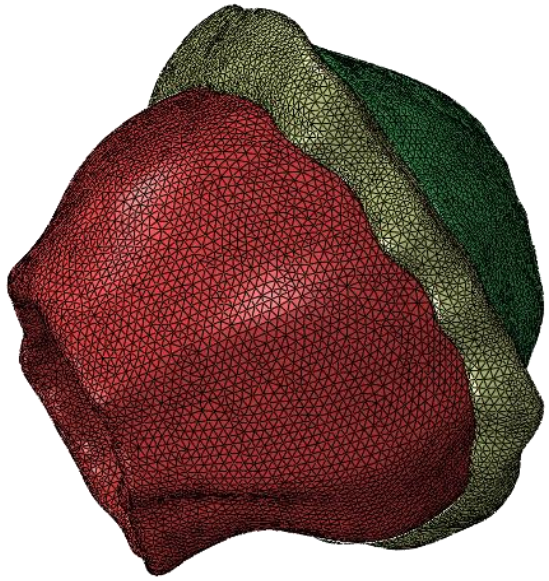

Figure 24: Case 2 - Complete FE mesh of the three structures of the hip joint. Red – femoral cartilage; Green – acetabular cartilage; Yellow – labrum.

5. Finite Element analysis: Results and discussion

Throughout this chapter the features and the numerical results of the FE analyses of the reconstructed models of the pathologic hip joints are presented. For simulation purposes the mechanical properties of the materials, as well as structural constraints of the models and specific loadings were defined.

For the two pathologic cases, and as already mentioned, the bony structures were considered as rigid bodies, therefore only the soft tissues are considered, and thus the material specifications were assigned to the cartilages and to the labrum. The soft tissues were considered as linear elastic and isotropic materials as in [53][8]. Regarding the mechanical properties of the articular cartilage and labrum, for the former a value of E=12MPa was assigned for the modulus of elasticity and a value of 0.4 for the Poisson's ratio, and for the latter a value of E=20MPa was assigned for the modulus of elasticity and a value of 0.4 for the Poisson's ratio [5][8]. These material specifications were considered in all the cases.

The numerical analyses were performed using Abaqus software and all the analyses were geometrically non-linear. Regarding structural constraints of the two models, the displacements of the outer nodes of the surface of the acetabular cartilage and of the outer part of the acetabular labrum, that are in contact with the acetabulum bone, were restricted. The regions of the acetabular cartilage and the labrum that are in contact were tied forming a singular contact surface. The contact between the merged surface of the acetabular cartilage and labrum with the surface of the femoral cartilage was considered frictionless. The nodes of the inner surface of the femoral cartilage were rigidly constrained to the node in the centroid of the femoral head. Moreover, an anatomical orientation was assigned to each hip joint model in order to simulate a physiological normal orientation of the femur in the human body (the anatomical orientation for each model of the hip joint was previously obtained from a detailed MATLAB script using geometrical data from the manual segmentation from Rhinocerus).

For the simulation purposes, the pathologic hip joints were submitted to a physiological normal compression force applied at the centroid of the femoral head. Being the hip joints subjected to this compression force, several physiological hip motions were mimicked by applying distinct rotational loadings, such as pure internal rotation or flexural rotation. For the analysis of the normal walking activity the magnitude of the compression force applied at each pathologic hip joint presented distinct values due to the variance of the body weight (BW) of each patient [50]. However, for simulation purposes, all the analyses were performed considering that all the patients have a BW of 750N and thus, the compression force simulating the normal daily walking activity has a y-component of 1875N and x-component of 450N (see figure 25). Regarding the rotational motions applied to the pathologic hip joints, and being the hip joints subjected to the compression force mentioned above, i) the pure internal rotation

was performed with an angle of 45º (along y-axis) and ii) the flexural rotation (along x-axis) was performed with an angle of 90º. The values for the rotational angles describe motions that are within a physiological range.

Regarding the rotational motions, and in order to evaluate the contact pressures in different regions of the femoral cartilage, some nodes were selected along the femoral cartilage. For the pure internal rotation, some nodes were selected defining a straight line, perpendicular to the rotation axis (y-axis), and for the flexural rotation, some nodes were selected also defining a straight line perpendicular to the rotation axis (x-axis). The nodes were selected in the region of the cam protuberance for the two pathologic hip joints. The nodes selected on the femoral cartilage for each rotational motion are presented in the following respective sections.

The maximum magnitudes of the contact pressures and of the von Mises stresses for each patient and for each loading path (compression and pure internal rotation or compression and pure flexural rotation) were registered on the femoral cartilage, on the acetabular cartilage and on the labrum. The contact pressures were also registered at each one of the selected points as function of the angle of rotation of the femoral head. The same analyses were also performed in the two hip joints in the case where there is absence of the labral tissue.

5.1. Pathological case 1 with alpha angle equal to 60º

5.1.1. FE analysis: compression force and pure flexural rotation

With the hip joint being subjected to a physiological compression force followed by a pure flexural rotation of 90º, the contact pressures distributions, at the end of the compression step and at the end of the flexural rotation step, are presented for the femoral cartilage, for the acetabular cartilage, and for the labrum. The maximum values observed for the contact pressures and for the von Mises stresses are also presented for all the three components. In Figure 25, the initial and the deformed mesh of all the three soft components of the hip joint is represented at the end of the loading path (compression followed by a pure flexural rotation). The initial mesh is presented regarding its anatomical normal orientation and the deformed form is presented at the end of the pure flexural rotation of 90º.

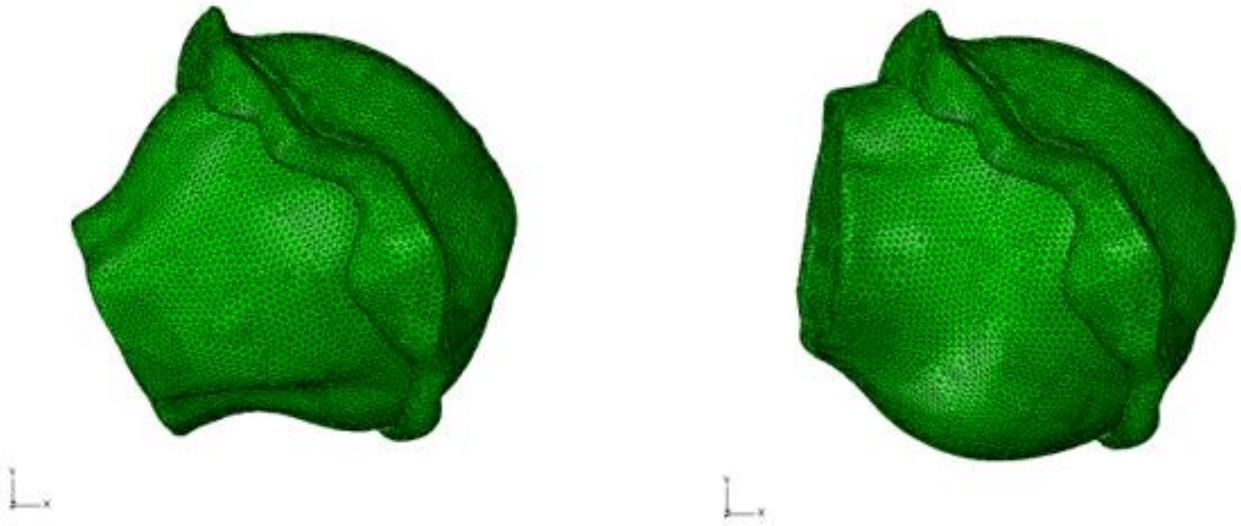

Figure 25: Case 1 - Representation of the initial and deformed meshes of the three components of the hip joint. Left – initial form representing the anatomical physiological orientation. Right – deformed form of the mesh at the end of the pure flexural rotation of 90º.

The maximum magnitude for the contact pressure and the contact pressures distribution on the femoral cartilage after the compressive step and after the pure flexural rotation are presented in Figure 26.

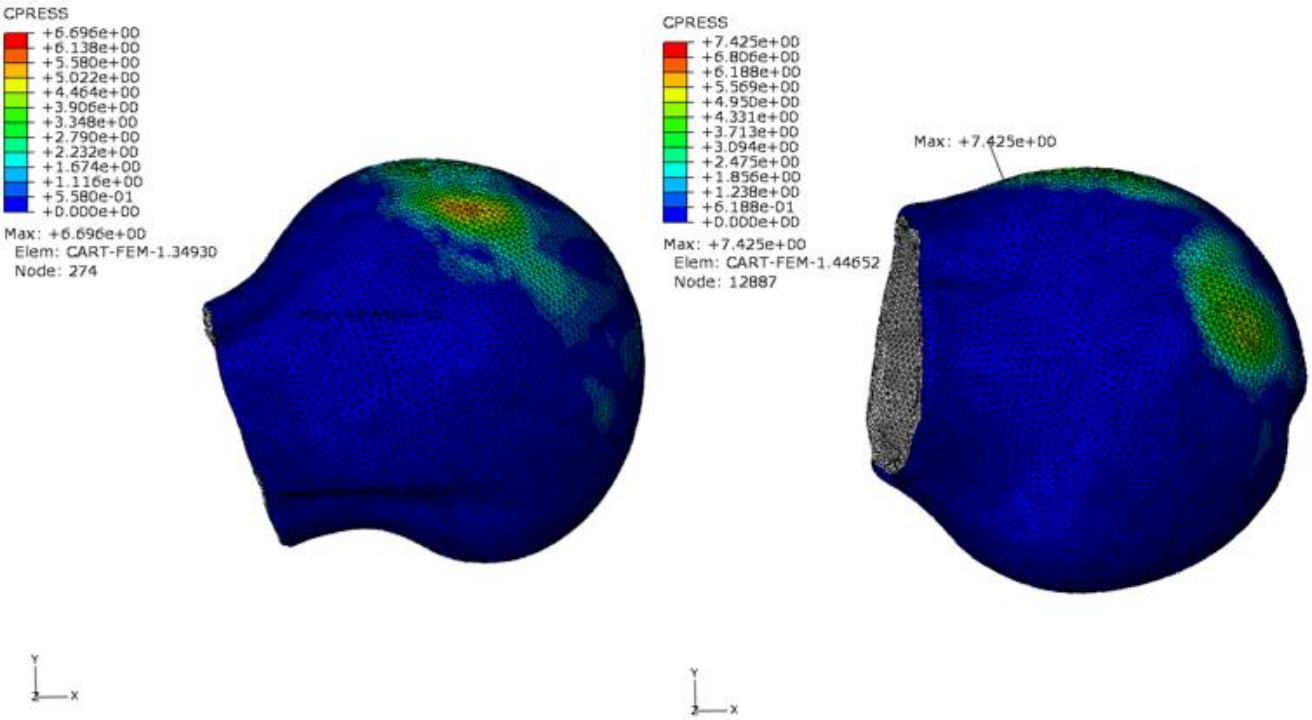

Figure 26: Case 1 - Representation of the contact pressures distribution and of the final maximum magnitude of the contact pressure on the femoral cartilage. Left – after the compressive step the maximum value was 6.696 MPa located on the anterosuperior region. Right – after the pure flexural rotation step the maximum value was 7.425 MPa located on the region of the cam deformity.

In the acetabular cartilage and labrum, the contact pressures distribution and the final magnitude after the compressive step and after the pure flexural rotation of 90º are presented in Figure 27.

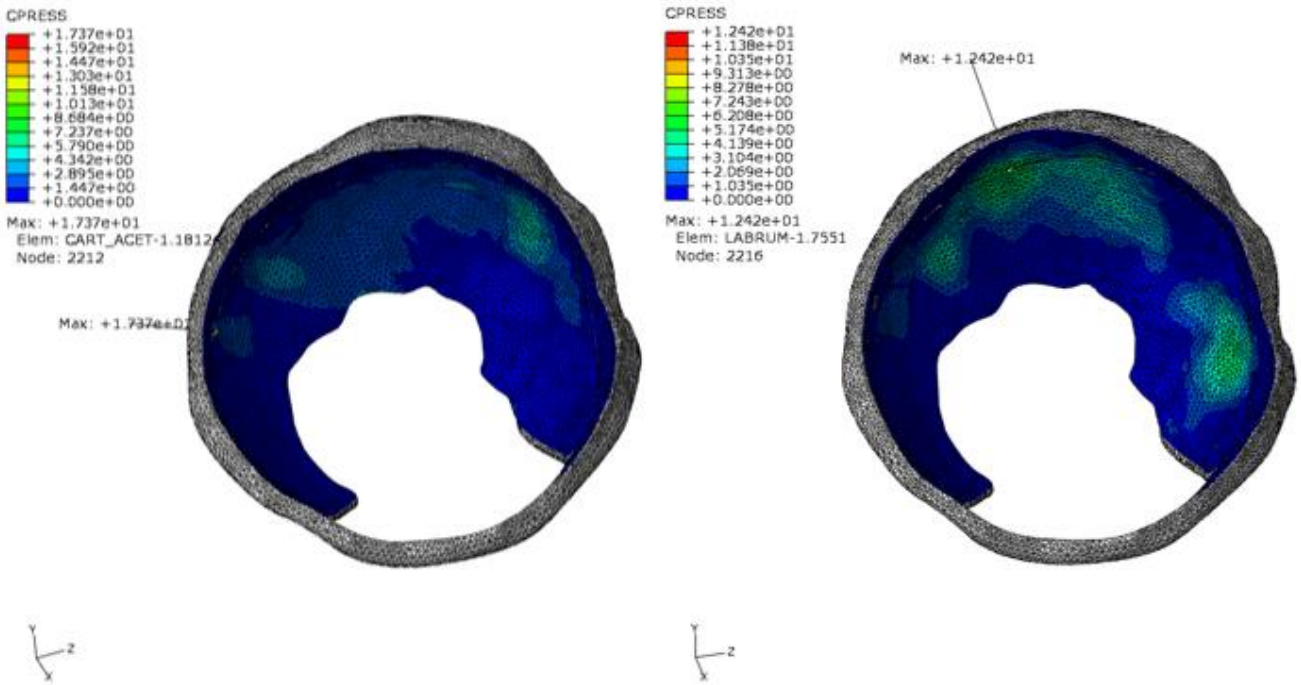

Figure 27: Case 1 - Representation of the contact pressure distribution and final magnitude on the acetabular cartilage and labrum. Left – after the compressive step. Right – after the pure flexural rotation.

The maximum magnitude of the contact pressure on the acetabular cartilage after the compressive step was 17.37 MPa and it is believed to result from an inadequate geometry reconstruction on the posterior region. The maximum magnitude of the contact pressure on the labrum after the compressive step was 2.068 MPa, located on the anterior region. After the pure flexural rotation step, the final maximum magnitude of the contact pressure on the acetabular cartilage was 5.666 MPa on the superior region and 12.42 MPa on the labrum also on the superior region, as it can be observed in figure 26. In addition, the maximum magnitude of the contact pressures was measured locally on the anterosuperior region of the acetabular cartilage where the cam deformity is more evident, with a value of 5.4 MPa after the compressive step and a value of 4.97 MPa after the pure flexural rotation. The value of 5.4 MPa measured locally on the acetabular cartilage, when compared with the maximum obtained value of 17.37 MPa, is believed to be more consistent with reality than the latter value.

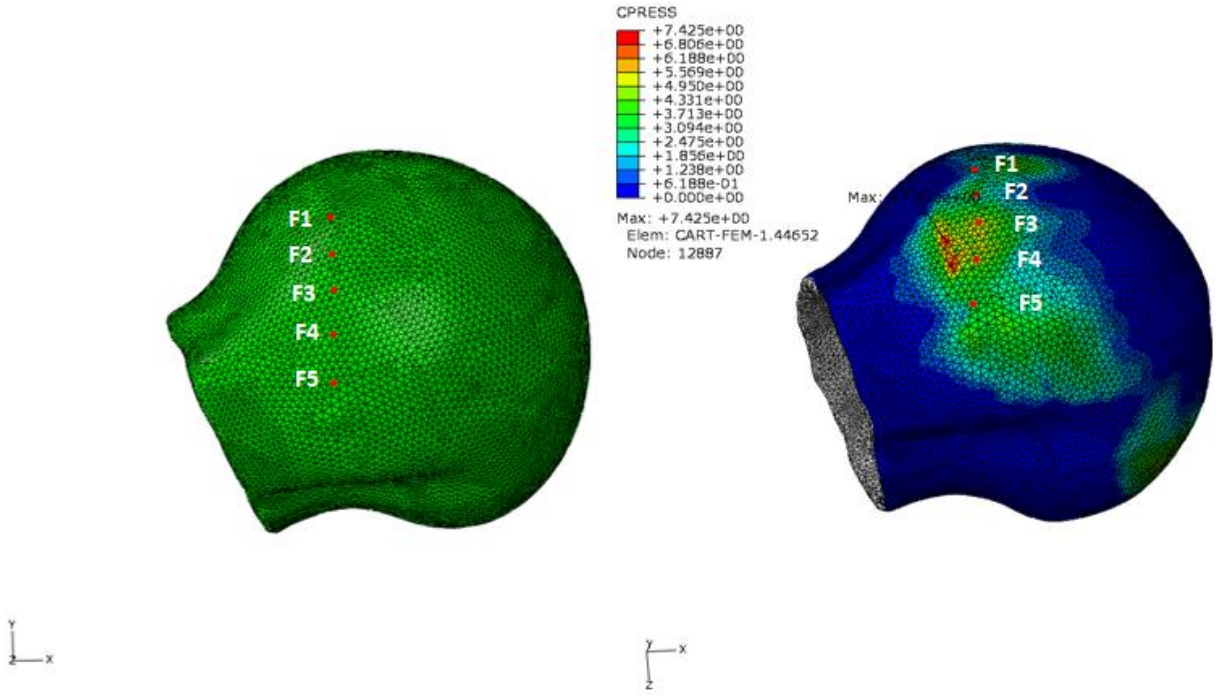

Figure 28: Case 1- Representation of the selected nodes (red points). Left – 5 nodes selected on the initial femoral cartilage defining a vertical line perpendicular to the axis of the flexural rotation. Right – representation of the same nodes after the flexural rotation and the corresponding contact pressures distributions.

Five nodes were selected along a straight vertical line perpendicular to the axis of the flexural rotation in the region of the cam deformity (see Figure 28). The contact pressures on the nodes selected perpendicularly to the flexural rotation axis are presented in Figure 29 as a function of the angle of rotation. The final maximum contact pressure observed on the femoral cartilage (7.425 MPa) does not occur in any of the selected nodes. It occurs near the node F3, which presents a maximum value of 4.954 MPa.

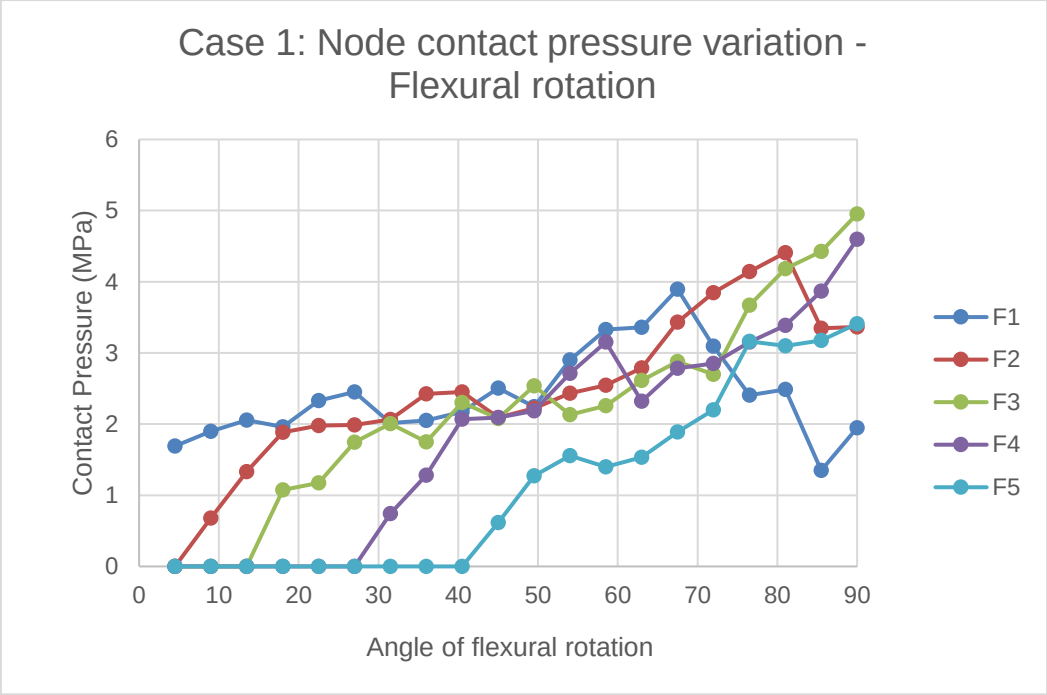

Figure 29: Case 1 - Contact pressures evolution in the selected nodes of the femoral cartilage as a function of the angle of flexural rotation.

The values of the contact pressures and von Mises stresses on the three components, the femoral cartilage (FC), the acetabular cartilage (AC) and the labrum (L), registered at the end of the compressive step, at the end of the pure flexural rotation of 90º and during these steps are presented in the Table 1 for the compressive step and in Table 2 for the pure flexural rotation step. The time step percentage is registered in order to observe the occurrence of the maximum values.

Table 1: Case 1 – Contact pressures and von Mises stresses at the end of the compressive step and during the compressive step on the three hip joint components. The maximum observed during the step and the final maximum magnitude are presented and the location is identified. (S – Superior; A – Anterior; I – Inferior; P – Posterior; AS – Anterosuperior)

		Contact Pressure		**Von Mises**	
		Maximum during step	**Final Maximum**	**Maximum during step**	**Final Maximum**
Compression	FC	**6.696 MPa** (100%) S region	**6.696 MPa** A region	**2.388 MPa** (100%) AS region	**2.388 MPa** AS region
	AC	**17.37 MPa** (100%) A region	**17.37 MPa** S region	**3.637 MPa** (100%) I region	**3.637 MPa** I region
	L	**2.357 MPa** (85% of the step) P region	**2.068 MPa** A region	**2.726 MPa** (100%) AS region	**2.726 MPa** AS region

Table 2: Case 1 – Contact pressures and von Mises stresses at the end of the flexural rotation and during the flexural rotation step on the three hip joint components. The maximum observed during the step and the final maximum magnitude are presented and the location is identified. (S – Superior; A – Anterior; I – Inferior; P – Posterior; AS – Anterosuperior)

		Contact Pressure		Von Mises	
		Maximum during step	Final Maximum	Maximum during step	Final Maximum
Flexural rotation 90º	FC	8.653 MPa (70% of the step) I region	7.425 MPa S region	3.546 MPa (65% of the step) AS region	2.337 MPa AS region
	AC	13.79 MPa (35% of the step) P region	5.666 MPa S region	14.84 MPa (40% of the step) P region	5.405 MPa S region
	L	12.42 MPa (100%) I region	12.42 MPa S region	17.67 MPa (40% of the step) P region	10.01 MPa S region

5.1.2. FE analysis: compression force and pure internal rotation

A FE analysis is performed in order to study the effect of a pure internal rotation of 45º on the same hip joint. As in the previous analysis, the joint is subjected to a physiological compression force and the second step consists in subjecting the joint to a pure internal rotation of 45º. The contact pressures distribution and the von Mises stresses, at the end of the compressive step are not presented in this section since the magnitudes are the same as in section 5.1.1. Thus, the contact pressure distributions and the corresponding final maximum magnitudes are presented just at the end of the internal rotation step, for the femoral cartilage, the acetabular cartilage, and the labrum. The initial and the deformed meshes of the three soft components of the hip joint are presented in Figure 30. The initial mesh is presented regarding its anatomical normal orientation and the deformed form is presented at the end of the pure internal rotation of 45º.

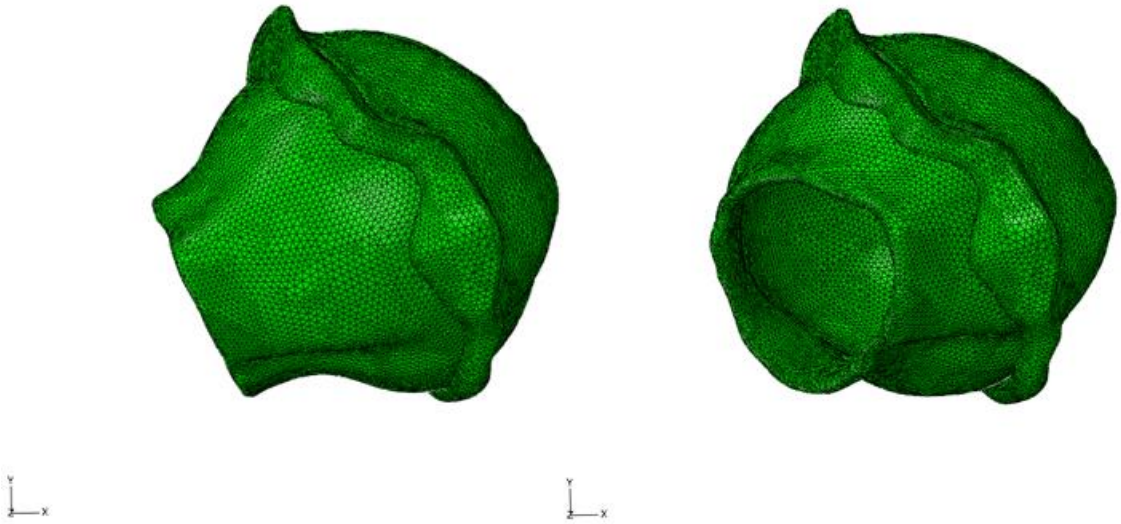

Figure 30: Case 1 - Representation of the initial and of the deformed meshes of the three components of the hip joint. Left – initial form representing the anatomical physiological orientation. Right – deformed form of the mesh at the end of the pure internal rotation of 45º.

The maximum contact pressures and the contact pressures distribution on the femoral cartilage after the pure internal rotation are presented in Figure 31. The final magnitude of the contact pressure presents a value of 10.45 MPa and is located on the inferior region of the femoral cartilage. The local value of the contact pressure at the end of the internal rotation step was also measured in the region of the cam deformity (anterosuperior region of the femoral head). The local value of the contact pressure in the region of the cam deformity was 8.44 MPa.

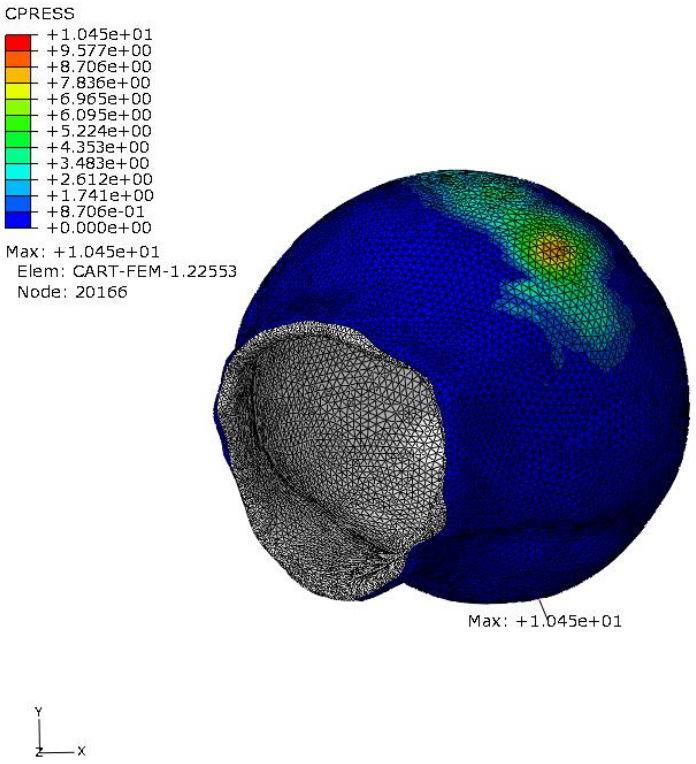

Figure 31: Case 1 - Representation of the contact pressures distribution and of the final maximum magnitude of the contact pressure on the femoral cartilage at the end of internal rotation step. The maximum value was 10.45 MPa located on the inferior region.

The contact pressures distributions and the final maximum magnitudes on the acetabular cartilage and labrum, can be observed in Figure 32. The final maximum magnitude is located on the posterior region of the acetabular cartilage and presents a value of 13.61 MPa. The final maximum magnitude of the contact pressure on the labrum was 10.96 MPa located on the postero inferior region. The local value of the contact pressure on the acetabular cartilage measured in the region in contact with the region where the cam deformity is more evident, the anterosuperior region, presented a magnitude of 8.489 MPa.

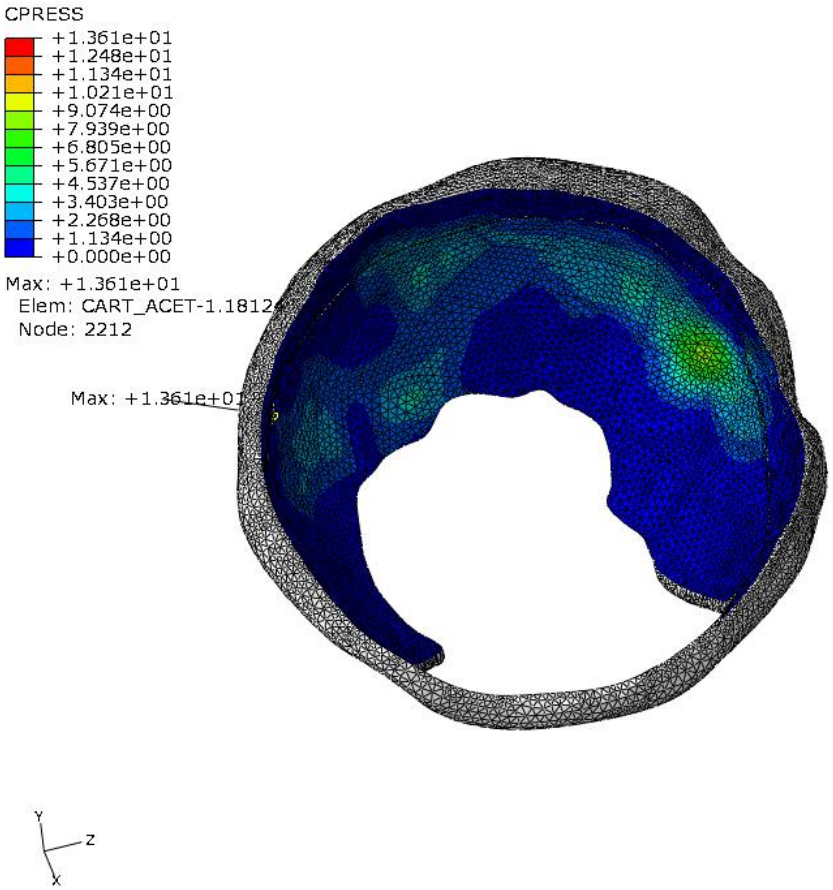

Figure 32: Case 1 - Representation of the contact pressures distribution and of the final maximum magnitude on the acetabular cartilage and labrum at the end of the pure internal rotation step. The maximum value registered for the acetabular cartilage was 13.61 MPa located in the posterior region and the maximum value for the labrum was 10.96 MPa also in the postero inferior region.

Five nodes were selected along a straight horizontal line perpendicular to the axis of the internal rotation in the region of the cam deformity (see Figure 33).

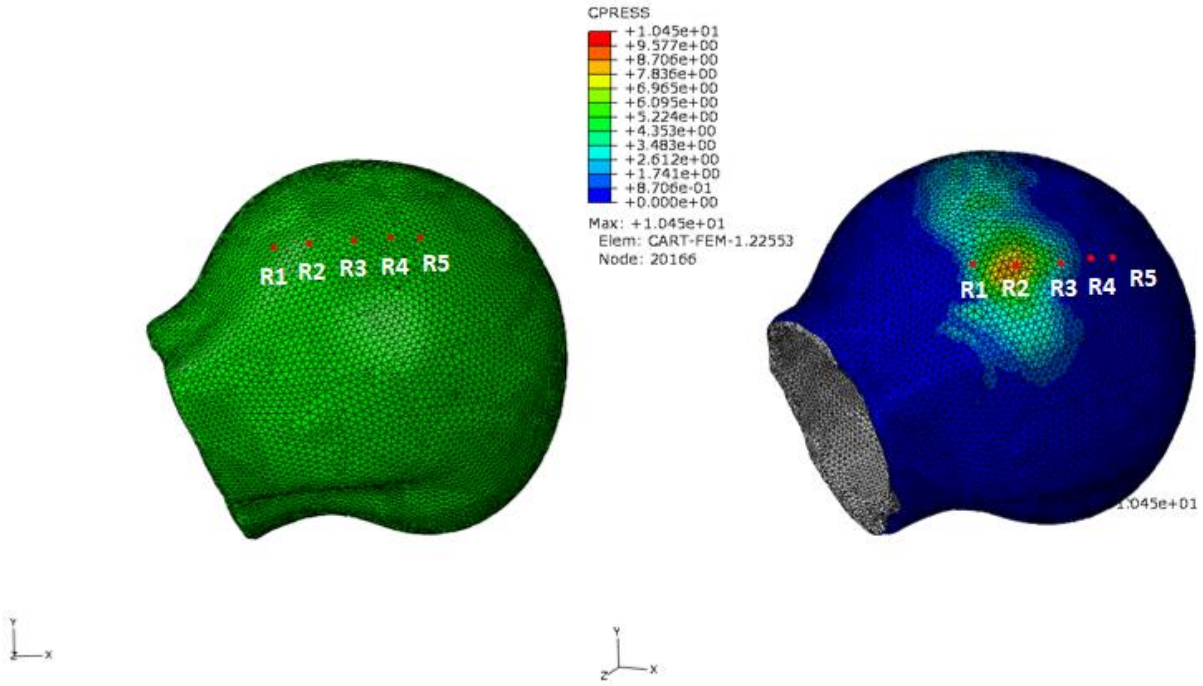

Figure 33: Case 1- Representation of the selected nodes (red points). Left – 5 nodes selected on the initial femoral cartilage defining a horizontal line perpendicular to the axis of the pure internal rotation. Right – representation of the same nodes after the internal rotation and the relative final position regarding the contact pressures distributions.

Similarly as in the previous section, an evolution of the contact pressures on the selected nodes is presented as a function of the angle of rotation (Figure 34). The final maximum contact pressure observed on the femoral cartilage (10.45 MPa) does not occur in any of the selected nodes. The measured local value of 8.44 MPa on the AS region is coeherent with the contact pressures in node R2, which presents a maximum magnitude of 8.908 MPa.

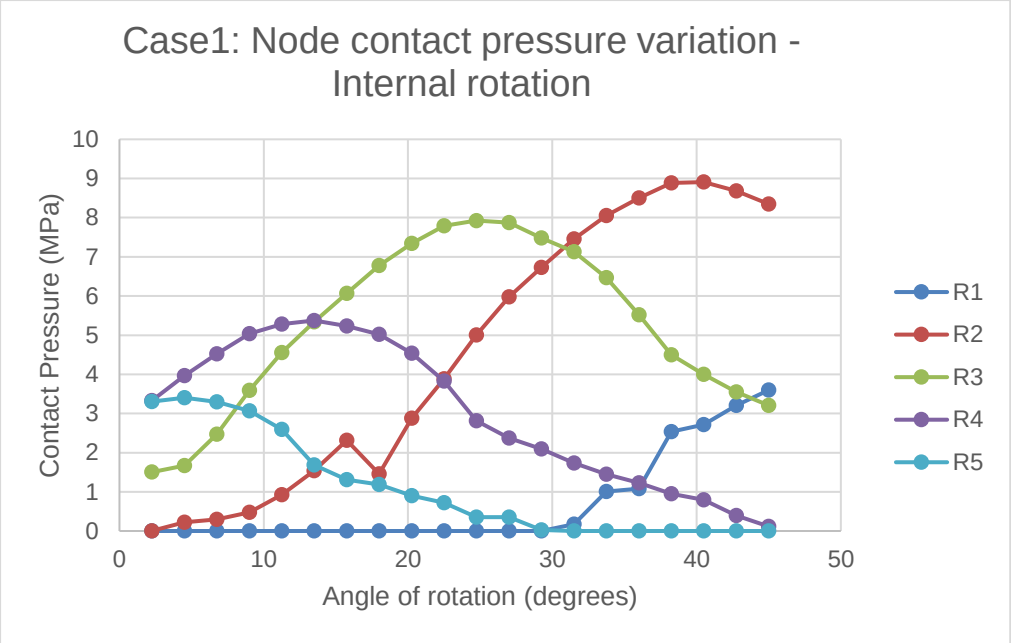

Figure 34: Case 1 - Contact pressure evolution in the selected nodes on the femoral cartilage as a function of the angle of pure internal rotation.

The values of the contact pressures and of the von Mises stresses on the three components, the femoral cartilage (FC), the acetabular cartilage (AC) and the labrum (L) at the end of pure internal rotation of 45º and during this step are presented in Table 3. The time step percentage is registered in order to observe the occurrence of the maximum values.

Table 3: Case 1 – Contact pressures and von Mises stresses at the end of the internal rotation and during the internal rotation step on the three hip joint components. The maximum observed during the step and the final maximum magnitude are presented and the location is identified. (I – Inferior; P – Posterior; AS – Anterosuperior; PI – Posteroinferior region)

		Contact Pressure		Von Mises	
		Maximum during step	**Final Maximum**	**Maximum during step**	**Final Maximum**
Internal rotation 45º	FC	**14.77 MPa** (70% of the step) I region	**10.45 MPa** I region	**4.174 MPa** (70% of the step) AS region	**3.828 MPa** AS region
	AC	**13.61 MPa** (100%) P region	**13.61 MPa** P region	**15.95 MPa** (60% of the step) PI Region	**10.56 MPa** PI region
	L	**18.44 MPa** (55% of the step) PI region	**10.96 MPa** P region	**15.99 MPa** (75% of the step) PI region	**9.784 MPa** PI region

5.2. Pathological case 2 with alpha angle equal to 81º

5.2.1. FE analysis: compression force and pure flexural rotation

As proceeded for the previous case, the contact pressures and the von Mises stresses are obtained on the pathologic hip joint being subjected to a physiological compression force and a pure flexural rotation of 90º. Regarding the present loading, and due to convergence problems, the simulation in ABAQUS stops when the flexural rotation reaches 23.4º, thus the results presented at the end of the flexural rotation correspond to an angle of rotation equal to 23.4º. The maximum values observed for the contact pressures after the compressive step and after the pure flexural rotation step are presented on the three components of the hip joint. The initial and the deformed meshes of the three hip joint components can be observed in Figure 35. The initial mesh corresponds to the anatomical normal orientation of the present hip and the deformed form corresponds to the end of the pure flexural rotation step of 23.4º.

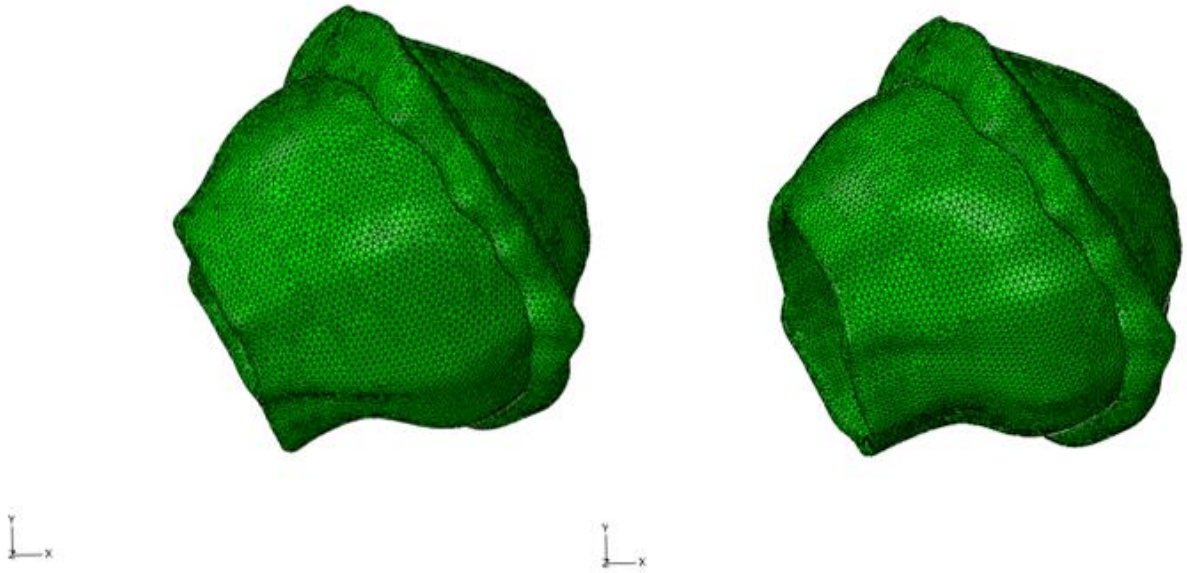

Figure 35: Case 2 - Representation of the initial and the deformed meshes of the three components of the hip joint. Left – initial form representing the anatomical physiological orientation. Right – deformed form of the mesh at the end of the pure flexural rotation of 23.4º.

The maximum final magnitude for the contact pressure and the contact pressures distribution on the femoral cartilage after the compressive step and after the pure flexural rotation are presented in Figure 36. The final maximum magnitude of the contact pressure on the femoral cartilage after the compressive step is 2.842 MPa on the superior region and at the end of the pure flexural rotation the final magnitude is 53.68 MPa on the inferior region. The latter magnitude represents an extremely elevated contact pressure, which is thought to be artificial due to geometry problems and may be an explanation for the convergence problems registered during the analysis.

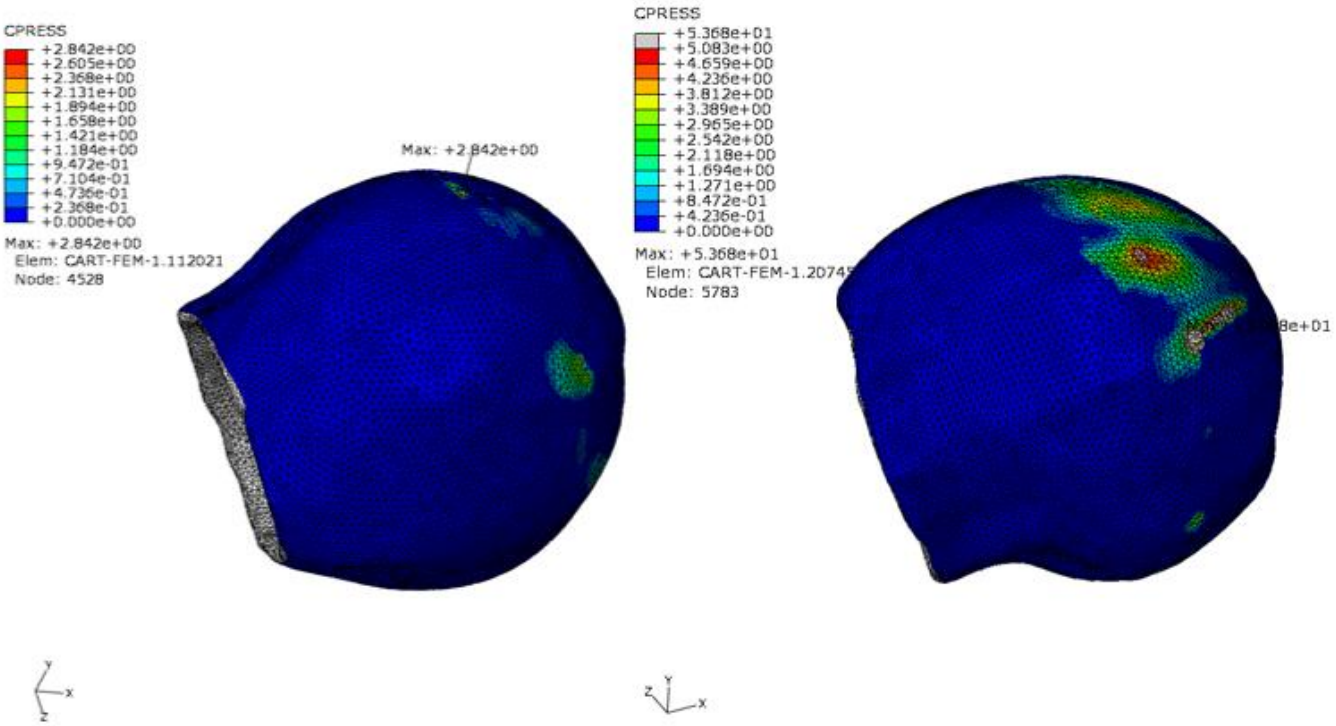

Figure 36: Case 2 - Representation of the contact pressures distribution and the final maximum magnitude of the contact pressure on the femoral cartilage. Left – after the compressive step the maximum value was 2.842 MPa located on the superior region. Right – after the pure flexural rotation step the maximum value was 53.68 MPa located on the inferior region.

In the acetabular cartilage and labrum, the contact pressures distribution and the final maximum magnitude after the compressive step and after the pure flexural rotation are presented in Figure 37. After the compressive step the magnitude of the contact pressure on the acetabular cartilage was 3.019 MPa in the superior region. The magnitude of the contact pressure on the labrum after the compressive step was 2.186 MPa located on the posteroinferior region. After the pure flexural rotation step, the final magnitude on the acetabular cartilage was 10.88 MPa, and was 57.45 MPa on the labrum, located both in the inferior region. In addition, the local value of the contact pressure on the acetabular cartilage was measured after the flexural rotation in the anterosuperior region (which is the region in contact with the cam deformity) and presented a magnitude of 6.47 MPa.

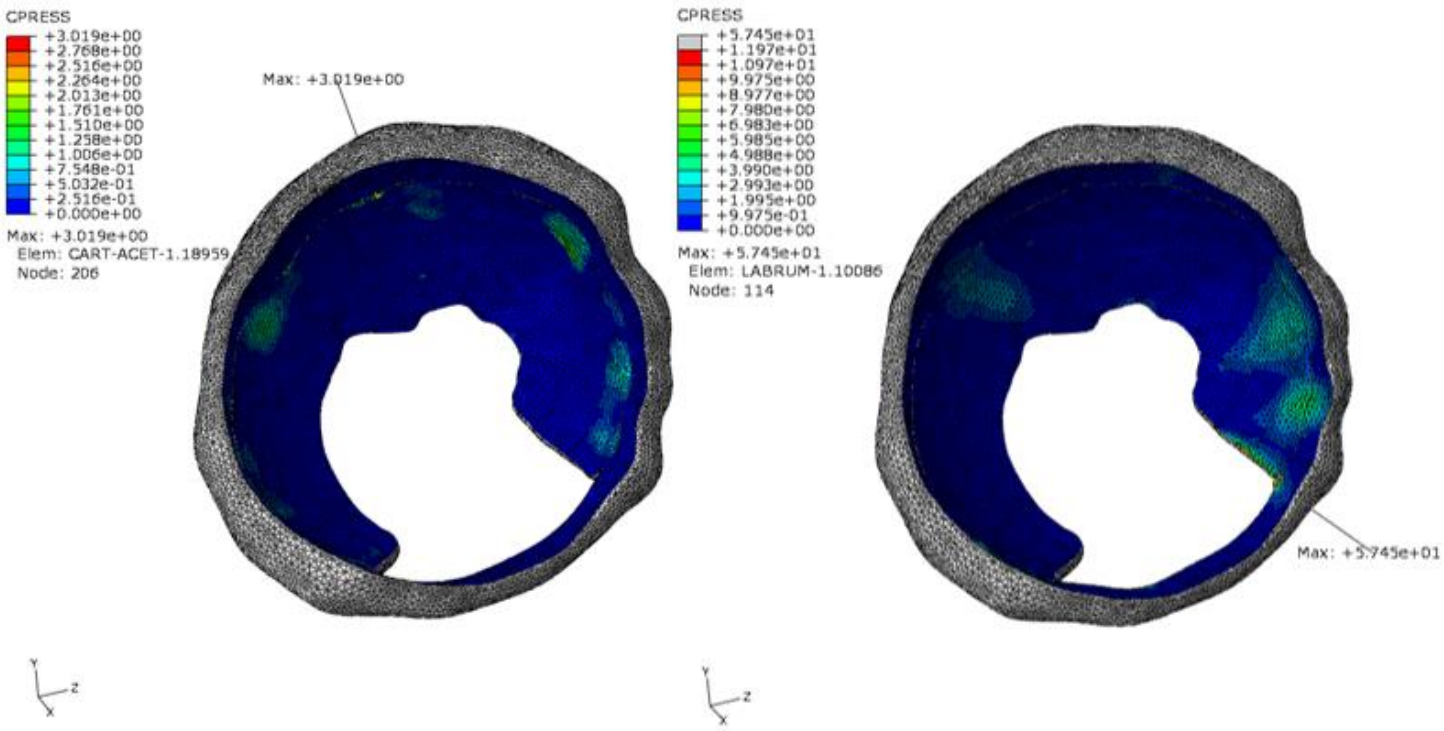

Figure 37: Case 2 - Representation of the contact pressures distribution and final maximum magnitude on the acetabular cartilage and labrum. Left – after the compressive step. Right – after the pure flexural rotation.

For the present analysis of the flexural rotation of the pathologic hip joint, the evolution of the contact pressures on the selected points of the femoral cartilage as function of the angular rotation was not computed due to lack of information.

The values of the contact pressures and von Mises stresses on the three components, the femoral cartilage (FC), the acetabular cartilage (AC) and the labrum (L) at the end of compressive step, at the end of pure flexural rotation of 90º and during these steps are presented in Table 4 for the compressive step and in Table 5 for the pure flexural rotation step. The time step percentage is registered in order to observe the occurrence of the maximum values.

Table 4: Case 2 – Contact pressures and von Mises stresses at the end of the compressive step and during the compressive step on the three hip joint components. The maximum observed during the step and the final maximum magnitude are presented and the location is identified. (S – Superior; AS – Anterosuperior; PI - Posteroinferior)

		Contact Pressure		Von Mises	
		Maximum during step	Final Maximum	Maximum during step	Final Maximum
Compression	FC	**3.006 MPa** (20% of the step) S region	**2.842 MPa** S region	**1.065 MPa** (100%) AS region	**1.065 MPa** AS region
	AC	**3.099 MPa** (100%) S region	**3.099 MPa** S region	**1.021 MPa** (65% of the step) AS region	**1.014 MPa** AS region
	L	**2.378 MPa** (85% of the step) PI region	**2.186 MPa** PI region	**1.099 MPa** (100%) PI region	**1.099 MPa** PI region

Table 5: Case 2 – Contact pressures and von Mises stresses at the end of the flexural rotation step on the three hip joint components. The final magnitudes are presented and the location is identified. (I – Inferior)

		Contact Pressure	Von Mises
		Final Maximum	Final Maximum
Flexural rotation 23.4º	FC	**53.68 MPa** I region	**7.043 MPa** I region
	AC	**10.88 MPa** I region	**10.11 MPa** I region
	L	**57.45 MPa** I region	**11.89 MPa** I region

5.2.2. FE analysis: compression force and pure internal rotation

For the pure internal rotation analysis, the procedure is identical to the one presented in section 5.1.2. The initial and the deformed forms of the three components of the pathologic hip joint are represented in Figure 38.

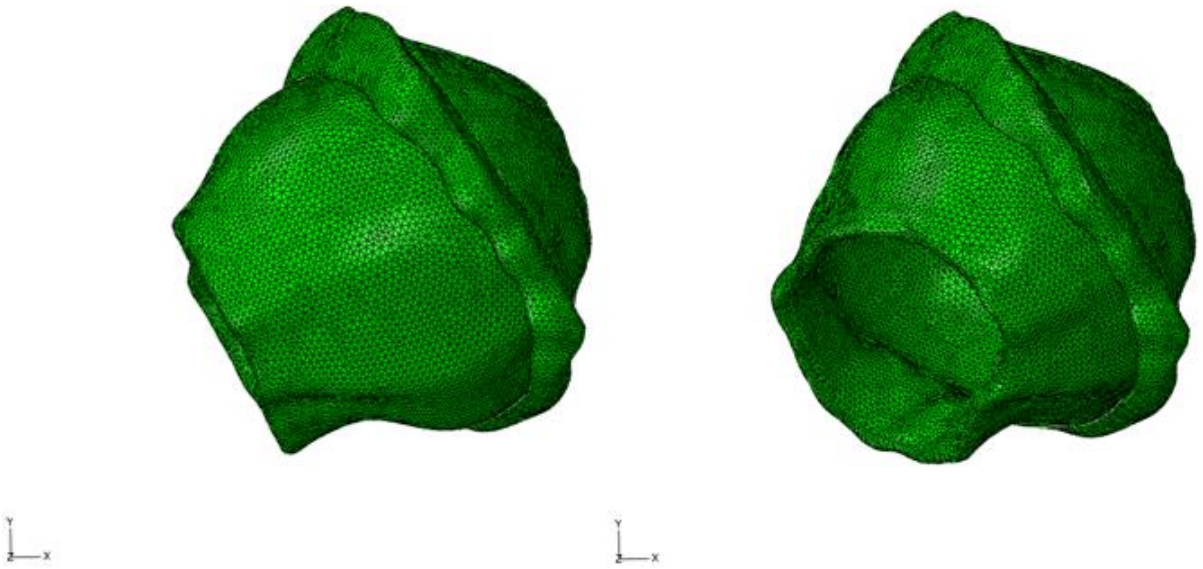

Figure 38: Case 2 - Representation of the initial and of the deformed meshes of the three components of the hip joint. Left – initial form representing the anatomical physiological orientation. Right – deformed form of the mesh at the end of the pure internal rotation of 45º.

The final magnitude of the contact pressures and the contact pressures distribution on the femoral cartilage at the end of the pure internal rotation step are presented in Figure 39. Two distinct views of the femoral cartilage are represented to better interpret the contact pressures distribution regarding the anatomical region of the cam pathology. In Figure 39 (right side) the osseous bump is clearly distinguished due to the increased alpha angle (81º) observed for the present patient and one can also observe that the maximum contact pressures distribution are concentrated in the region of the pathology. The final maximum magnitude of the contact pressure presents a value of 9.775 MPa and is located on the anterosuperior region of the femoral cartilage, where the cam deformity is more evident.

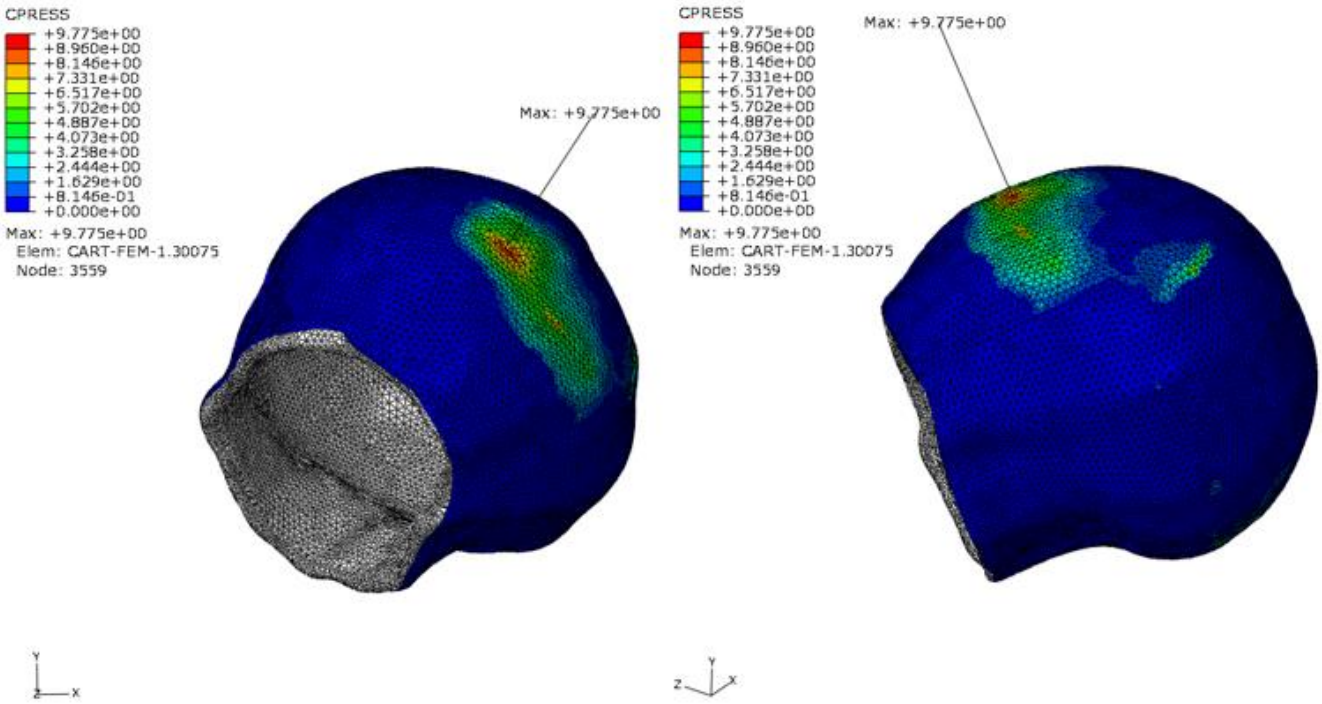

Figure 39: Case 2 – Representation in distinct views of the contact pressures distribution and of the final maximum magnitude of the contact pressure on the femoral cartilage at the end of internal rotation step. The final magnitude was 9.775 MPa located on the anterosuperior region (region of the cam deformity).

In the articular cartilage and labrum, the contact pressures distribution and the final maximum magnitude can be observed in Figure 40. The final maximum magnitude is located on the anterosuperior region of the acetabular cartilage and presents a value 9.158 MPa, and for the labrum the final magnitude is 17.59 MPa located in the anterosuperior region. As one can observe the contact pressures distribution for the acetabular cartilage and the labrum are concentrated in the region in contact with the pathology.

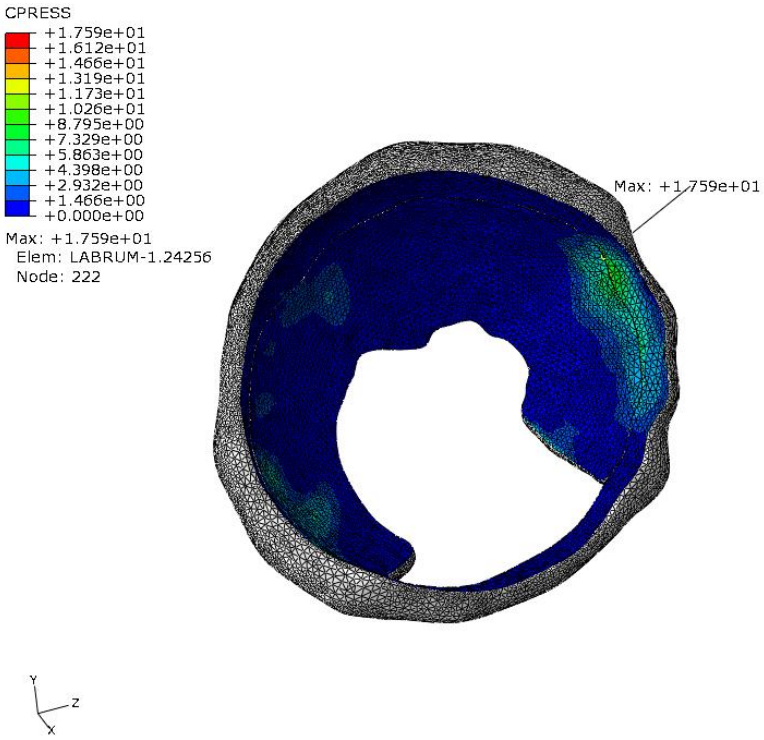

Figure 40: Case 2 - Representation of the contact pressures distribution and the final maximum magnitudes on the acetabular cartilage and labrum at the end of the pure internal rotation step. The maximum value registered for the acetabular cartilage was 9.158 MPa in the anterosuperior region and the maximum value on the labrum was 17.59 MPa also in the anterosuperior region (region in contact with the cam proturbence).

Six nodes were selected along a straight horizontal line perpendicular to the axis of internal rotation in the region of the cam deformity (see Figure 41).

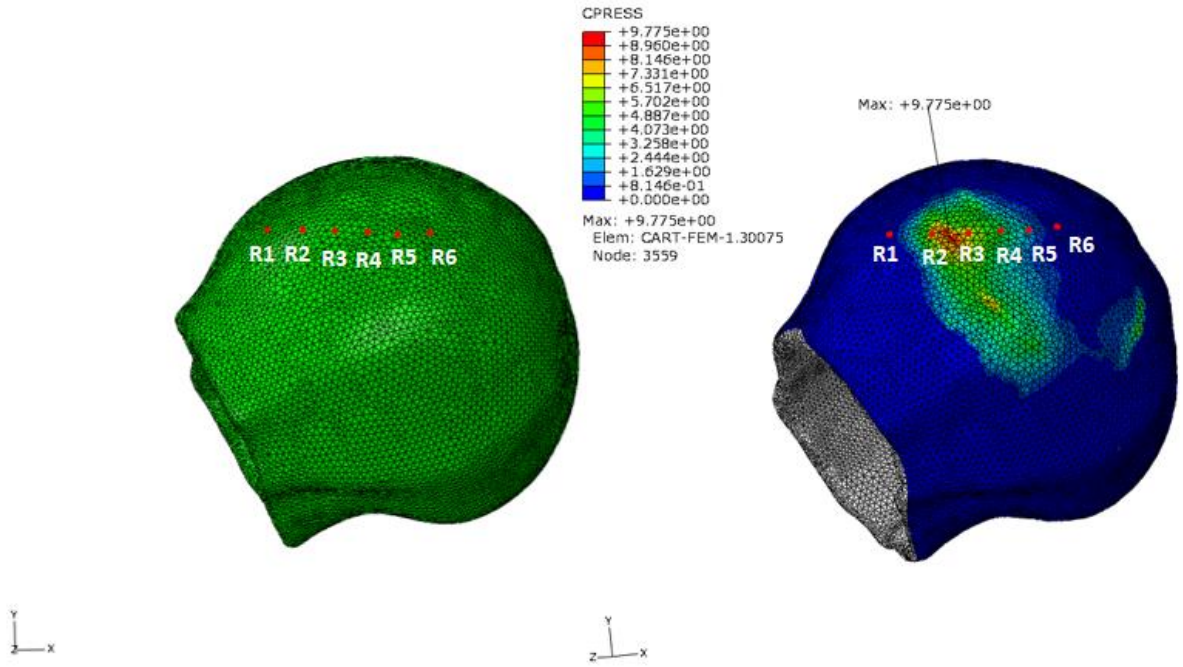

Figure 41: Case 2- Representation of the selected nodes (red points). Left – 6 nodes selected on the initial femoral cartilage defining a horizontal line perpendicular to the axis of the pure internal rotation. Right – representation of the same nodes after the internal rotation and the relative final position regarding the contact pressures distributions.

The plot that describes the evolution of the contact pressures in the selected nodes as a function of the angle of rotation can be observed in Figure 42. The final maximum contact pressure observed on the femoral cartilage (9.775 MPa) does not occur in any of the selected nodes. It occurs near node R3 which presents a maximum value of 7.65 MPa.

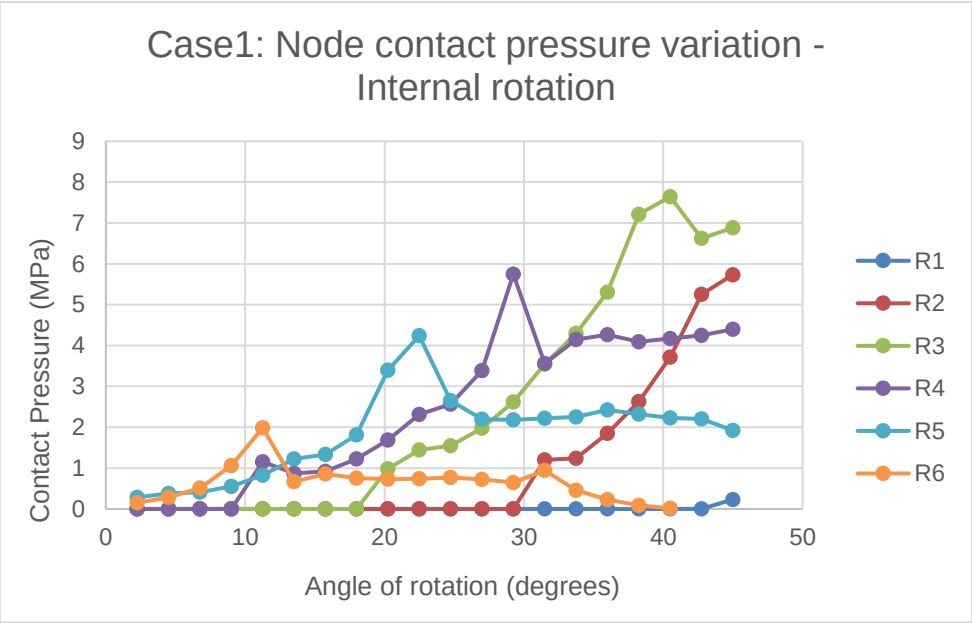

Figure 42: Case 2 - Contact pressures evolution in the selected nodes on the femoral cartilage as function of the angle of pure internal rotation.

The values of the contact pressures and of the von Mises stresses on the three components, the femoral cartilage (FC), the acetabular cartilage (AC) and the labrum (L) at the end of pure internal rotation of 45º and during this step are presented in Table 6. The time step percentage is registered in order to observe the occurrence of the maximum values.

Table 6: Case 2 – Contact pressures and von Mises stresses at the end of the internal rotation and during the internal rotation step on the three hip joint components. The maximum observed during the step and the final maximum magnitude are presented and the location is identified. (I – Inferior; AS – Anterosuperior; AI – Anteroinferior region)

		Contact Pressure		Von Mises	
		Maximum during step	Final Maximum	Maximum during step	Final Maximum
Internal rotation 45º	FC	36.84 MPa (35% of the step) I region	9.775 MPa AS region	5.477 MPa (40% of the step) AI region	4.183 MPa AS region
	AC	10.12 MPa (50% of the step) AS region	9.158 MPa AS region	10.36 MPa (35% of the step) I region	6.194 MPa AS region
	L	51.40 MPa (45% of the step) AI region	17.59 MPa AS region	18.01 MPa (100%) AS region	18.01 MPa AS region

5.3. Pathological case 1 without labrum

5.3.1. FE analysis: compression force and pure flexural rotation

In this section the FE analysis of the pathologic hip joint from the Case 1 but without the labral tissue is presented. The two mesh components that compose the hip joint are the femoral cartilage and the acetabular cartilage. The same loadings and procedures were performed as for the case including the labral tissue. No differences in the initial and in the deformed form of the final meshes when compared with Figure 25 are observed.

The magnitude of the maximum contact pressure and the contact pressures distribution on the femoral cartilage at the end of the compressive step and at the end of the pure flexural rotation of 90º are represented in Figure 43. The magnitude of the contact pressure on the femoral cartilage after the compressive step was 5.402 MPa located on the anterosuperior region of the tissue. At the end of the pure flexural rotation step, the final magnitude of the contact pressure was 5.168 MPa. Also, during the pure flexural rotation step, a maximum value of 8.131 MPa was registered for 70% of the step time, suggesting that the maximum magnitude of the contact pressure occurs at an angle of rotation of 63º.

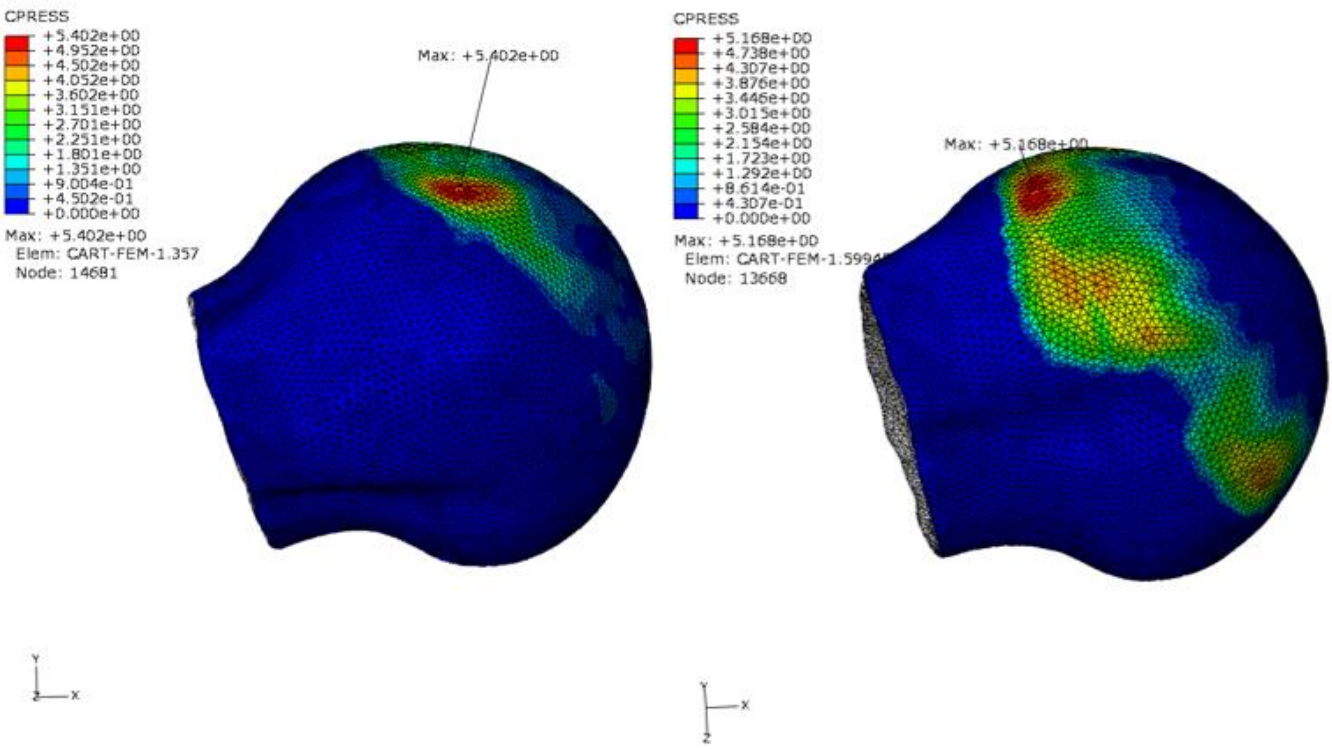

Figure 43: Case 1 without labrum - Representation of the contact pressures distribution and final maximum magnitude of the contact pressure on the femoral cartilage. Left – after the compressive step the maximum value was 5.402 MPa located on the anterosuperior region. Right – after the pure flexural rotation step the final maximum value was 5.168 MPa located on the superior region.

The maximum magnitude of the contact pressures and the contact pressure distribution at the end of the compressive step and at the end of the pure flexural rotation of 90º on the acetabular cartilage, are presented in Figure 44. At the end of the compressive step the maximum magnitude was 5.371 MPa located on the anterosuperior region. At the end of the pure flexural rotation, the maximum magnitude observed was 5.227 MPa located on the superior region. A maximum was observed at 65% of the time step with a value of 8.085 MPa located on the anterosuperior region (region of the cam deformity). For the acetabular cartilage, and during the pure flexural rotation of 90º, the observed value suggests that the maximum magnitude of the contact pressure occurs for an angle of rotation of 58.5º.

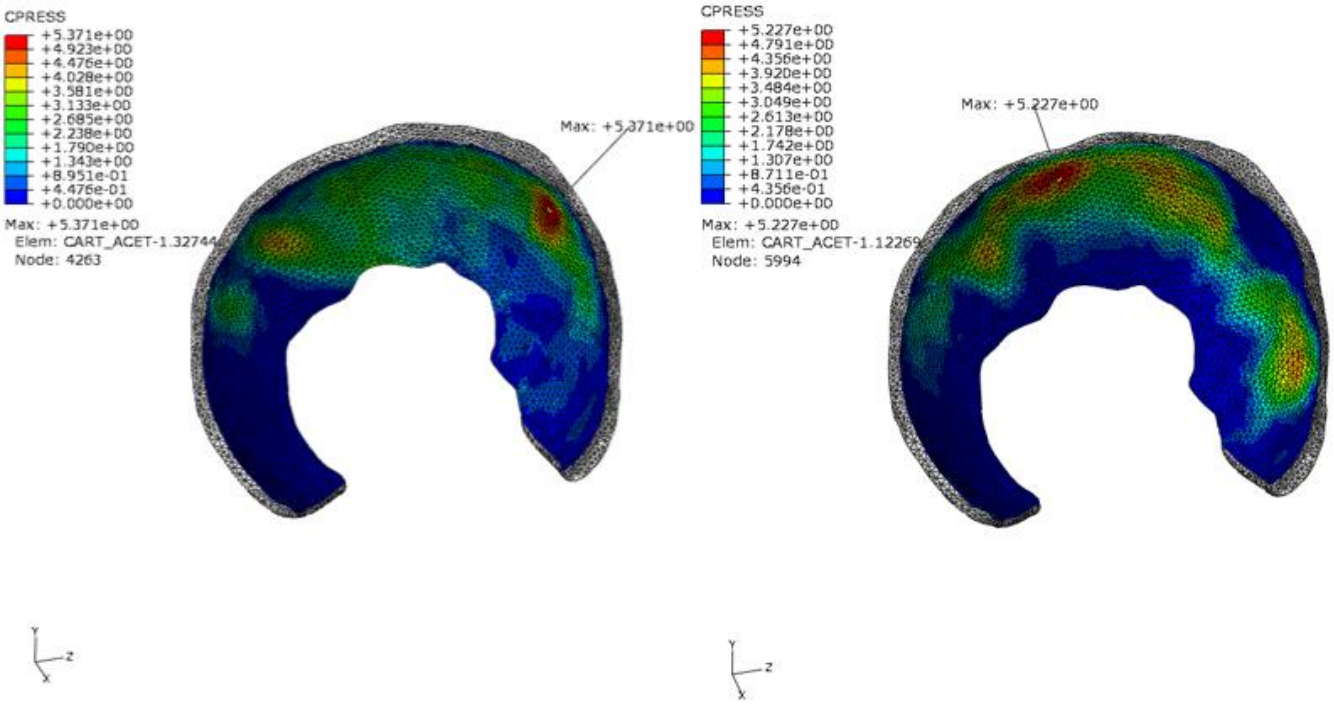

Figure 44: Case 1 without labrum - Representation of the contact pressures distribution and final maximum magnitude on the acetabular cartilage. Left – after the compressive step. Right – after the pure flexural rotation.

The evolution of the contact pressures on the selected nodes on the femoral cartilage is also presented in the case of the model without labrum. For comparative purposes, the selected nodes are the same as the ones selected for the case 1 (Figure 28) with the labral tissue. The contact pressures evolution on the selected nodes on the femoral cartilage is represented in Figure 45 as a function of the angle of rotation. The final maximum contact pressure observed on the femoral cartilage (5.168 MPa) does not occur in any of the selected nodes. It occurs near the node F3 which presents a maximum value of 4.837 MPa.

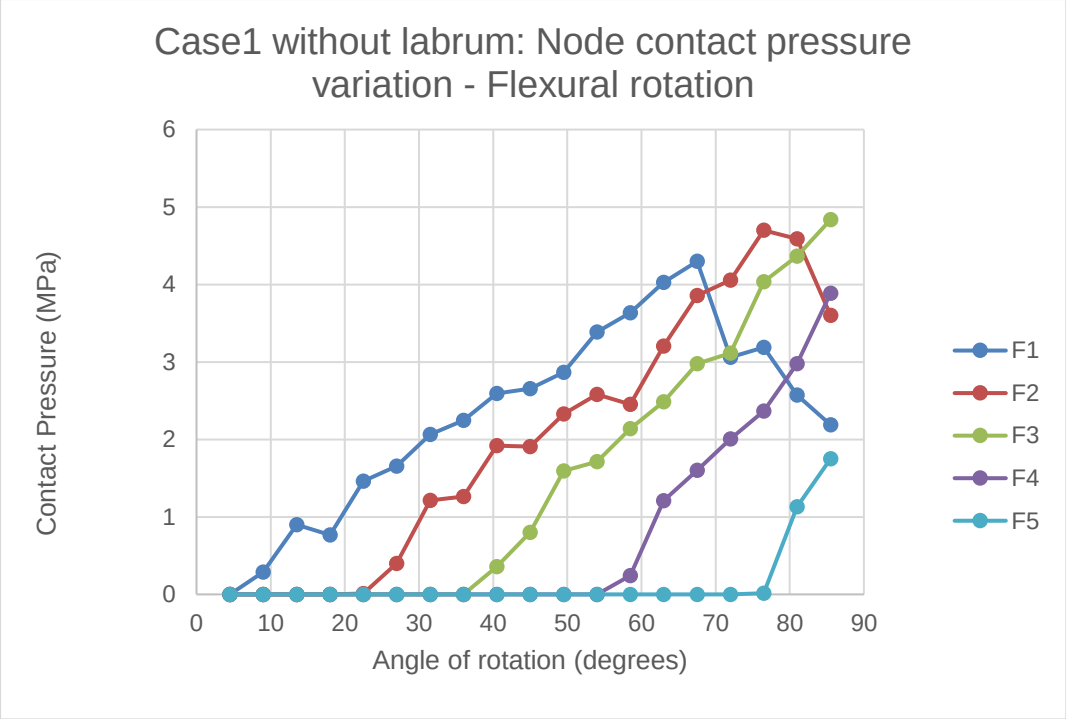

Figure 45: Case 1 without labrum - Contact pressures evolution in the selected nodes on the femoral cartilage as a function of the angle of flexural rotation.

The magnitudes of the contact pressures and of the von Mises stresses on the two components of the hip joint, the femoral cartilage (FC) and the acetabular cartilage (AC) at the end of compressive step and at the end of the pure flexural rotation of 90º are presented in Table 7 and in Table 8, respectively. The time step percentage for which a maximum value occurs during the step is also registered.

Table 7: Case 1 without labrum – Contact pressures and von Mises stresses at the end of the compressive step on the two hip joint components. The maximum magnitudes are presented and the location is identified. (AS – Anterosuperior)

		Contact Pressure	Von Mises
		Final Maximum	Final Maximum
Compression	FC	5.402 MPa AS region	2.404 MPa AS region
	AC	5.371 MPa AS region	3.999 MPa AS region

Table 8: Case 1 without labrum – Contact pressures and von Mises stresses at the end of the flexural rotation and during the flexural rotation step on the two hip joint components. The maximum observed during the steps and the final magnitude are presented and the location is identified. (S – Superior; A – Anterior; I – Inferior; AS – Anterosuperior)

		Contact Pressure		Von Mises	
		Maximum during step	Final Maximum	Maximum during step	Final Maximum
Flexural rotation 90º	FC	8.131 MPa (70% of the step) I region	5.168 MPa S region	3.697 MPa (65% of the step) AS region	2.467 MPa AS region
	AC	8.085 MPa (65% of the step) A region	5.227 MPa S region	8.500 MPa (100%) S region	8.500 MPa S region

5.3.2. FE analysis: compression force and pure internal rotation

The pure internal rotation of 45º is performed with the hip joint being subjected to a compressive force. As mentioned for the flexural rotation analysis without labrum, there are no differences in the initial and the deformed shape of the articular cartilage meshes, when comparing to the meshes observed in Figure 30 (Case 1 with labrum).

The contact pressures distribution and maximum magnitude of the contact pressure on the femoral cartilage at the end of the pure internal rotation step, visualized in two different views, can be observed in Figure 46. The results at the end of the compressive step are not presented since the values are equal to the ones presented in section 5.3.1. The final magnitude for the contact pressure at the end of the pure internal rotation step is 8.868 MPa on the anterosuperior region of the tissue. In addition, a maximum value was measured at 85% of the time step during the rotation step with magnitude equal to 9.070 MPa on the anterosuperior region. This suggests that the maximum magnitude of the contact pressure on the femoral cartilage occurs at an angle of rotation of 38.25º.

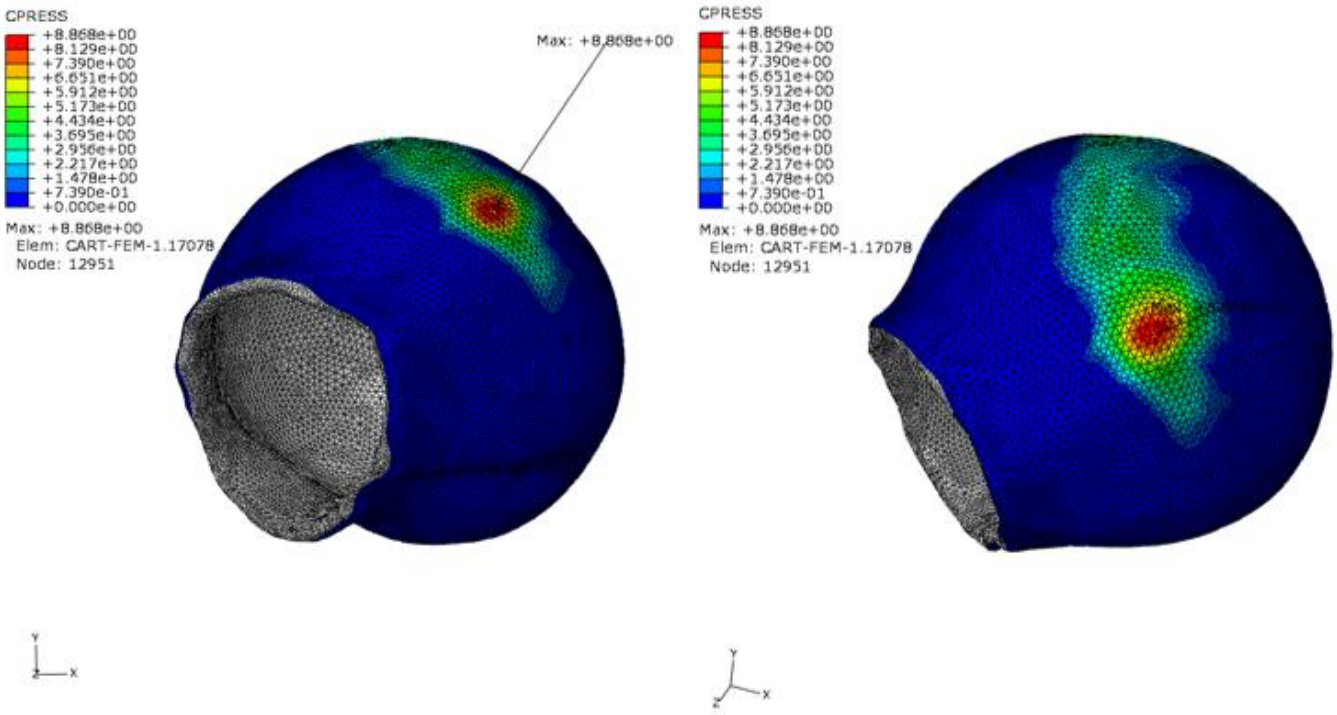

Figure 46: Case 1 without labrum – Representation in distinct views of the contact pressures distribution and the final maximum magnitude of the contact pressure on the femoral cartilage at the end of the internal rotation step. The final magnitude was 8.868 MPa located on the anterosuperior region (region of the cam deformity).

The maximum magnitude of the contact pressure and the contact pressures distribution in the acetabular cartilage at the end of the rotational step can be observed in Figure 47. The maximum magnitude at the end of the pure internal rotation step is 8.812 MPa on the anterosuperior region (region in contact with the protuberance). A maximum value was measured during the rotation step with a value of 9.078 MPa at 75% of the time step, suggesting that the maximum magnitude of the contact pressure on the acetabular cartilage occurs for an angle of rotation of 33.75º.

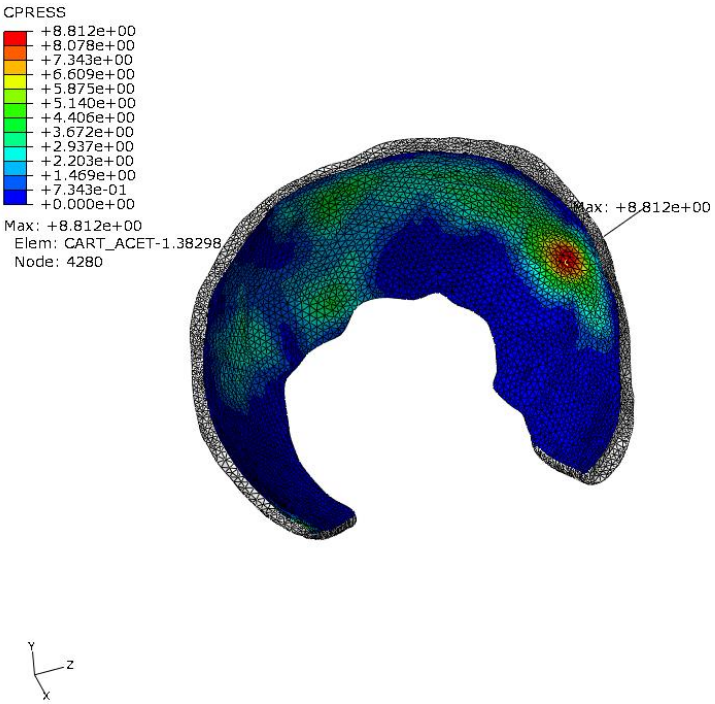

Figure 47: Case 1 without labrum - Representation of the contact pressures distribution and of the maximum magnitude on the acetabular cartilage at the end of the pure internal rotation step. The final magnitude registered for the acetabular cartilage was 8.812 MPa located in the anterosuperior region.

The evolution of the contact pressures on the selected nodes of the femoral cartilage, is represented in Figure 49 as a function of the rotation angle. The nodes are also represented in Figure 48 together with the contact pressures distribution at the end of the pure internal rotation step and are the same that were selected in the case of the complete model (see Figure 33).

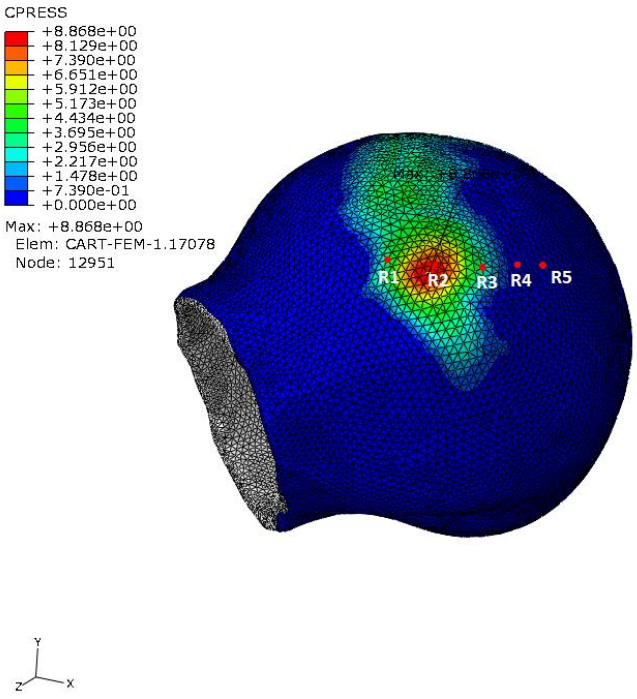

Figure 48: Case 1 without labrum - Representation of the 5 nodes selected on the femoral cartilage defining a horizontal line perpendicular to the axis of the pure internal rotation.

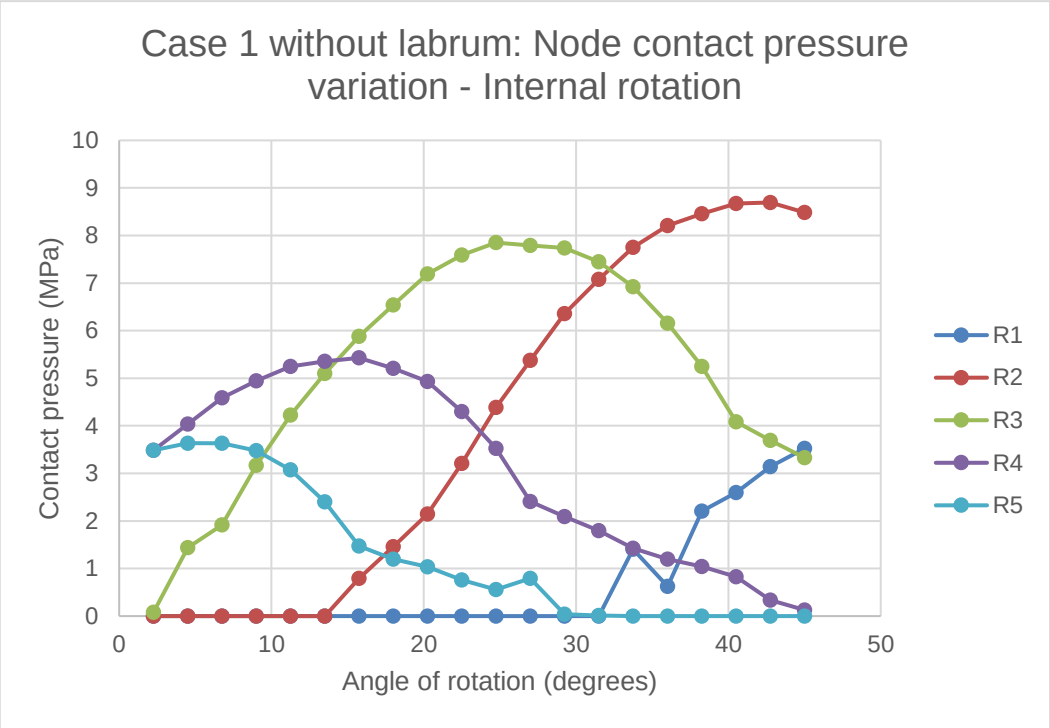

Figure 49: Case 1 without labrum - Contact pressures evolution in the selected nodes on the femoral cartilage as a function of the angle of pure internal rotation.

The magnitude of the contact pressures and of the von Mises stresses on the femoral cartilage (FC) and on the acetabular cartilage (AC) at the end of the rotational step and during the rotational step can be observed in Table 9 together with the corresponding locations.

Table 9: Case 1 without labrum – Contact pressures and von Mises stresses at the end of the internal rotation and during the internal rotation step on the two hip joint components. The maximum observed during the step and the final maximum magnitude are presented and the location is identified. (S – Superior; AS – Anterosuperior; PI – Posteroinferior region)

		Contact Pressure		**Von Mises**	
		Maximum during step	**Final Maximum**	**Maximum during step**	**Final Maximum**
Internal rotation 45º	**FC**	**9.070 MPa** (85% of the step) AS region	**8.868 MPa** AS region	**4.126 MPa** (90% of the step) AS region	**4.047 MPa** AS region
	AC	**9.078 MPa** (75% of the step) AS region	**8.812 MPa** AS region	**7.157 MPa** (65% of the step) PI region	**5.786 MPa** S region

5.4. Pathological case 2 without labrum

5.4.1. FE analysis: compression force and pure flexural rotation

In this section the FE analysis of the pathologic hip joint from the Case 2 but without the labral tissue is presented. The two mesh components that compose the hip joint are the femoral cartilage and the acetabular cartilage. As mentioned in the section 5.2.1, the pure flexural rotation stops when reaches 23.4º of the total flexural rotation and thus, the results presented at the end of the pure flexural rotation correspond to an angle of 23.4º.

The maximum magnitude of the contact pressure and the contact pressures distribution on the femoral cartilage at the end of the compressive step and at the end of the pure flexural rotation of 23.6º are represented in Figure 50. The maximum magnitude of the contact pressure on the femoral cartilage after the compressive step was 1.960 MPa on the anterosuperior region. The maximum magnitude was identified at 20% of the total compression step with a value of 2.33 MPa on the anterosuperior region. At the end of the pure flexural rotation of 23.4º, the maximum magnitude of the contact pressure presented a value of 9.920 MPa on the anteroinferior region.

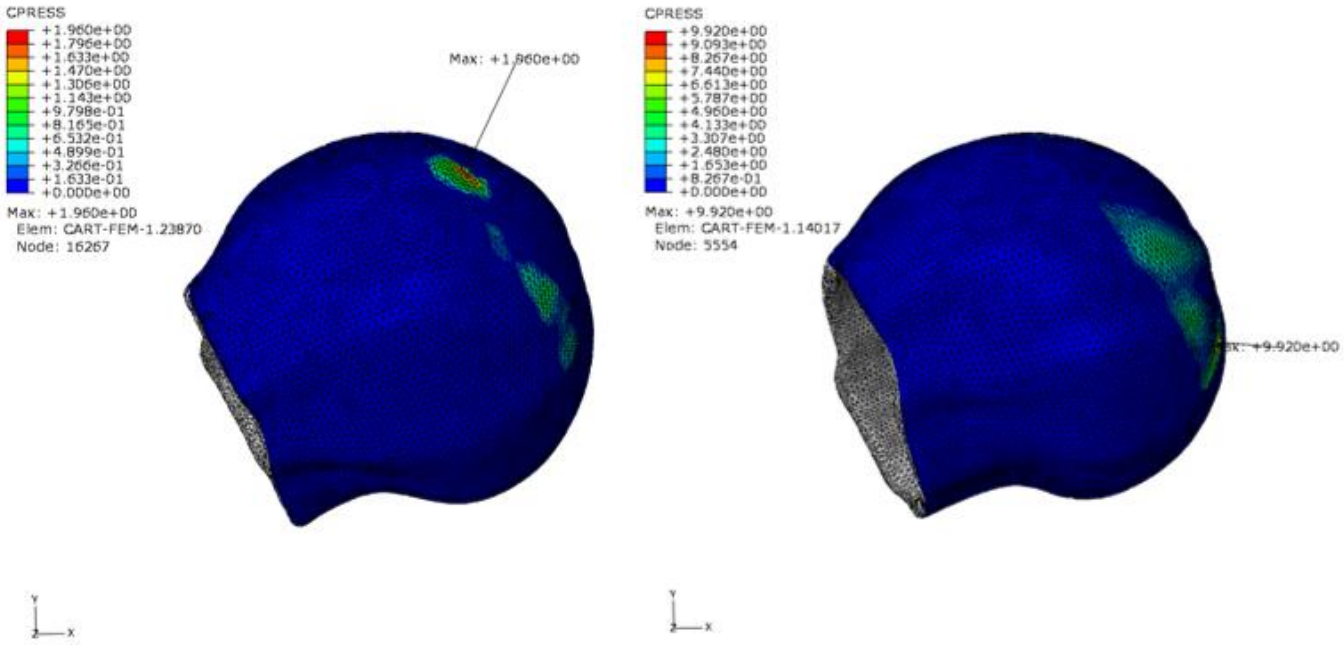

Figure 50: Case 2 without labrum - Representation of the contact pressures distribution and of the final maximum magnitude of the contact pressure on the femoral cartilage. Left – after the compressive step the maximum value was 1.960 MPa located on the anterosuperior region. Right – after the pure flexural rotation step the final maximum value was 9.920 MPa located on the anteroinferior region.

The maximum magnitude of the contact pressure and the contact pressures distribution at the end of the compressive step and at the end of the pure flexural rotation on the acetabular cartilage, are presented in Figure 51. The maximum magnitude of the contact pressure registered at the end of the compression step was 2.279 MPa on the anterosuperior region. The maximum magnitude of the contact pressure was identified at 20% of the total step with a value of 2.323 MPa on the same region. For the pure flexural rotation the maximum magnitude presented a value of 10.75 MPa on the anterosuperior region.

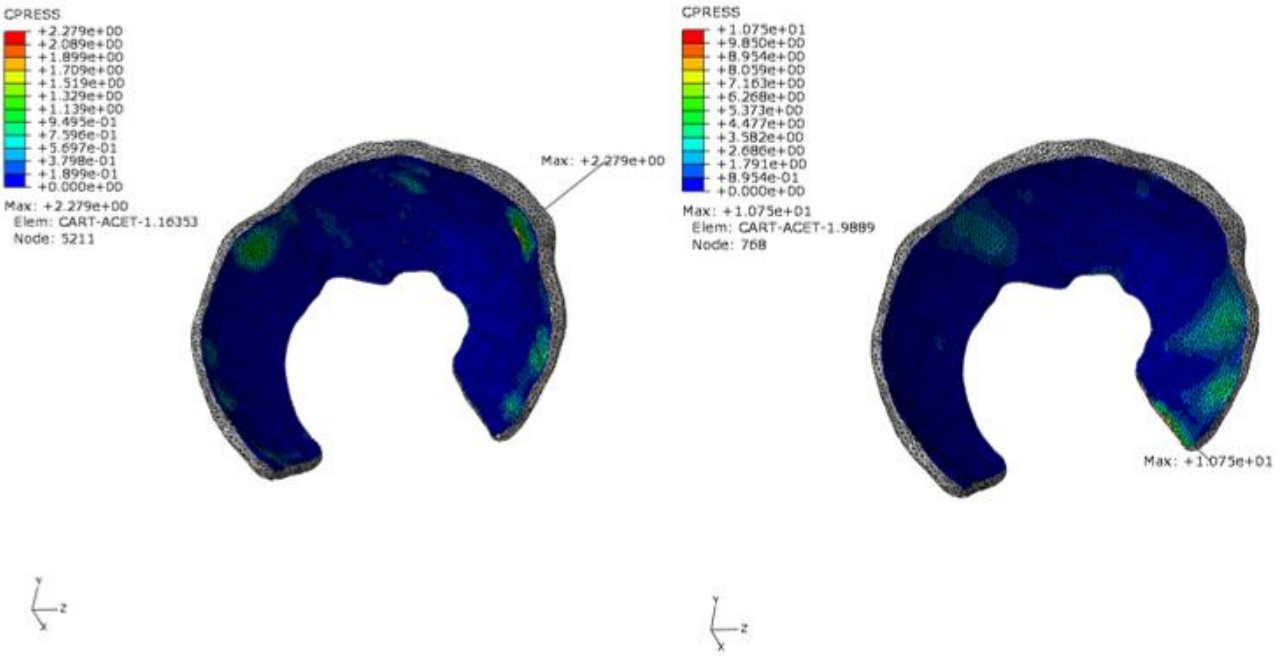

Figure 51: Case 2 without labrum - Contact pressures distribution and final maximum magnitude of the contact pressures on the acetabular cartilage. Left – at the end of the compression step. Right – at the end of the pure flexural rotation of 23.4º.

The values of the contact pressures and von Mises stresses on the two components, the femoral cartilage (FC) and the acetabular cartilage (AC) at the end of the compressive step, at the end of pure flexural rotation of 23.6º and during these steps are presented in Table 10 for the compressive step and in Table 11 for the pure flexural rotation step. The time step percentage is registered in order to observe the occurrence of the maximum values.

Table 10: Case 2 without labrum – Contact pressures and von Mises stresses at the end of the compressive step and during the compressive step on the two hip joint components. The maximum observed during the step and the final magnitude are presented and the location is identified. (AS – Anterosuperior)

		Contact Pressure		Von Mises	
		Maximum during step	Final Maximum	Maximum during step	Final Maximum
Compression	FC	**2.33 MPa** (20% of the step) AS region	**1.960 MPa** AS region	**1.018 MPa** (20% of the step) AS region	**0.8212 MPa** AS region
	AC	**2.323 MPa** (20% of the step) AS region	**2.279 MPa** AS region	**1.043 MPa** (40% of the step) AS region	**1.023 MPa** AS region

Table 11: Case 2 without labrum – Contact pressures and von Mises stresses at the end of the flexural rotation and during the flexural rotation step on the two hip joint components. The maximum observed during the step and the final magnitude are presented and the location is identified. (AI – Anteroinferior; AS – anterosuperior)

		Contact Pressure	Von Mises
		Final Maximum	Final Maximum
Flexural rotation 23.4º	FC	**9.920 MPa** AI region	**3.143 MPa** AI region
	AC	**10.75 MPa** AS region	**13.04 MPa** AI region

5.4.2. FE analysis: compression force and pure internal rotation

The pure internal rotation step was performed under the same loading conditions as Case 2 with labrum in section 5.2.2. The results for the compressive step are not presented for this section since the magnitudes are equal to the ones presented in section 5.4.1. The contact pressures distribution on the femoral cartilage at the end of the pure internal rotation step of 45º and the final maximum magnitude of the contact pressure registered are presented in Figure 52 in distinct anatomical views. The final magnitude observed on the femoral cartilage presents a value of 8.018 MPa on the anterior region.

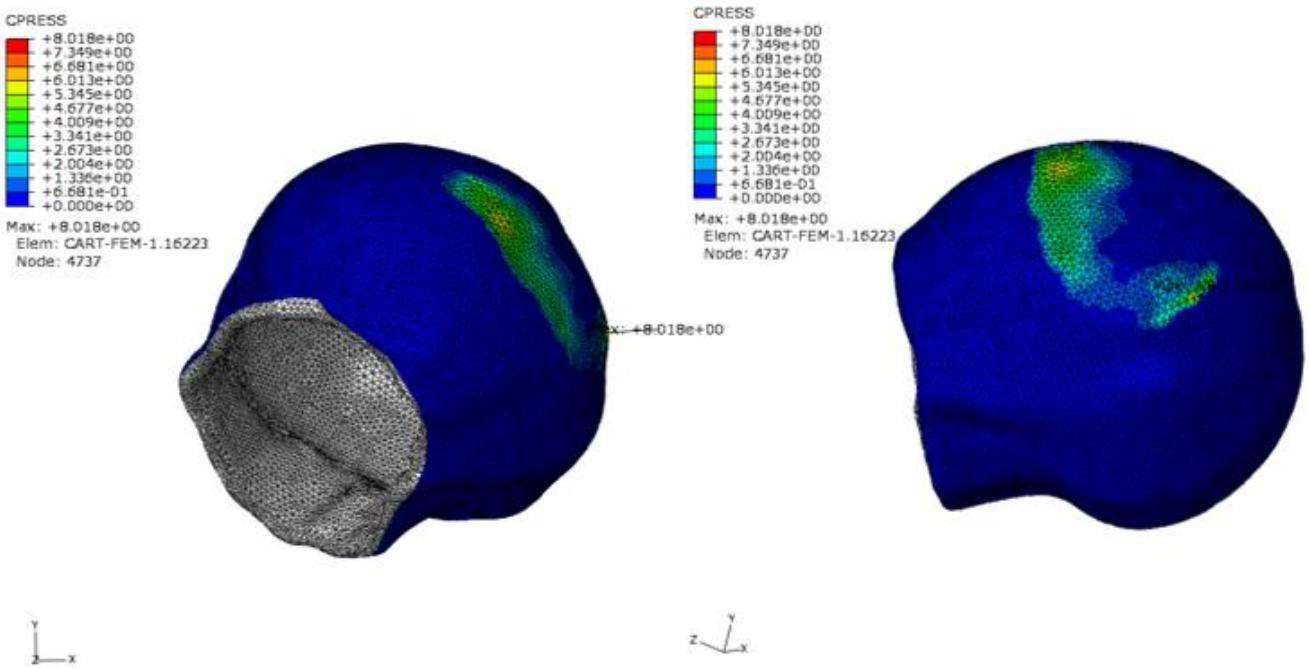

Figure 52: Case 2 without labrum – Representation in distinct views of the contact pressures distribution and of the final maximum magnitude of the contact pressure on the femoral cartilage at the end of the internal rotation step. The final magnitude was 8.018 MPa located on the anterior region.

The maximum magnitude of the contact pressure and the contact pressures distribution in the acetabular cartilage at the end of the rotational step can be observed in Figure 53. The maximum magnitude at the end of the pure internal rotation step was 7.010 MPa located on the anteroinferior region. The maximum magnitude was identified at 50% of the total step time with a value of 9.88 MPa located also on the anteroinferior region of the tissue. The magnitude of the contact pressure at the end of the internal rotation step on the anterosuperior region in contact with the cam deformity was 5.671 MPa.

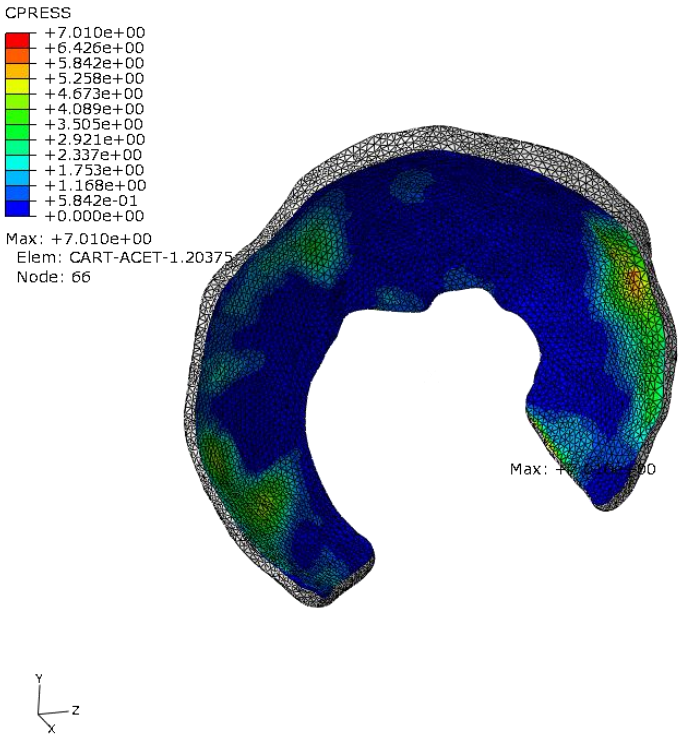

Figure 53: Case 2 without labrum - Representation of the contact pressures distribution and of the maximum magnitude on the acetabular cartilage and labrum at the end of the pure internal rotation step. The maximum magnitude registered for the acetabular cartilage was 7.010 MPa located in the anteroinferior region.

The evolution of the contact pressures on the selected nodes of the femoral cartilage, is represented in Figure 55 as a function of the rotation angle. The nodes are also represented in Figure 54 together with the contact pressures distribution at the end of the pure internal rotation step and are the same that were selected in the case of the complete model (see Figure 41).

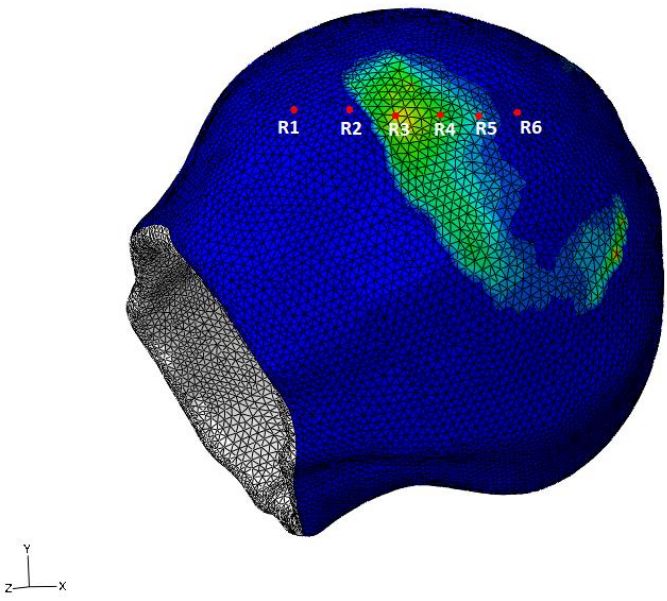

Figure 54: Case 2 without labrum - Representation of the 5 nodes selected on the femoral cartilage defining a horizontal line perpendicular to the axis of the pure internal rotation.

The final magnitude observed on the femoral cartilage (8.018 MPa) occurs slightly below the region of the selected nodes.

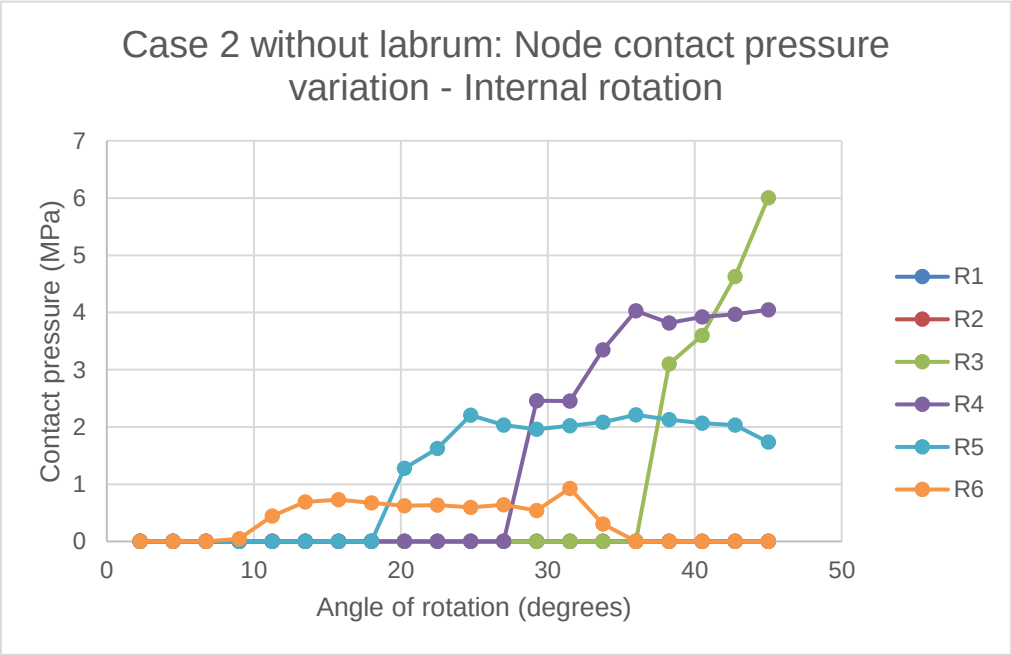

Figure 55: Case 2 without labrum - Contact pressures evolution in the selected nodes on the femoral cartilage as a function of the angle of pure internal rotation.

The maximum magnitude of the contact pressures and of the von Mises stresses on the femoral cartilage (FC) and on the acetabular cartilage (AC) at the end of the rotational step and during the rotational step can be observed in Table 12 together with the corresponding locations.

Table 12: Case 2 without labrum – Contact pressures and von Mises stresses at the end of the internal rotation and during the internal rotation step on the two hip joint components. The maximum observed during the step and the final magnitude are presented and the location is identified. (AI - Anteroinferior; AS – Anterosuperior)

		Contact Pressure		**Von Mises**	
		Maximum during step	**Final Maximum**	**Maximum during step**	**Final Maximum**
Internal rotation 45º	FC	**8.018 MPa** (100%) A region	**8.018 MPa** AS region	**2.970 MPa** (100%) AS region	**2.970 MPa** AS region
	AC	**9.88 MPa** (50% of the step) A region	**7.010 MPa** AI region	**13.64 MPa** (30% of the step) AI region	**10.69 MPa** AS region

5.5. Discussion

This section aims to analyze and compare the values obtained from the numerical simulations of the two pathological cases with distinct degrees of the cam deformity (with alpha angles of 60º and 81º, respectively) and also to evaluate the effect of the absence of the labral tissue in the hip joints. Validation of the results with already existing data [8] [9] is also performed.

Several limitations in the models used in these analyses are to be considered. The analyses are performed based on the real patient-specific hip anatomy using sets of arthro-MRI images provided by a physician. The reconstructed 3D models of the hip joint were manually segmented and several software tools were used in order to obtain the final 3D models. The manually obtained models of the hip joints are, in our opinion, more consistent with the reality than the automatically generated models. Nonetheless, some deviations from the reality are to consider due to the reduced contrast and resolution specifications of the arthro-MRI images. The fact that the segmentation was totally manually conducted and not automatically computer-based executed may lead to geometric discrepancy in the reconstructed soft tissues specifications, such as the tissue thickness and anatomical real dimensions. Also, joint incongruity and material properties are to be appraised.

Specific characteristics of the soft tissues and model approximations were considered. The hip joint models used in the analyses do not include other tissues that surround and involve the cartilages and the labrum. Regarding the behavior of the cartilage, linear elastic behavior was attributed to the femoral and acetabular cartilages, and the bones were considered rigid. Such characteristics attributed to the present models are the major limitations to be considered in the analyses. Despite the presented limitations of the models, the FE analyses yielded magnitudes of the contact pressures that are in coherence with the published data.

The obtained values of the contact pressures in the present thesis, in the overall, are in the range of the published works. The obtained maximum magnitudes of the contact pressure for the articular compressive loading of the cam joints are in the range of 3 – 6 MPa, which is in coherence with the published data in Jorge et al. [8] and Lourenço et al. [9]. This suggests that the compressive loading is not the determinant factor for the existence of high intra-articular contact pressures in hips with cam deformity. Also, the severity of FAI of the cam-type does not affect the magnitudes of the contact pressures for the compressive articular loading. In Lourenço et al. [9] the magnitudes of the contact pressures obtained at the end of the compressive step for a normal hip joint and for a pathological hip joint (alpha angle of 90º) presented values that are in the range of 5 MPa on the femoral cartilage. Moderately higher values of the contact pressures were observed on the acetabular cartilage and magnitudes in the range of 3 – 4 MPa were observed on the labrum. Regarding the obtained results for the present analysis of the two pathologic cases, the maximum magnitudes of the contact pressure at the end of the compressive step for the pathologic case 1 with alpha angle of 60º were approximately 6.5 MPa on the femoral cartilage on the region of the deformity, 5.4 MPa on the acetabular cartilage (in

the region in contact with the femoral deformity) and approximately 2.5 MPa on the labrum (also in the region in contact with the pathology). In addition, for the same case (case1), extremely high magnitudes of the contact pressures (17.37 MPa) were obtained on the acetabular cartilage on the superior region of the tissue. This value is believed to be artificial, possibly due to geometric incoherence during the reconstruction procedures. For case 2 with alpha angle of 81º, the maximum contact pressure obtained was 3 MPa on the femoral cartilage, 3.1 MPa on the acetabular cartilage and approximately 2.4 MPa on the labrum. The magnitude of the contact pressures obtained for the pathologic case 2 appear to be decreased when comparing with the pathologic case 1. This occurrence may be explained by differences in the cartilage thickness or by any inaccuracies resulting from the manual segmentation. This suggests that the alpha angle does not influence the articular compression without further movement. Therefore, the severity of the cam pathology, during the compressive hip action, is probably not responsible for any chondral or labral damage.

High values of the contact pressures were observed for the selected hip joint movements, such as pure flexural rotation and pure internal rotation. Rotational movements of the pathologic cam joints play thus a major role in the genesis of augmented magnitudes of the contact pressure on the articular and labral structures of the joints. It is when the cephalic deformity of the femoral head enters the acetabulum, that the abutment mechanism occurs which leads to an abnormal non-physiological contact of the femoral cartilage with the acetabular cartilage and labrum. Over time, this mechanism may lead to aggression of the intra-articular structures and to labral detachment. For the pure flexural rotational motion, the magnitudes of the contact pressures were considerably higher when comparing with the magnitudes after the compressive step. The maximum magnitudes of the contact pressures obtained in Jorge et al [8] for the pure flexural rotation of 90º and for a patient presenting a cam pathologic hip with an alpha angle of 98º, were 11.6 MPa on the acetabular cartilage at 90º of the pure flexural motion, 8.6 MPa on the femoral cartilage for 32º of the flexural rotation observed on the region where the cam deformity is more evident, and 14.4 on the labrum at the end of the rotational step. In Lourenco et al. [9] the maximum magnitudes of the contact pressures were computed in a model with cam type impingement with an alpha angle of 90º and in a normal hip joint model. For the patient presenting a cam-type impingement with an alpha angle of 90º, the obtained magnitudes of the contact pressures at the end of the pure flexural rotation of 90º were 7.1 MPa on the femoral cartilage in the region of the cam pathology, 10.2 MPa on the acetabular cartilage in the region of the tissue that is in contact with the femoral deformity and approximately 7.1 MPa on the labrum also in the region in contact with the deformity. For the normal joint (alpha angle in the range 40º-50º), Lourenco et al. [9] reported the occurrence of numerical problems that blocked the simulation at 40º of rotation. The obtained magnitudes of the contact pressures at the end of a pure flexural rotation of 40º were 14.0 MPa on the femoral cartilage, 13.6 MPa on the acetabular cartilage and 13.1 MPa on the labrum. The values are considerably high and it was believed to result from reconstruction problems. Regarding the present analysis of the two pathologic cases 1 and 2, with alpha angles of 60º and 81º respectively, the obtained maximum magnitudes of the contact pressures at the end of the flexural step in case 1 are in the range of the values presented in the previous works. Due to reconstruction problems and/or geometry incoherence, the flexural rotation step for case 2 stops when it reaches the rotational angle of 23.4º and

thus it was not possible to compare values with case 1. However, the final magnitudes of the contact pressures obtained for a rotational angle of 23.4º were considerably higher than the ones obtained for the compressive step and also higher than the ones obtained in case 1 for the same rotational angle.

For case 1 and considering the pure flexural rotation of the hip joint of 90º, a progressive increase of the magnitude of the contact pressures was observed on the femoral cartilage during the flexural step. The maximum magnitude of the contact pressure obtained on the femoral cartilage presented a value of 8.7 MPa for an angle of flexural rotation of 63º, and the final magnitude of the contact pressure for 90º rotation was 7.4 MPa located on the region of the cam deformity. For the acetabular cartilage, an increase of the magnitudes of the contact pressure was observed on the anterosuperior and peripheric region near the chondro-labral transition as a result of the increased contact between the cam deformity and the acetabular cavity. The maximum magnitude was of 13.8 MPa registered during the flexural rotation step for an angle of rotation of 31.5º and was observed on the transitional region of the chondral and labral tissue. The final magnitude of the contact pressure registered at the end of the 90º of rotation, was of 5.7 MPa located on the superior periphery and 5 MPa on the anterosuperior region of the acetabular cavity, the region that is contact with the osseous bump. It is also observed that the contact pressures distribution on the acetabular cartilage presents a large and wide-reaching distribution within the acetabular cavity. In the labral tissue, a superior and peripheric migration of the contact pressures was observed during the flexural step. The maximum and final contact pressure was 12.4 MPa registered also on the superior periphery of the acetabular cavity, coincident with the location of the final maximum magnitude of the contact pressure on the acetabular cartilage. The presented magnitudes obtained on the acetabular cartilage and labral tissue are coincident with intra operative observations, that identified the major chondral and labral damages on the peripheric region of the acetabular cavity between the limits of the chondral and labral tissues in contact with the location of the femoral cam pathology. Regarding the evolution of the contact pressures in the selected nodes in the region of the deformity of the femoral cartilage as a function of the angle of flexural rotation (Figure 29 in section 5.1.1), it is observed a gradual growth of the magnitudes of the contact pressure on the selected nodes. The nodes were selected perpendicularly to the axis of flexural rotation with the aim of including the closest and furthest regions to the cam pathology. From the plot one can observe that the maximum magnitude occurs at the end of the flexural step with a value of 4.95 MPa on node F3. Lower pressures are observed on the nodes that are closer to the superior region of the femoral cartilage (nodes F1 and F2), in contrast, higher pressures are identified in the nodes F3, F4 and F5, being these nodes located closer to the region of the femoral deformity in the anterosuperior region of the femoral head.

Although for case 2 (largest alpha angle), the final and maximum magnitudes of the contact pressures obtained on the femoral cartilage and labrum for the pure flexural rotation of the hip are higher than for case 1, it is believed that they are artificial due to geometric reconstruction incoherence of the hip model and not resulting from the increased severity of the cam impingement. The final magnitude observed on the femoral cartilage was 54 MPa located on the inferior region of the femoral cartilage and a similar magnitude of 57 MPa was identified on the labrum on the same region. For the acetabular

cartilage a value of 10.9 MPa was identified on the inferior region of the acetabular cavity which is not extremely deviated from reality, as similar values were obtained in previous works for alpha angles of 90º and 98º, as already referred.

The fact that rotational motions of the hip joints with cam deformity are the major factor for the genesis of the higher contact pressures within the intra articular structures is also confirmed in the case of the pure internal rotational motion. Moreover, higher magnitudes of the contact pressure were registered on the labral and chondral tissues in the case of the pure internal rotation when comparing with the pure flexural rotation motion. Also, and in contrast with the pure flexural rotation, the contact pressures distribution on the acetabular cartilage in the pure internal rotation motion, is narrower and confined to a specific area in the chondro-labral transitional region. The abutment mechanism of the femoral head into the acetabular cavity leads to increased pressures on the region of the femoral deformity and thus, major tissue aggression and lesion may develop. The obtained magnitudes of the contact pressure for the present cases 1 and 2 are in the range of the published values. The maximum magnitudes of the contact pressures obtained in Jorge et al [8] for a pure internal rotation of 24º and for a patient presenting a cam pathologic hip with an alpha angle of 98º, were 12.8 MPa on the femoral cartilage on the region where the cam deformity is more evident, 13.6 MPa on the acetabular cartilage and 14.7 on the labrum at the end of the rotational step. In Lourenço et al. [9], after the pure internal rotational motion of 40.5º and for a cam type hip joint with an alpha angle equal to 90º, a magnitude of 12.5 MPa was registered in the anterosuperior region of the femoral cartilage. The anterosuperior region is the region where the cam deformity is more evident. A magnitude of 16 MPa was registered on the acetabular cartilage and a magnitude of 15.8 MPa was registered on the labrum. The registered contact pressures on the acetabular cartilage and labrum were identified in the region that is in contact with the femoral deformity. For a normal hip joint, at the end of the pure internal rotation, a magnitude of 10.5 MPa was registered on the femoral cartilage, in a distinct region when comparing with the cam hip joint. The maximum contact pressure was registered on the superior region of the femoral cartilage, whereas for the cam joint the final magnitude of the contact pressure on the femoral cartilage was registered on the anterosuperior region, which is the region of the femoral deformity. A maximum magnitude of 9.4 MPa was observed on the acetabular cartilage and a maximum magnitude of 11.1 MPa was observed on the labrum.

For the pure internal rotation motion, a complete rotation of 45º was performed in the two pathological cases 1 and 2. A change of the location of the final and maximum magnitudes of the contact pressure was observed when comparing with the flexural rotation motion. For case 1, the maximum magnitude of the contact pressure presented a value of 14.8 MPa located on the inferior region of the femoral cartilage for an angle of internal rotation of 31.5º, whereas the final magnitude was of 10.5 MPa located on the same region. The maximum contact pressures were not observed on the region of the femoral deformity. The location of the obtained maximum magnitudes on the femoral cartilage may be related to the patient-specific characteristics of this joint. The magnitude of the maximum contact pressure on the acetabular cartilage was 13.6 MPa observed on the posterior region on the chondro-labral transitional region. The maximum magnitude of the contact pressure on the labrum was 18.4 MPa,

on the posteroinferior region, coherent with the contact pressures distribution of the acetabular cartilage. Analyzing the evolution of the contact pressure in the selected nodes on the region of the deformity of the femoral cartilage as a function of the angle of pure internal rotation (Figure 32 section 5.1.2), maximum magnitudes were observed for an angle of rotation of approximately 25º (on node R3) with a magnitude of 8 MPa and 40º (on node R2) with a magnitude of 9 MPa. A pattern of pressure growth is found as the distance of the node to the center of rotation increases. The nodes that are located precisely on the region of the osseous bump are constantly under higher pressures than the other slightly apart from the bump.

For case 2, the maximum magnitude of the contact pressures observed on the femoral cartilage at the end of the step was 9.8 MPa located on the anterosuperior region of the femoral cartilage (the region where the cam pathology is more evident). The maximum magnitude of the contact pressures observed on the acetabular cartilage was 10.1 MPa on the anterosuperior region of the acetabular cavity for an angle of rotation of 22.5º. At the end of the rotational step, a final magnitude of 9.1 MPa was observed on the same region, which is the region in contact with the femoral deformity. The maximum magnitude of the contact pressures observed on the labral tissue was 17.6 MPa at the end of the rotational step and also in the region in contact with the cam deformity. However, very large pressures were obtained in the femoral cartilage and in the labrum during the rotational step for an angle of rotation in the range 15º-20º. This suggests that the high pressures obtained on these structures are the result of the cam impingement, characteristic of the present joint with a cephalic deformity of 81º. Analyzing the evolution of the contact pressure in the selected nodes on the region of the deformity of the femoral cartilage as a function of the angle of pure internal rotation (Figure 40 in section 5.2.2), maximum magnitudes were observed for an angle of rotation of approximately 28º (on node R4) with a magnitude of 6 MPa and 40º (on node R3) with a magnitude of 8 MPa. As in case 1, a pattern of pressure growth is found as the distance of the node to the center of rotation increases. The nodes that are located precisely on the region of the osseous bump characteristic of the cam deformity, are constantly under higher pressures than the other nodes slightly apart from the region of the osseous bump.

Comparing the obtained magnitude of the contact pressures on both pathological cases at the end of the pure internal rotation step, the final magnitude on the labrum was higher for case 2 than for case 1. The increased value of the contact pressure for case 2 is the consequence of the increased severity of the cam impingement, characterized by an higher alpha angle. For the acetabular cartilage and femoral cartilage, the obtained contact pressures in case 1 are higher when comparing with normal hips. In case 2 the obtained contact pressures in the femoral cartilage and in the labrum are higher when comparing with case 1. This suggests that major impact and major damage may be observed on the femoral cartilage and on the labrum of the patient with cam-type impingement with an alpha angle of 81º as a result of the cam pathology. This observation is in coherence with the intraoperative observations, since the labral and chondral damages are observed on the femoral cartilage and on the chondro-labral transitional region that is in contact with the cam deformity. In addition, in case 2, the contact pressures distribution on the acetabular cartilage (section 5.2.2) is more confined to the chondro-labral transitional region of the acetabular cavity that is in contact with the region where the femoral

head is most aspherical (anterosuperior region). The acetabular contact pressures distribution in case 1 is more widely spread in the same regions. One may conclude that tissue damage is influenced by the severity of the cam-type impingement in pathologic hip joints; a major localized tissue aggression is observed in the hip of the patient with alpha angle equal to 81º than in the hip of the patient presenting an alpha angle equal to 60º.

A comparative study was performed by analyzing the effect of the absence of the labral tissue in the pathologic hip joints for the selected motions. The magnitudes of the contact pressure obtained in the analyses without labrum are compared with the cases where the labrum is present. Although the obtained magnitudes of the contact pressure observed on the intra-articular structures when the labrum is absent were moderately decreased when comparing with the magnitudes in complete hip joints, a trend in the contact pressures distributions was observed in both pathological cases without labrum. The contact pressures distribution in the pathological cases without labrum were more extended and widely spread throughout the soft tissues. This is straightforwardly identified in the case of the acetabular cartilage of both pathologic cases (section 5.3 and 5.4). The maximum magnitudes of the contact pressures are diminished when compared with the ones obtained in the complete models but the regions that are subjected to pressure are amplified. The labral tissue is important in the maintenance and support of the articular structures protecting some regions of the acetabular cartilage from the effect of high stresses. Due to the lack of the labral tissue, its supportive action is not present, leading to wider distributions of pressures on the acetabular cartilages. This suggests that, in a patient presenting labrum detachment, no supportive nor protective action is performed by this tissue and thus larger regions of the cartilage structures are less preserved from the subjected pressures, resulting in increasing chondral damage. Thus, early surgical treatment and labral reattachment, may help to prevent, or delay, the joint degeneration. A change in the region of maximum contact pressures was also observed in case 1 when a pure internal rotation is applied. When the labrum is not present, the maximum magnitude of the contact pressure is obtained in the region of the cam deformity.

Comparing the effects of the two rotational motions of the hip joint, the pure flexural rotation and the pure internal rotation, the internal rotation appears to be the determinant hip joint motion for the genesis of the high intra-articular contact pressures, and the critical angle of rotation is in the range of 15º-30º. This was observed in both cases when the labrum is or is not present. In [9] it was shown that the surgical treatment that restores the normal anatomy of the joint effectively reduces these high intra-articular pressures and stresses approaching the values obtained in a normal hip.

6. Conclusions

The main objectives of the performed analysis are a) to compare the intra-articular von Mises stresses and contact pressures in hips with femoroacetabular impingement of the cam-type with various degrees of morphological deformity, b) to evaluate the effect of the abscence of the labral tissue in hip joints in order to c) validate the current treatment techniques.

The magnitudes of the contact pressures obtained in the two pathological cases are in coherence with published data and are higher than the ones obtained in normal hip joints. As a consequence of the increased severity of the cam impingement, increased contact pressure magnitudes are observed in the pathologic hip with larger alpha angle.

For the imposed physiological rotational motions, the internal rotation appears to be the determinant hip joint motion for the genesis of the high intra-articular contact pressures. For the pure flexural rotation, it was not possible to compare the effect of the alpha-angle since the FE analysis for case 2 did not converge. However, higher magnitudes of the contact pressure were obtained in case 2, with higher alpha angle, when compared with the magnitudes obtained in case 1 for the same flexural loading. For the pure internal rotation, in both cases, the obtained contact pressures on the femoral and acetabular cartilages are higher when comparing with normal hips. In case 2, with higher alpha angle, the obtained contact pressures in the femoral cartilage and in the labrum are higher when comparing with case 1. It is thus conclusive that the tissue aggression is influenced by the severity of the cam-type impingement in pathologic hip joints; major intra-articular pressures and stresses are observed in the hip of the patient with alpha angle equal to 81º than in the hip of the patient presenting an alpha angle equal to 60º. When the labrum is absent from the model, the magnitudes of the contact pressures are moderately smaller than the ones obtained in the complete models. However, the regions that are now subjected to pressure are wider, suggesting that the labrum has a supportive and protective action that preserves some regions of the cartilage structures from high pressures. In the cases where the labral tissue is damaged, an early surgical intervention may also be a key aspect in preventing major joint degeneration.

This study confirms the abnormal functioning of the hip joints with cam-type impingement. The increased magnitudes of the contact pressures on the intra-articular structures may justify the origin of the observed damage, and thus, the early surgical intervention may prevent the outset of the articular complications. Regarding the future developments, major achievements in the simulations may be accomplished by considering the bony structures as non-rigid materials (elastic materials) and the cartilages as porous materials. Also, including the tissues that surround the hip joint such as ligaments, would represent a hip joint environment more consistent with reality.

References

[1] M. Leunig, P. E. Beaulé, and R. Ganz, “The concept of Femoroacetabular impingement: Current status and future perspectives,” *Clin. Orthop. Relat. Res.*, vol. 467, no. 3, pp. 616–622, 2009.

[2] S. Wagner *et al.*, “Early osteoarthritic changes of human femoral head cartilage subsequent to femoro-acetabular impingement,” *Osteoarthr. Cartil.*, vol. 11, no. 7, pp. 508–518, 2003.

[3] R. Ganz, M. Leunig, K. Leunig-Ganz, and W. H. Harris, “The etiology of osteoarthritis of the hip: An integrated mechanical concept,” *Clin. Orthop. Relat. Res.*, vol. 466, no. 2, pp. 264–272, 2008.

[4] J. Parvizi, M. Leunig, and R. Ganz, “Femoroacetabular Impingement,” *J. Am. Acad. Orthop. Surg.*, vol. 15, no. 9, pp. 561–570, 2007.

[5] S. Chegini, M. Beck, and S. J. Ferguson, “The effects of impingement and dysplasia on stress distributions in the hip joint during sitting and walking: A finite element analysis,” *J. Orthop. Res.*, vol. 27, no. 2, pp. 195–201, 2009.

[6] B. D. Kuhns, A. E. Weber, D. M. Levy, and T. H. Wuerz, “The Natural History of Femoroacetabular Impingement,” *Front. Surg.*, vol. 2, no. November, pp. 1–7, 2015.

[7] P. Banerjee and C. R. McLean, “Femoroacetabular impingement: A review of diagnosis and management,” *Curr. Rev. Musculoskelet. Med.*, vol. 4, no. 1, pp. 23–32, 2011.

[8] J. P. Jorge *et al.*, “Finite element simulations of a hip joint with femoroacetabular impingement.,” *Comput. Methods Biomech. Biomed. Engin.*, vol. 17, no. 11, pp. 1275–1284, 2014.

[9] J. Lourenço, F. M. F. Simões, and P. A. Rego, “Finite element analyses of femoroacetabular impingement before and after hip arthroscopy.,” *Biomed. Mater. Eng.*, vol. 26, no. 3–4, pp. 193–206, 2015.

[10] E. S. and U. Schumacher, *THIEME Atlas of Anatomy - General Anatomy and Musculoskele- tal System*. 2010.

[11] B. S. Standring, *Gray' s Anatomy , 40th Edition*. 2008.

[12] D. E. Lunn, A. Lampropoulos, and T. D. Stewart, “Basic biomechanics of the hip,” *Orthop. Trauma*, vol. 30, no. 3, pp. 239–246, 2016.

[13] K. F. Bowman, J. Fox, and J. K. Sekiya, “A clinically relevant review of hip biomechanics,” *Arthrosc. - J. Arthrosc. Relat. Surg.*, vol. 26, no. 8, pp. 1118–1129, 2010.

[14] M. M. Groh and J. Herrera, “A comprehensive review of hip labral tears,” *Curr. Rev. Musculoskelet. Med.*, vol. 2, no. 2, pp. 105–117, 2009.

[15] S. J. Ferguson, J. T. Bryant, R. Ganz, and K. Ito, “The influence of the acetabular labrum on hip

joint cartilage consolidation: A poroelastic finite element model," *J. Biomech.*, vol. 33, no. 8, pp. 953–960, 2000.

[16] P. Bocchiaro and A. Zamperini, "World's largest Science , Technology & Medicine Open Access book publisher c," *RFID Technol. Secur. Vulnerabilities, Countermeas.*, 2016.

[17] Carol A. Oatis, PhD "Kinesiology - The Mechanics and Pathomechanics of Human Movement, Second Edition", Lippincott Williams & Wilkins.

[18] J. Buckwalter, M. Lotz, J.F. Stoltz, "Osteoarthritis, Inflammation and Degradation: A continuum" , IOS Press.

[19] M. Tannast, D. Goricki, M. Beck, S. B. Murphy, and K. A. Siebenrock, "Hip damage occurs at the zone of femoroacetabular impingement," *Clin. Orthop. Relat. Res.*, vol. 466, no. 2, pp. 273–280, 2008.

[20] M. Stephanie Pun, MD, Deepak Kumar, PT, PhD, and Nancy E. Lane, "Femoroacetabular Impingement," *Nih*, vol. 67, no. 1, pp. 17–27, 2016.

[21] K. Ito, M. a Minka, M. Leunig, S. Werlen, and R. Ganz, "Femoroacetabular impingement and the cam-effect. A MRI-based quantitative anatomical study of the femoral head-neck offset.," *J. Bone Joint Surg. Br.*, vol. 83, no. September 1997, pp. 171–176, 2001.

[22] M. Leunig, W. J. Robertson, and R. Ganz, "Femoroacetabular Impingement: Diagnosis and Management, Including Open Surgical Technique," *Oper. Tech. Sports Med.*, vol. 15, no. 4, pp. 178–188, 2007.

[23] M. Lavigne *et al.*, "Anterior Femoroacetabular Impingement," *Clin Orthop*, no. 418, pp. 61–66, 2004.

[24] L. Dubs, "The contour of the femoral head-neck junction as a predictor for the risk of anterior impingment: Commentary," *Praxis (Bern. 1994).*, vol. 92, no. 11, pp. 475–477, 2003.

[25] P. L. Leunig *et al.*, "Young Adult Hip A Systematic Approach to the Plain Radiographic Evaluation of the A Systematic Approach to the Plain Radiographic Evaluation of the Young Adult Hip," *J. Bone Jt. Surg. Copyr. BY J. BONE Jt. Surg.*, vol. 90, pp. 47–66, 2008.

[26] C. Barton, M. J. Salineros, K. S. Rakhra, and P. E. Beaulé, "Validity of the alpha angle measurement on plain radiographs in the evaluation of cam-type femoroacetabular impingement," *Clin. Orthop. Relat. Res.*, vol. 469, no. 2, pp. 464–469, 2011.

[27] A. Kassarjian, "Hip MR arthrography and femoroacetabular impingement," *Semin. Musculoskelet. Radiol.*, vol. 10, no. 3, pp. 208–219, 2006.

[28] K. K. Gosvig *et al.*, "A new radiological index for assessing asphericity of the femoral head in cam impingement," *J Bone Jt. Surg [Br]*, vol. 8989, no. 10, pp. 1309–16, 2007.

[29] M. R. Nouh, M. E. Schweitzer, L. Rybak, and J. Cohen, "Femoroacetabular impingement: Can

the alpha angle be estimated?," *Am. J. Roentgenol.*, vol. 190, no. 5, pp. 1260–1262, 2008.

[30] K. A. Siebenrock, "Gender-dependent discrepancies in femoroacetabular impingement Paper No . 214 • 55th Annual Meeting of the Orthopaedic Research Society," vol. 26, no. 214, p. 2008, 2008.

[31] L. B. Laborie, T. G. Lehmann, I. Engesæter, F. Sera, L. B. Engesæter, and K. Rosendahl, "The alpha angle in cam-type femoroacetabular impingement: New reference intervals based on 2038 healthy young adults," *Bone Jt. J.*, vol. 96 B, no. 4, pp. 449–454, 2014.

[32] A. A. Wright, G. S. Naze, A. E. Kavchak, D. Paul, B. Kenison, and E. J. Hegedus, "Radiological variables associated with progression of femoroacetabular impingement of the hip: A systematic review," *J. Sci. Med. Sport*, vol. 18, no. 2, pp. 122–127, 2015.

[33] A. Bedi, N. Chen, W. Robertson, and B. T. Kelly, "The Management of Labral Tears and Femoroacetabular Impingement of the Hip in the Young, Active Patient," *Arthrosc. - J. Arthrosc. Relat. Surg.*, vol. 24, no. 10, pp. 1135–1145, 2008.

[34] J. C. McCarthy, P. C. Noble, M. R. Schuck, J. Wright, and J. Lee, "The Otto E. Aufranc Award: The role of labral lesions to development of early degenerative hip disease.," *Clin. Orthop. Relat. Res.*, no. 393, pp. 25–37, 2001.

[35] K. Ito, M. Leunig, and R. Ganz, "Histopathologic features of the acetabular labrum in femoroacetabular impingement.," *Clin. Orthop. Relat. Res.*, no. 429, pp. 262–71, 2004.

[36] R. H. Fitzgerald, "Acetabular labrum tears. Diagnosis and treatment.," *Clin. Orthop. Relat. Res.*, no. 31, pp. 60–68, 1995.

[37] J. B. Volpon, "Femoroacetabular impingement," *Rev. Bras. Ortop. (English Ed.*, vol. 51, no. 6, pp. 621–629, 2016.

[38] A. K. Gupta, G. D. Abrams, and S. J. Nho, "What's New in Femoroacetabular Impingement Surgery: Will We Be Better in 2023?," *Sports Health*, vol. 6, no. 2, pp. 162–170, 2014.

[39] C. L. Peters, J. A. Erickson, L. Anderson, A. A. Anderson, J. Weiss, and B. L. Christopher Peters, "Hip-Preserving Surgery: Understanding Complex Pathomorphology," *J Bone Jt. Surg Am*, vol. 91, pp. 42–58, 2009.

[40] C. R. Freeman, M. G. Azzam, and M. Leunig, "Hip preservation surgery: surgical care for femoroacetabular impingement and the possibility of preventing hip osteoarthritis," *J. Hip Preserv. Surg.*, vol. 1, no. 2, pp. 46–55, 2014.

[41] W. A. Hodge, R. S. Fijan, K. L. Carlson, R. G. Burgess, W. H. Harris, and R. W. Mann, "Contact pressures in the human hip joint measured in vivo.," *Proc. Natl. Acad. Sci. U. S. A.*, vol. 83, no. 9, pp. 2879–83, 1986.

[42] T. Macirowski, S. Tepic, and R. W. Mann, "Cartilage stresses in the human hip joint.," *J. Biomech.*

Eng., vol. 116, no. 1, pp. 10–18, 1994.

[43] R. Von Eisenhart, C. Adam, M. Steinlechner, M. Muller-Gerbl, and F. Eckstein, “Quantitative determination of joint incongruity and pressure distribution during simulated gait and cartilage thickness in the human hip joint,” *J. Orthop. Res.*, vol. 17, no. 4, pp. 532–539, 1999.

[44] A. E. Anderson, B. J. Ellis, S. A. Maas, C. L. Peters, and J. A. Weiss, “Validation of Finite Element Predictions of Cartilage Contact Pressure in the Human Hip Joint,” *J. Biomech. Eng.*, vol. 130, no. 5, p. 51008, 2008.

[45] E. Genda, N. Iwasaki, G. Li, B. A. MacWilliams, P. J. Barrance, and E. Y. S. Chao, “Normal hip joint contact pressure distribution in single-leg standing-effect of gender and anatomic parameters,” *J. Biomech.*, vol. 34, no. 7, pp. 895–905, 2001.

[46] H. Yoshida, A. Faust, J. Wilckens, M. Kitagawa, J. Fetto, and E. Y. S. Chao, “Three-dimensional dynamic hip contact area and pressure distribution during activities of daily living,” *J. Biomech.*, vol. 39, no. 11, pp. 1996–2004, 2006.

[47] H. H. Huberti and W. C. Hayes, “Patellofemoral contact pressures,” *J. Bone Jt. Surg. Inc.*, vol. 66, no. 5, pp. 715–724, 1984.

[48] D. A. Michaeli, S. B. Murphy, and J. A. Hipp, “Comparison of predicted and measured contact pressures in normal and dysplastic hips,” *Med. Eng. Phys.*, vol. 19, no. 2, pp. 180–186, 1997.

[49] D. E. Shepherd and B. B. Seedhom, “A technique for measuring the compressive modulus of articular cartilage under physiological loading rates with preliminary results.,” *Proc. Inst. Mech. Eng. H.*, vol. 211, no. 2, pp. 155–165, 1997.

[50] G. Bergmann *et al.*, “Hip forces and gait patterns from rountine activities,” *J. Biomech.*, vol. 34, pp. 859–871, 2001.

[51] Q. Liu, W. Wang, A. R. Thoreson, C. Zhao, W. Zhu, and P. Dou, “Finite element prediction of contact pressures in cam-type femoroacetabular impingement with varied alpha angles,” *Comput. Methods Biomech. Biomed. Engin.*, vol. 5842, no. April, pp. 1–8, 2016.

[52] M. Dalstra, R. Huiskes, and B. Section, “Load Transfer Across the Pelvic,” *Biomechanics*, vol. 28, no. 6, 1995.

[53] Joana Lourenço, “Biomechanical Modelling of the Femoroacetabular Impingement of the Cam Type Thesis to obtain the Master of Science Degree in Biomedical Engineering,” no. December, 2013.

[54] J. C. Carr, R. K. Beatson, and J. B. Cherrie, “Reconstruction and representation of 3D objects with radial basis functions,” *Proc. 28th …*, no. August, pp. 12–17, 2001.

[55] L. Ombregt, “Clinical examination of the hip and buttock,” *A Syst. Orthop. Med.*, p. 617–626.e1, 2013.